ON-CHIP LIQUID/SOLID CHROMATOGRAPHY FOR CONTINUOUS ANALYSIS

THÈSE N^{O} 3866 (2007)

PRÉSENTÉE LE 31 AOÛT 2007

À LA FACULTÉ DES SCIENCES ET TECHNIQUES DE L'INGÉNIEUR

Laboratoire de microsystèmes 4

SECTION DE MICROTECHNIQUE

ÉCOLE POLYTECHNIQUE FÉDÉRALE DE LAUSANNE

POUR L'OBTENTION DU GRADE DE DOCTEUR ÈS SCIENCES

PAR

Mario SCHLUND

ingénieur en microtechnique diplômé EPF
de nationalité suisse et originaire de Aesch (ZH)

acceptée sur proposition du jury:

Prof. R. Salathé, président du jury
Prof. Ph. Renaud, directeur de thèse
Prof. J. Brugger, rapporteur
Prof. A. Dommann, rapporteur
Prof. S. Verpoorte, rapporteur

ÉCOLE POLYTECHNIQUE
FÉDÉRALE DE LAUSANNE

Lausanne, EPFL
2007

La succession de chercheurs est comparable à un seul homme qui apprend indéfiniment

Blaise Pascal (1623 - 1662)

Abstract

This thesis reports on the development of technologies and methods for a microfiuidic device for continuous pressure-driven flow-injection analysis.

Chip based, pressure-driven liquid chromatographic (LC) systems are often avoided due to the difficulties encountered when it comes to flow control. The complexity involved precludes, for the time being commercializable, on-chip integration of valves and micropumps for microfluidic devices. However, LC is still the workhorse analytical method in most laboratories for small molecule analysis. There is a growing demand from the industry to have LC sensors being capable of direct sampling on the production lines, hence obviating the time-consuming detour to the lab.

As a possible solution to this demand, the concept of a chromatographic device is presented. It incorporates continuously flowing analyte and mobile phase streams and is capable of aliquoting samples from meso scale flows. Plugs are injected by momentarily change the flow distribution within the microfluidic channels by exploiting the method of gated flow injection in pressure-driven microchannels. The theoretical concept and experimental evidence is shown for two possible implementations; thermal plug injection through local homogenous bubble nucelation and pressure-drop plug injection. For the microfabricated device, a sol-gel technique is adapted to coat the open-tubular column walls with a C_8

stationary phase. Multi-compound phenolic solutions and vitamins are successfully separated to characterize the performance and limits of the chromatographic columns.

The last chapter of this work introduces the concept of size-exclusion enhanced, open-tubular chromatography (SOHS) on chip, where a porous column wall is excluding larger molecules and thus increases the separation power of the hydrodynamic separation generated through the parabolic flow profile of the pressure driven flow. The encouraging results are very promising for future applications such as polymer separations or DNA separation.

keywords: *microfluidics, lab-on-a-chip, μ-TAS, pressure-driven flow, hydrodynamic separation, liquid/solid chromatography, size-exclusion chromatography, electrochemical detection, amperometric detection, plug injection, continuous sampling, continuous analysis, porous silicon, fluorescence*

Version abrégée

Cette thèse traite du développement de technologies et méthodes de nouvelles pour la fabrication d'un dispositif microfluidique pour l'analyse en continu dans des systèmes hydrodynamiques miniaturisés.

Les systèmes hydrodynamiques de chromatographie liquide (LC) sur puce sont souvent évités en raison des difficultés relatives au contrôle des flux. En effet, l'intégration des valves et micropompes dans des puces microfluidique est d'une telle complexité que la production des systèmes intégrés commercialisable n'a pas pour le moment été réalisée. Néanmoins, la chromatographie liquide reste une des méthode préférée pour l'analyse en laboratoires chimiques. La demande de capteurs LC de la part de l'industrie, capable de l'échantillonnage en continu de lignes de production et évitant tout détour par un laboratoire d'analyse, ne cesse d'augmenter.

Un dispositif hydrodynamique pour l'analyse chromatographique sur puce est présenté dans cette thèse comme une solution possible à cette demande. Il utilise des flux d'analyte et de phase mobile en mouvement continue et il est capable de prélever des échantillons sur des flux à l'échelle mésoscopique.

L'injection d'un échantillon dans la colonne de séparation se fait par un changement momentané de la distribution de pression dans les canaux microfluidiques, en exploitant la méthode de l'injection dite aiguillée (gated injection). Deux méthodes pour l'implémentation de cette technique sur puce sont

présentées d'une façon théorique et validées expérimentalement: l'injection thermique par génération homogène d'une bulle dans le canal et l'injection par baisse de pression. Dans le dispositif microfluidique, une technique de sol-gel est utilisée afin de couvrir les parois de la colonne chromatographique d'une phase stationnaire C_8. La performance ainsi que les limites de cette colonne chromatographique sont caractérisés par la séparation de composants phenoliques ainsi que de vitamines.

La dernière partie de ce travaille introduit le concept de la chromatographie hydrodynamique assistée par une méthode de chromatographie d'exclusion en canal ouvert (SOHS) sur puce. Une paroi poreuse exclut des molécules de plus grande taille que celle des pores et augmente ainsi la puissance de séparation hydrodynamique générée par le profil parabolique du flux dans la microcolonne. Les résultats sont très prometteurs et laissent espérer une utilisation future du dispositif dans la séparation des polymers ou de l'ADN.

mots-clés: *microfluidique, lab-on-a-chip, μ-TAS, flux hydrodynamique, séparation hydrodynamique, chromatographie liquide/solide, chromatographie d'exclusion, détection électrochimique, ampérometrie, injection d'échantillon, échantillonnage en continu, analyse en continu, silicium poreux, fluorescence*

Acknowledgements

I would like to express my deepest gratitude to follwing people who contributed to the outcome of this thesis:

Prof. Philippe Renaud, who invited me to his group, first for a CTI project, and then for my PhD. The savant mix of creative freedom combined with fruitful discussions was the stimulating background of this thesis.

Prof. Sabeth Verpoorte, Prof. Jürgen Brugger and Prof. Alex Dommann for their participation in the thesis jury and Prof. René Salathé for having accepted to be its unpartial president. I highly appreciated your valuable comments and feedback.

Dr. Scott E. Gilbert from Crystal Vision Microsytems LLC who introduced me to the fascinating field of on-chip chromatography and particularly their industrial applications.

Prof. em. Ervin sz. Kováts for fruitful discussions about chromatography and analytical chemistry in general.

Prof. Ian Marison and Patrick Pugeaud for having me introduced to practical applications and laboratory use of HPLC.

Dr. Dirk Janasek and Prof. Andreas Manz from the Institute for Analytical Sciences, ISAS in Dortmund,

who kindly gave me access to their laboratory for one week. Even though the outcome was not what expected, we learned a lot! Thank you for your hospitality and support.

Dr. Arnaud Bertsch, not only as long-time office mate, but also for being probably the toughest proofreader the world has ever seen. I really appreciated your help in reading this manuscript as well as your hands-on explications for chemical and other scientific issues.

My actual and former office mates, Dr. Ana Valero, Dr. Ronit Zvitov and Prof. Karen Cheung for their everlasting good mood! It surely was not always that easy with me - especially when I couldn't stop whistling the same tune over and over again...

The semester and diploma students David Widmer, Gregoire Dao and Silvan Schnydrig, who contributed not only notably to the outcome of this thesis but also greatly influenced my time of flight...

Prof. Harald Fischer and Prof. Alessandro Stefani whom I got to know during the European research project netMED and with whom I shared numerous valuable discussions. And yes Alessandro, we'll chop that antenna whenever you like!

All the actual and former members of the CMI for their expert advice and support in clean room processing. I particularly appreciated the support of Dr. Philippe Flückiger, Dr. Cyrille Hibert, Faouzi Khechana, Guy Clerc and Roberto Mancini, and of course the indefatigable commitment of Irene Magnenat. Thank you very much!

Claude Amendola, Jean-Jacques Crausaz, Jean-Pierre Rougnon and Pascal Zbinden at the EPFL ATPR Workshop. Your precision and quality in making the chip holders is legendary and certainly contributes to the reputation of the *Swiss Made* label.

The administrative experts Rose-Mary Apothéloz, Claudia D'Agostino and Mary Halm. Your help is inestimable when it comes to taking care of bills, hotel reservations, orders, and any other imaginable administrative matter. Thank you very much for having made my life a lot easier.

The team at ACORT for producing the circuit boards.

ZEOCHEM AG for the free samples of N-dimethylaminodimethyl-octadecylsilane/octylsilane solutions for liquid phase coatings of the separation columns.

All my former an actual collegues and friends in the LMIS4 and EPFL, especially Alessandro, André, Anja, Claudia, Daniel (×2), Elie, Frédéric, Giancarlo, Harald, Harsha, Jeroen, Joël, Karine, Lynda, Marc (×2), Matteo, Mina, Nicolas (×2), Pontus, Raphaël (×2), Reto, Sébastien (×2), Shady, Stefan, Thomas, Tobias, uRBAN, Vincent and all the others I might have forgotten. We had a great time and without you I would not have made it!

All my family, who did not always understand why it had to be Lausanne and why those things have to be that small. Thank you for your indulgence and encouragement!

And finally Florence and Peyo, who show me that there are things much more important than science...

Contents

Nomenclature

Variables and constants

α	separation factor	[-]
χ	surface to volume ration	[-]
Δp	appplied pressure drop	[Pa]
ΔT	temperature différence	[°K]
η	viscosity	$[\mathrm{kg\,m^{-1}\,s^{-1}}]$
$\hat{U}$	applied voltage	[V]
κ	thermal conductivity	$[\mathrm{W\,m^{-1}\,{}^{\circ}K^{-1}}]$
λ_i	aspect ratio of molecule i with respect to column height	[-]
$\overline{\sigma}$	average standard deviation of peak width	[m]
ρ	density	$[\mathrm{kg\,m^{-3}}]$
σ	standard deviation of peak width	[m]
τ	temporal standard deviation of peak width	[s]
φ	channel aspect ration w_c/h_c	[-]
$a_{0.1}$	left-side peak half-width at 10% of height	[s]

NOMENCLATURE

A_c	column surface	$[\mathrm{m}^2]$
$b_{0.1}$	right-side peak half-width at 10% of height	[s]
b_c	quadratic channel side length	[m]
C	concentration	$[\mathrm{mol\,m}^{-3}]$
$c_{mobile,i}$	concentration of compound i in mobile phase	$[\mathrm{mol\,l}^{-1}]$
c_p	specific heat capacity	$[\mathrm{J\,kg}^{-1}\,{}^{\circ}\mathrm{K}^{-1}]$
$c_{stat/mob}$	compound concentration in stationary/mobile phase	$[\mathrm{mol\,l}^{-1}]$
D_c	diffusion constant	$[\mathrm{m}^2\,\mathrm{s}^{-1}]$
d_c	characteristic length	[m]
d_f	layer thickness of stationary phase	[m]
D_m	diffusion constant in mobile phase	$[\mathrm{m}^2\,\mathrm{s}^{-1}]$
E	energy	[Pa]
G	fixed pressure gradient	$[\mathrm{Pa\ m}^{-1}]$
H	plate height	[m]
h_c	channel (column) height	[m]
I_{meas}	measured current at amperometric detector	[A]
k	retention factor	[-]
k_b	Boltzmann constant ($= 1.3806503 \cdot 10^{23}$)	$[\mathrm{m}^2\ \mathrm{kg\ s}^{-2}\ {}^{\circ}\mathrm{K}^{-1}]$
K_e	efficiency factor	[-]
K_i	distribution coefficient of compound i	[-]
k_i	retention factor of compound i	[-]

$K_{SEC,i}$	SEC exclusion coefficient of compound i	[-]
l	characteristic length of scale factor	[m]
L^*	normalized straight segment length	[-]
L_c	channel (column) length	[m]
L_h	latent vapor heat	[$\mathrm{J\,kg^{-1}}$]
L_s	straight segment length	[m]
M	molar mass	[$\mathrm{kg\,mol^{-1}}$]
m	mass	[kg]
N	plate number	[-]
$n_{stat/mob}$	# of molecules of compound in stationary/mobile phase	[-]
N_s	noise level of the amperometric signal	[V]
P	power	[W]
p	pressure	[Pa]
Pe	Peclet number	[-]
Q	volumic flow rate	[$\mathrm{m^3\,s^{-1}}$]
R	chromatographic resolution	[-]
r	coordinate in channel/column radial direction	[m]
r^*	normalized turn radius	[-]
r_0	external turn radius	[m]
r_c	channel/column radius	[m]
$r_{eff,i}$	effective radius of molecule i	[m]

R_{fl}	flow resistance	$[\mathrm{N\,s\,m^{-5}}]$
R_{gc}	universal gas constant (= 8.314472)	$[\mathrm{m^3\,Pa\,K^{-1}\,mol^{-1}}]$
R_h	heater electrical resistance	$[\Omega]$
r_i	internal turn radius	[m]
r_p	particle size	[m]
R_{tot}	total electrical resistance	$[\Omega]$
Re	Reynold's number	[-]
S_i	detector sensitivity with respect to compound i	$[\mathrm{V\,mol^{-1}}]$
T	temperature	[°K]
T_0	initial temperature	[°K]
t_0	column hold–up time or dead time	[s]
$t_{adv.}$	advection time	[s]
t_D	diffusion time	[s]
T_g	glass transition temperature	[°K]
T_p	tailing of peak	[-]
$t_{R,i}$	retention time of molecule i	[s]
$t_{R,rel,i}$	relative retention time of molecule i	[s]
t_R	retention time	[s]
t'_R	net (or adjusted) retention time	[s]
u	flow rate	$[\mathrm{m\,s^{-1}}]$
u_{max}	maximum flow rate	$[\mathrm{m\,s^{-1}}]$

u_m	mean flow rate of the mobile phase	$[\mathrm{m\,s^{-1}}]$
u_{opt}	optimum flow rate	$[\mathrm{m\,s^{-1}}]$
V	volume	$[\mathrm{m^3}]$
V_0	interstitial column volume	$[\mathrm{m^3}]$
V_c	column volume	$[\mathrm{m^3}]$
V_i	elution volume of sample i	$[\mathrm{m^3}]$
V_{pores}	total pore volume	$[\mathrm{m^3}]$
$V_{stat/mob}$	Volume of compound in stationary/mobile phase	$[\mathrm{m^3}]$
V_{tot}	total elution volume	$[\mathrm{m^3}]$
w	peak width at the baseline	[s]
$w_{1/2}$	peak width at half-height	[s]
w_c	channel (column) width	[m]
x	coordinate in channel/column width direction	[m]
y	coordinate in channel/column height direction	[m]
z	coordinate in channel/column length direction	[m]

Abbreviations

μ-TAS	Micro-total-analysis system
ACN	Acetonitrile
BHF	Buffered hydrofluoric acid
CCD	Charge-coupled device
CE	Capillary electrophoresis

NOMENCLATURE

CEC	Capillary electrochromatography
CMI	Center of MicroNanoTechnology, EPFL
DC	Direct current
DMP	2,6 dymethylphenol
DNA	Deoxyribonucleic acid
EOF	Electroosmotic flow
ETFE	Ethylene-tetrafluoroethylene
HDC	Hydrodynamic chromatography
HF	Hydrofluoric acid
HPLC	High performance liquid chromatography
LC	Liquid chromatography
LOD	Limit of detection
LSC	Liquid/solid chromatography
MEKC	Micellular electrokinetic chromatography
MHD	Magneto-hydrodynamic pumping
OPPC	Open parallel plates chromatography
OT	Open-tubular
OTC	Open-tubular chromatography or open-tubular column
PAD	Pulsed amperometric detection
PDF	Pressure-driven flow
PDMS	Poly-dimethyl siloxane

PEEK	Polyetheretherketones
PP	4 pentylphenol
SDC	Shear-driven chromatography
SEC	Size-exclusion chromatography
SEM	Scanning electron microscopy
SNR	Signal-to-noise ration
SOHS	Size-exclusion enhanced, OT hydrodynamic chromatography
TAS	Total analysis system
TEOS	Tetraethoxysilane
TEOS-C_8	Octyltriethoxysilane
THF	Tetrahydrofuran
TMP	2,3,5 trimethylphenol
UV	Ultraviolet

Chapter 1

Introduction

Microtechnology first and nanotechnology subsequently provided scientist and engineers with tools to scale down sensors, actuators and even entire laboratories to chip level. Miniaturization is used not only for the sake of being small, but rather to take benefit of physical, chemical and fabricational advantages such as high surface-to-volume ratio, small reagents volumes or rapid batch fabrication.

A particular interest exists in miniaturizing analytical separation devices. Analytical chemistry, the science of providing information about composition and quantities of a substance, is done in laboratories, using mainly hand operated equipment. With the upcoming of electronics and computers, the qualitative and quantitative chemical analysis became more and more automatized. New technology with enhanced performance offered new possibilities. The total analysis system (TAS) introduced in the 1980s (Widmer, 1983) was addressing the high demand in laboratory automation. The TAS approach consists in integrating the analytical process into flowing systems, advantaging machine handling over hand labor; different analytical steps are put together by fluidic interconnection to perform the desired analysis.

Although the first analytical miniaturized device integrated on a chip was fabricated more than 30 years ago (Terry, 1975), it took another

15 years and a lot of progress in microfabrication technology until the introduction of the concept of micro-total-analysis systems (μ-TAS) by Manz *et al.* (1990a) and thus the starting shot to an exciting new variety of devices. Macroworld tubing is henceforth integrated into planar substrates and sampling volumes are reduced to μl, nl or even pl. Keywords such as 'Microfluidics' and 'Lab-on-a-Chip' were born. Since then, chip based separation devices for gas and liquid separation techniques have continuously grown in number and importance. One of the main accomplishments of miniaturized analytical chemistry was the sequencing of DNA (Huang *et al.*, 1992). However, while already widely present in research laboratories, μ-TAS are still an emerging species in industrial applications, the step from prototypes to market-ready devices being steep and difficult to handle.

1.1 Liquid handling

1.1.1 Pressure-driven flow

The most immediate way of moving a liquid in a conduit is applying a pressure difference between in- and outlets, thus inducing a pressure-driven flow (PDF). In microchannels, the no-slip condition at the walls results in a parabolic flow profile following the law of J. Poiseuille (1797-1869) and thus limits the flow rates. When considering separation technology, this can be an unwanted consequence causing dispersion of sample plugs in case of liquid/solid chromatography. But this effect can also be made use of, as for example in the field-flow fractionating technique presented by Giddings in 1966, or hydrodynamic chromatography introduced by Dimarzio and Guttman (1971) and later shown in microcapillary tubes (Tijssen *et al.*, 1983, 1986).
Applying PDF to microchannels is a rather challenging excercice. Common setups are using syringe pumps or hydrostatic pressure to drive liquids. However, reducing dimensions often results in a raise in required pressure-drop, which finds its limits usually in the interconnection in-

between the microchannel and the macro-world. Precise control of flow rates and switching and valving is cumbersome and hence the integration onto the miniaturized devices is complex (Shoji and Esashi, 1994).

1.1.2 Electroosmotic Flow

When a conductive liquid is in contact with a charged surface, charge separation induces electrical double-layers. One charge is immobilized at the surface, while the other, opposite charge moves freely within its layer. This layer can migrate under the application of an electrical field parallel to the surface and thus drags the liquid close by shear forces. In very small channels this drag can be of sufficient power to induce a net flow, called electroosmotic flow (EOF). The inherent advantages of EOF over PDF in miniaturized systems is ease of integration, and the flat *plug flow* (Manz *et al.*, 1994). Flow direction is easily changed by switching the sign of the applied electrical field. Plug flow and ease of scalability and integration are the reasons why most of the microfluidic applications are making use of EOF, such as capillary electrophoresis (CE), where molecules and ions of different charges and sizes are separated by electrophoretic and EOF-driven hydrodynamic forces (Manz *et al.*, 1992).

1.2 Chip based chromatography

The concept of performing separations on chip is driven by different motivations: Improvement of the system in terms of separation power and speed, reduction of carrier and reagent solution consumption and probably also the prospect of a cheap mass production of on-chip columns (Szumski and Buszewski, 2002). One of the most important advantages is the increased mass sensitivity, as chromatographic dilution (= initial solute concentration/concentration at peak maximum) is increasing with the squared column diameter.
There are two main concepts of liquid chromatography: Historically,

pressure microcolumns in glass capillary tubes with 1mm internal diameter were shown already in 1967, as resumed by Szumski and Buszewski (2002). The first analytical miniaturized device integrated on a chip, a gas chromatograph, was fabricated more than 30 years ago. In 1975, and later in 1979, it was Terry *et al.* who showed his microfabricated gas chromatograph with the separation column integrated on a silicon chip. However, as pointed out in the review on μ-TAS by Reyes *et al.* (2002), it never found the scientific echo it deserves, mainly due to its new technology to that date unknown amongst the separation scientists. The first system using separation columns on a chip for liquid chromatography was presented by Manz *et al.* (1990b) in their pioneering work using PDF and by Harrison *et al.* and Manz *et al.* (1992), using CE. As detailed in the previous paragraph, the application of high voltage on chip level is less complex than the application of pressure and its related problems of sealing and interconnections. Hence the major part of research focused on chip-based CE separation techniques, showing very high efficiencies, such as the work presented by Culbertson *et al.* (2000).

However, pressure-driven systems present important advantages over EC systems; the free choice of solvents and buffers and related to this a significantly larger versatility. Ocvirk *et al.* showed in 1995 an on-chip HPLC (High-performance liquid chromatography) system with a packed column and laser fluorescence detection. Five years later, McEnery *et al.* presented a pressure-driven chip etched in silicon with both, an external UV-detector and an electrochemical detector consisting of two platinum electrodes integrated on the chip and an external $Ag/AgCl$ reference electrode. Vahey *et al.* (2000) fabricated LC-chips by bonding PDMS (poly-dimethyl siloxane) containing microchannels to glass plates, together with an interesting plug injection method, called flow programming method by the authors. This method was taking advantage of the laminar flow behavior on small-scale fluidic systems.

In addition to the fabrication part of microfluidic devices, which constantly improved with the expericence taken from the MEMS (micro-

electro-mechanical systems) community (Verpoorte and De Rooij, 2003), fundamental research focuses on the mathematical modeling of the physical effects within the microfluidic channels and for miniaturized separation columns in particular. This is important as conventional columns are in general of cylindrical format, while on-chip columns, due to their inherently layer-based clean-room fabrication method, are mostly rectangular. Poppe (2002) adressed the problem of mass transfer in rectangular, open-tubular channels. He specifically showed that the approximation of an infinite channel width used by Giddings *et al.* (1983) in rectangular channels is having little influence on retained solutions while the approximation is almost an order of magnitude off for unretained species. The authors are proposing modified coefficients for the equation for the reduced plate height in rectangular channels by Golay (1981).

Li (2001) showed the influence of the electro-viscous effects on the fluidic resistance in pressure-driven flows in microchannels, especially for low-concentration ionic solutions. Dutta and Beskok (2001) showed analytical solutions to the electrical double layer influence on pressure-driven flows. Qiao and Aluru (2002) proposed an interesting model to compute flow rates and pressure in microfluidic devices, by using an analogy to electrical circuits.

Different approaches have been made to overcome the large dead volumes generated by chip-external sample injection. Verheggen *et al.* showed already back in 1988 the T-injection, where the direct injection of sample into the column rendered any moving parts for valving unnecessary. Kirby *et al.* and Hasselbrink *et al.* (2002) incorporated electrokinetic pressure actuated valves directly into the chip. A photosesitive monomer solution is pumped into the channels and solidified by UV-light in order to created movable pistons in the microchannel. Bai *et al.* (2002a,b) introduced the concept of pressure pinched injection, in order to minimize the analyte plug volume. Prior to injection the analyte flow is pinched from both side by the mobile phase in order to minimize the injected plug volume. Solignac and Gijs (2003) presented an injection method

based on the application of pressure pulses for EC-systems, where plugs generated by electrokinetic injection can lead to biased concentrations in the plugs.
Most of the pressure-driven systems use external pumps and valving, which provide the pressure through a more or less complicated interconnection to the chip. A common method is the use of a certain number of syringe-pumps, where each pump is providing a different liquid (analyte, mobile phase) to the chip. This type of setup presents several disadvantages such as complex interconnection, as well as and tedious purging and cleaning processes. In order to simplify the pressure interconnection, research has been carried out on alternative liquid handling, such as evaporation driven systems proposed by Goedecke *et al.* (2002), where the driving force of the liquid is generated by evaporation at the channel end combined with capillary forces. Other liquid actuation methods have been proposed, mainly in the field of electro- and magneto-hydrodynamic pumping (MHD), where the Lorentz-force is used to drive dielectric fluids. Bart *et al.* (1990) discussed electrohydrodynamic pumping and issues concerning its use in μ-scaled systems; Richter *et al.* (1991) showed a silicon electro-hydrodynamic injection pump; Jang and Lee (2000) showed a small-scale MHD micropump. However they experienced electrolysis in the pumped liquid; Lin *et al.* (2001) showed an interesting electrophoresis microchip capable of performing flow-through sampling using MHD pumping coupled to an electrokinetic gated injection: And Zhong *et al.* (2002) used MHD pumping on a device made of low-temperature co-fired ceramic tapes.

1.3 Motivation

Microfabricated planar separation devices have been extensively studied for the past 17 years and touted for their size, speed and low cost compared to conventional instrumentation. The literature contains hundreds of articles describing electrophoretic and electrokinetically driven devices, such as capillary electrophoresis, (CE), reversed-phase capillary

electrochromatography (CEC) and micellular electrokinetic chromatography (MEKC) (Jinno and Sawada, 2000; Kricka, 1998; Moore *et al.*, 1995; Verpoorte, 2002).
These devices utilize the principle of electroosmotic flow for fluid propulsion, which is more amenable to miniaturization on a planar chip format. In addition, electrophoretic techniques find abundant application in biomolecular analysis, a tremendous market driver at the present time. On the other hand, chip-based pressure-driven liquid chromatographic (LC) systems have been slow to find extensive interest, and have been pioneered by a handful of workers.
This is mainly due to lack of ease of flow control as is the case with electrokinetically driven devices where mechanical pumps and valves are obviated, and to the difficulty in integration of injectors and valves onto the chip. Despite these handicaps, there is much motivation to develop microfabricated LC systems, as LC is still the workhorse analytical method in most laboratories for small molecule analysis. Pressure-driven capillary LC systems in the form of microbore and nanobore HPLC columns have proven their superiority to conventional HPLC columns in terms of resolution, speed and solvent and sample conservation, as well as their ability to be coupled to mass spectrometers for proteomics analysis and as a high throughput analytical tool for combinatorial drug and metabolome screening. There is a growing need for miniaturizing LC by combining a capillary column with injectors and detectors small enough to take advantage of the ultra-small column volume presented by the nanobore capillary. This is best done by microfabrication, using clever design of a microfluidic network to combine a robust injection system with a capillary column, and a detector based on integrated electrodes,fluorescence microscopy, diffraction grating or a total internal reflectance surface in a fully integrated planar package.
Although most of the motivation for miniaturization of pressure-driven LC comes from the need to fulfill niches in the biotechnology arena, an application that has been overwhelmingly overlooked is that of online analysis in chemical and pharmaceutical production. Conventional

HPLC has not been widely employed as an on-line analytical tool because of slowness, size, sampling complexities and running expense. Microfabricated LC offers many solutions that address these issues and lower the barrier to implementation of the technique.

1.4 Research objective and limitations

The objective of this thesis was to develop new concepts for the application of pressure-driven chromatography as a fast sensor for continuous analysis.
Specifically this included the development of novel concepts for continuous flow injection techniques, in order to obtain representative sampling and reproducible injections over a long period of time, and the development of a novel, open-tubular approach to combined hydrodynamic and size-exclusion separations (SOHS) through pressure-driven chromatography.
This necessitated on one hand the fabrication of a device including a reliable sample plug injection and a detector, capable of performing representative sampling and reproducible analysis over a long period of time. On the other hand the recycling of the well-known technology of porous silicon allowed to fabricate a separation column for SOHS chromatography.

1.5 Thesis structure

In *Chapter 2* the fundamental basics of microfluidics governing equation and pressure-driven chromatography are presented. Scaling laws for miniaturization are introduced and the theoretical framework for the subsequent chapters is laid out.
Chapter 3 presents the device from fabrication to its application. The novel microfluidic design is introduced, as well as the sample injection principles.

In *Chapter 4*, chromatographic test separations are shown and the separation column's performance is characterized and discussed. Vitamin separations are shown as possible application of the system.
Chapter 5 introduces the concept of a porous column wall that enhances hydrodynamic separation in pressure-driven columns. Experimental verifications of the theoretical predictions are shown and discussed.
The thesis concludes in *Chapter 6* with a discussion of the methods and results presented in the previous chapters.

Chapter 2

Microfluidics for pressure-driven chromatography

Summary This chapter presents the fundamental basics of microfluidic laws and pressure-driven chromatography. Subsequent calculations for the chip design will be based on this theoretical framework.

2.1 Microfluidics

If not otherwise state, the following section is based on Kovacs (2000) and Tabeling (2003).

Laminar flow and Reynolds number When reducing channels in size, the surface-to-volume ratio increases in a way to pass from the inertia to the viscosity dominated regime. For a flow rate u, as a function of fluid density ρ and fluid viscosity η, the Reynolds number Re is defined as the ratio:

$$Re = \frac{\rho \cdot u \cdot d_c}{\eta} \tag{2.1}$$

Where d_c is the characteristic length of the system. In case of a circular tube, d_c is its diameter, while for rectangular channels d_c is the hydraulic

diameter, in case of one dimension being much smaller than the other, d_c can be set to the smallest dimension.
Flow is turbulent for Reynolds numbers above 3000 and laminar for Re lower than 2000. While the behavior of an infinitesimally small volume in turbulent flows is chaotic and to a large extent unpredictable, in laminar flow it can be described analytically. In case of channels with characteristic dimensions between 1 and 50μm and flow rates in the order of several hundreds of μm/s the flow regime is well in the laminar region.

Diffusion The time t_D for a particle to diffuse across a distance x depends on its diffusion constant D_c:

$$t_D = \frac{x^2}{D_c} \tag{2.2}$$

where the diffusion constant D_c is a function of the particle size r_p, the temperature T and of the viscosity η of the surrounding medium, given by the Stokes-Einstein equation:

$$D_c = \frac{k_b T}{6\pi\eta r_p} \tag{2.3}$$

with k_b being the Boltzmann constant.

Péclet Number The dimensionless Péclet number Pe relates the rate of advection of a flow to its rate of diffusion, and it is defined as:

$$Pe = \frac{\text{advection}}{\text{diffusion}} = \frac{u\delta C/d_c}{D_c\delta C/d_c^2} = \frac{u \cdot d_c}{D_c} \tag{2.4}$$

with δC a typical concentration variation over the distance d_c.

Flow profile Incompressible fluids are governed by the Navier-Stokes (N-S) equation:

$$\rho[\frac{\partial \vec{u}}{\partial t} + (\vec{u} \cdot \nabla)\vec{u}] = -\nabla p + \eta \nabla^2 \vec{u} \ , \tag{2.5}$$

∇p being the pressure gradient. At low Reynolds numbers Re, the equation can be simplified according to Brody *et al.* (1996), as the inertial terms on the left hand side of the N-S equation can be ignored, which yields to the Stokes equation:

$$\eta \nabla^2 \vec{u} = \nabla p \ . \tag{2.6}$$

One can see that the above equation is independent of time, which leads to the property that flow lines are the same whether a channel is actuated from one end or the other (pumping or suction).
For a circular conduit of radius r_c with no-slip conditions at the walls ($u(r_c) = 0$), equation 2.6 expresses the parabolic flow profile of flow velocity u at a radial position r in the conduit as follows:

$$u(r) = \frac{G}{4\eta}(R^2 - r^2) \tag{2.7}$$

with G the fixed pressure gradient $-\partial p/\partial z$ between in- and outlet of the channel. If one considers not a circular cross-section but rather a flow

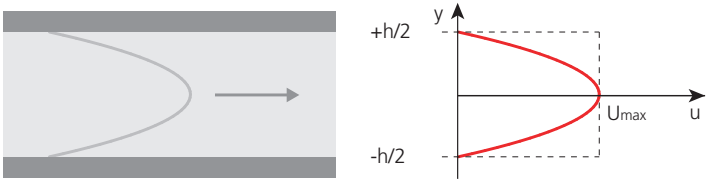

Figure 2.1: Poiseuille flow between two parallel plates

between two parallel plates, the resulting parabolic flow profile follows the law of J. Poiseuille (1797-1869), as illustrated in figure 2.1:

$$u(r) = \frac{G}{2\eta}\left(\left(\frac{h}{2}\right)^2 - y^2\right) \tag{2.8}$$

For rectangular conduits, one has to consider a channel of width w_c and height h_c and thus:

$$\left(\frac{\delta^2}{\delta x^2} + \frac{\delta^2}{\delta y^2}\right) u = -\frac{G}{\eta} \tag{2.9}$$

with boundary conditions $u(-w_c/2, y) = u(w_c/2, y) = u(x, -h_c/2) = u(x, h_c/2) = 0$.
Using Fourier series and subsitutional approach for the resulting differential equation, one obtains the following expression:

$$\begin{aligned} u(x,y) = &\left(\frac{Gh^2}{8\eta}\right)\frac{32}{\pi^2}\sum_{j=0}^{\infty}\left\{\frac{(-1)^j}{(2j+1)^3}\right. \\ &\times\left(1 - \frac{cosh\left[(2j+1)\pi x/h_c\right]}{cosh\left[(2j+1)\pi x/2h_c\right]}\right) \\ &\left.\times\, cos\left[(2j+1)\pi y/h_c\right]\right\} \end{aligned} \tag{2.10}$$

The y-averaged velocity then becomes

$$\begin{aligned} \overline{u} =& \frac{1}{h_c}\int_{-h_c/2}^{h_c/2} u(x,y)\mathrm{d}y \\ =& \left(\frac{Gh^2}{12\eta}\right)\frac{96}{\pi^4}\sum_{j=0}^{\infty}\left\{\frac{1}{(2l+1)^4}\right. \\ &\left.\times\left(1 - \frac{cosh[(2l+1)\pi x/h_c]}{cosh[(2l+1)\pi x/2h_c]}\right)\right\} \end{aligned} \tag{2.11}$$

Parabolic flow is a serious constraint in solute transport across a channel, as the velocity gradient disperses or dilutes a solute inserted in plug form, as shown by Taylor (1953).
Particularly in the case of chromatographic separations in a microchannel one desires a plug transport, in which the average velocity of the solute across the crossection is constant. The flow has a plug profile at a velocity $u_{max}/2$ (with u_{max} being the maximum flow velocity in the center of the channel), if the diffusion time $t_D = d_c^2/D_c$ across the channel is smaller than $t_{adv.} = d_c/u_{max}$. This can be resumed in the two following conditions:

$$D_c \gg d_c \cdot u_{max} \qquad \text{(plug transport)} \tag{2.12}$$

$$D_c \ll d_c \cdot u_{max} \qquad \text{(parabolic transport)} \tag{2.13}$$

Flow resistance The flow resistance of a channel depends on its cross-section and on its length. For channels with circular cross-sections of radius r_c and length L_c, the flow resistance is given by:

$$R_{fl} = \frac{8\eta L_c}{\pi {r_c}^4} \tag{2.14}$$

For rectangular channels, the diameter $2r_c$ of equation 2.14 can be replaced by the hydraulic diameter of a rectangular channel $\frac{4h_c w_c}{2(h_c+w_c)}$, which yields:

$$R_{fl} = \frac{8\eta L_c (w_c + h_c)^2}{(w_c h_c)^3} \tag{2.15}$$

For rectangular channels of width w_c much larger than the channel height h_c ($w_c \gg h_c$), the flow resistance can be approximated by:

$$R_{fl} = \frac{12\eta L_c}{w_c h_c^3} \tag{2.16}$$

It can be shown that equation 2.16 can be used for aspect ratios w_c/h_c larger than 4.44.

2.2 Chromatography

2.2.1 Introduction

When compounds migrate at different velocities through a column, separation occurs. Following the explications by Bidlingmeyer (1987) and Ganetsos (1993), the Russian botanist M. S. Tswett is generally credited with the discovery of what is today commonly called chromatographic separation. During his research on plant pigments at the beginning of the 20th century he used a column of powdered calcium carbonate to separate green leaf pigments into a series of colored bands by allowing a solvent to percolate through the column bed. He also coined the term chromatography (color writing) from Greek for color (chroma) and write (graphein) to describe the process (Figure 2.2).
Chromatography in which separation is based on differences between the solubility of the sample components (*analyte*) in the *mobile phase* and *stationary phase* is called *partition chromatography*. In liquid/solid chromatography (LSC), the mobile phase is a liquid, while the stationary phase consists of a solid. This latter can either be the column walls or packing materials in their bare state, or coated with a retentive layer.

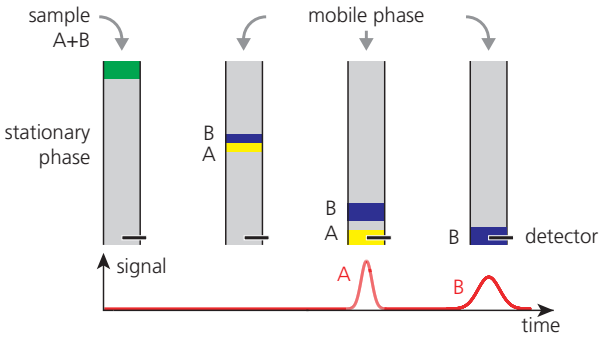

Figure 2.2: Separation of a analyte with two components A and B in a chromatographic column.

Chromatography in general comprises all separation techniques in which analytes partition in-between different phases that move relative to each other, or where the analytes have different migration velocities. It is predominantly an analytical separation technique, used to detect and quantify mixtures of components. However, for the sake of completeness, its use for isolation and purification of compounds also has to be mentioned. Figure 2.3 gives an overview of the wide field of partition chromatography. The marked sequence is illustrating the domain in which this thesis is taking place.

Present-day liquid chromatography was introduced by Nobel Price winners Martin and Synge (1941), who showed that in theory, the stationary phase requires very small particles for high efficiency and this lead to the modern columns packed with μm-size particles, resulting in a high driving pressure reaching up to several hundreds of bars. This

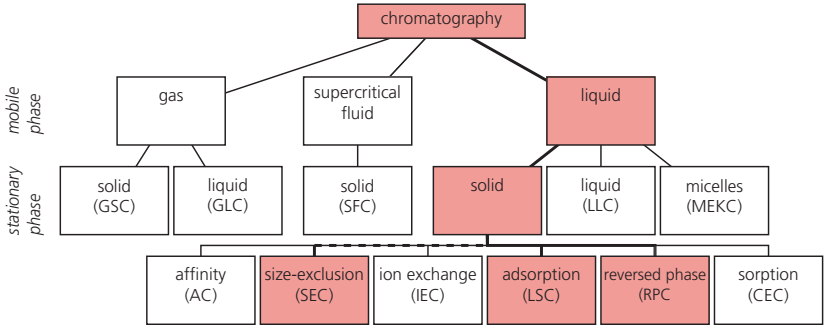

Figure 2.3: Family tree of column chromatographic methods. GSC = gas-solid chromatography; GLC = gas-liquid chromatography; SFC = supercritical fluid chromatography; LLC = liquid- liquid chromatography; MEKC = micellar electrokinetic chromatography; AC = affinity chromatography; SEC = size-exclusion chromatography; IEC = ion-exchange chromatography; LSC = liquid/solid chromatography; RPC reversed phase chromatography; and CEC = capillary electrochromatography. The figure was inspired by Poole (2003).

is characterized by the term high-performance (or high-pressure) liquid chromatography (HPLC).
In normal-phase chromatography, the stationary phase is polar and the mobile phase is nonpolar, while for reversed-phase chromatography the stationary phase is nonpolar, and the mobile phase is polar. A typical stationary phase consists of a long-chain hydrocarbon (typically C_8 or C_{18}) attached to a support, while a typical mobile phase comprises mixtures of water or buffer with polar solvents such as methanol (MeOH), acetonitrile (ACN), or tetrahydrofuran (THF). Today, reversed-phase chromatography is by far the most popular HPLC technique as illustrated by Neue and Fallah (1997). According to Ho *et al.* (2003), it owes its popularity to the following reasons:

- Versatile separation method with stationary phase chemistry meeting the need of a wide range of samples.
- The stationary phase material can be manufactured to high quality and is reasonably stable under normal operating conditions.
- The elution order of the compounds being separated can be predicted easily and is based upon their hydrophobicity.
- Mobile phases are mixtures of aqueous, polar solvents. Water, which is usually the predominant component, is inexpensive, safe and abundant.

2.2.2 Principles

2.2.2.1 Separation process

Chromatography is a separation process in which the analyte is distributed between two phases, stationary phase and mobile phase. It is essential to understand, that the separation of different compounds will depend on how much time they will spend in the stationary phase. All compounds spend the same amount of time in the mobile phase, which is equal to the time required by an unretained solute, that is a solute

that does not interact with the stationary phase, to travel through the separation column. This time is called the column dead or hold–up time, t_0. The time the compound spends in the stationary phase is called the adjusted retention time $t_{R'}$. The time a compound needs to elute, that is to pass through the separation column is called the retention time t_R, where $t_R = t_0 + t_{R'}$. It is obvious that compounds preferring to reside in the mobile phase will elute faster than those preferring the stationary phase. This can be expressed through either the distribution coefficient K for a compound i:

$$K_i = \frac{c_{stat}}{c_{mob}} \tag{2.17}$$

Where $c_{stat/mob}$ is the concentration in the stationary/mobile phase, or the retention factor k, of compound i:

$$k_i = \frac{n_{stat}}{n_{mob}} = \frac{V_{stat} \cdot c_{stat}}{V_{mob} \cdot c_{mob}} = K_i \frac{V_{stat}}{V_{mob}} \tag{2.18}$$

Where $n_{stat/mob}$ is the number of molecules and $V_{stat/mob}$ the respective volumes of the compound i in the stationary/mobile phase. In this thesis the retention factor k will be used for all subsequent calculations.
It is evident that only compounds with retention factors will be separated by the chromatographic column.

2.2.2.2 Stationary phase

The stationary phase plays a key role for the separation. The focus will be on stationary phases for reversed phase liquid/solid chromatography, as they are the most widely used in LSC. The surfaces of reversed-phase columns are hydrophobic. Most of the reversed stationary phases are based on long chain hydrocarbons (Figure 2.4). This hydrophobic surface interacts with the hydrophobic part of the compounds in the analyte. Retention increases with increasing hydrocarbon chain length. Prior to the deposition of the long chain hydrocarbons, the column wall and/or the packing material surface is composed of hydrophilic silanols and silox-

ane bridges, which serve as reactive centers for surface modification, e.g. to prepare a so-called bonded stationary phase.

2.2.2.3 Mobile phase

The mobile phase generally consist of mixtures of water or aqueous buffer solutions with various water-miscible solvents, (e.g. Methanol, Acetonitrile, Ethanol, Isopropanol, Tetrahydrofuran). If one looks at the viscosity of a solvent, acetonitrile is the preferred organic modifier in reversed phase chromatography. Acetonitrile-based mobile phases can give an up to 2-fold lower pressure drop than methanol-based mobile phases at equal flow rate (Figure 2.5).
Varying the solvent strength of the mobile phase controls analyte retention. A strong solvent decreases retention, while a weak solvent increases it. According to Neue and Fallah (1997), retention change is roughly 10% for every 1% change in the concentration of organic solvent. The importance of choosing the right composition of mobile phase in term of organic solvent concentration is shown in figure 2.6. Generally it cannot be recommended to use mobile phases with less than 10% organic solvent content in water. Under such conditions, brush-type stationary phases with e.g. C_8 or C_{18} alkyl chains are in an ill-defined conformation and

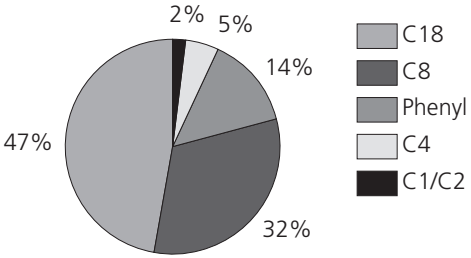

Figure 2.4: Stationary phases used in reversed phase chromatography as shown by Dolan and Snyder (1989).

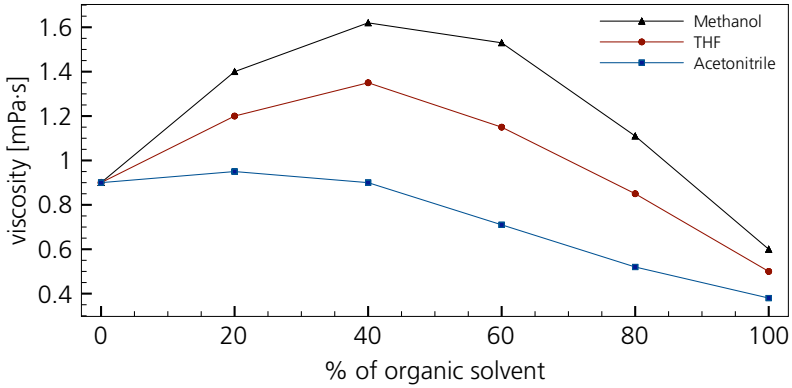

Figure 2.5: Viscosity of mixtures of water and organic solvents at 25°C. Data from Dolan and Snyder (1989).

equilibration takes a long time. This phenomenon is called *hydrophobic collapse* as described by Meyer (2004). From a physical point of view this means that the mobile phase is driven out of the pores as result of an unfavorable wetting angle.

Elution problem Chromatographic systems can be set up either for isocratic or gradient elution. Isocratic elution means constant separation conditions throughout the entire analysis, with no gradient, especially solvent gradient. Te exact opposite is gradient elution, where the mobile phase composition is steadily changed during analysis. This is of particular interest for complex mixtures with a large number of compounds. Under isocratic conditions, these mixtures will likely present poorly resolved initial peaks, while the final peaks will be broad and flat and even undetectable due to background noise. This is called the *general elution problem*. It can be dealt with using solvent, temperature or flow gradients as well as column switching, where different columns are used subsequently. These methods all attempt to separate the initial peaks

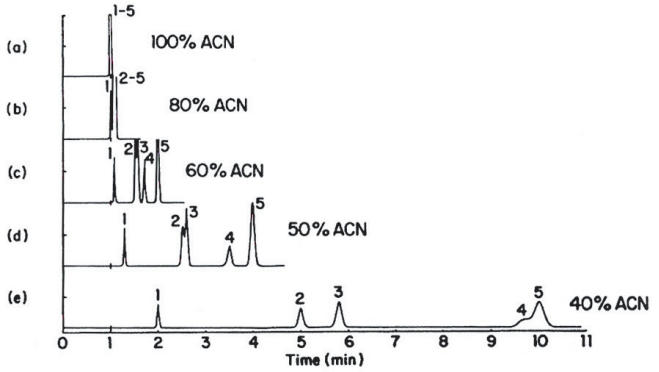

Figure 2.6: Effect of solvent content in mobile phase in reversed-phase chromatography (Poole, 2003).

and to accelerate the elution of the final peaks. For the scope of this thesis, only isocratic elution will be used.

2.2.2.4 Peak detection

Besides the separation column, the detector is to be considered as the most important part of a chromatographic system. The detector translates the changes in the composition of the column effluent during the chromatographic run into an electrical signal. This signal can then be recorded and processed to give the required information about the sample composition. The choice of the detector to be used depends on several sample-related factors: the chemical properties of the analytes, the desired range of sample concentrations to be determined, the complexity of the analyte, but also on the chromatographic system used for separation. The requirements for separation and the detection for a specific analytical problem is complementary: the higher the quality in terms of selectivity and sensitivity, the less demands are put on the separation

system, and vice versa. According to Meyer (2004), the ideal detector should:

- either be equally sensitive to all eluted peaks or record only those of interest.
- not be affected by changes in temperature or mobile phase composition (as happens in gradient solution).
- be able to monitor small amounts of compound (trace analysis).
- not contribute to band broadening; hence the detector volume should be small.
- react quickly to pick up correctly narrow peaks, which pass rapidly through the cell.
- be easy to manipulate, robust and cheap.

Still, only a few types of detectors have found general application (Katz *et al.* (1998))

- UV- detectors
- refractive index detectors
- fluorescence detectors
- electrochemical (amperometric) detectors
- light scattering detectors
- others: conductivity, photoconductivity, infrared and radioactivity detectors

2.2.3 Separation Column

Liquid/solid chromatography (LSC) utilizes a liquid mobile phase to separate the components of a mixture. These components (or analyte) are first dissolved in a solvent, and then forced under high pressure to flow through a chromatographic column. In the column, the mixture is resolved into its components. The separation resolution is dependent upon the extent of interaction between the solute components and the solid stationary phase. The interaction of the solute with mobile and stationary phases can be manipulated through different choices of both solvents and stationary phases.
Standard LSC systems are consisting of an external pump, delivering the pressure necessary to drive the liquids, a separation column with typical diameters of several milimeters and a length of several tens of centimeters. To obtain sufficient separation power, the column is filled with μm-sized particles in order to increase the internal surface of the column (packed column). Such systems are providing separation results after dozens of minutes up to several hours.
Instead of packed columns, one can imagine to use columns of very small size, in order to approach the size of the channels in-between the particles of a packed column. Such systems are called open-tubular columns (OTC); the stationary phase is coated to the column walls, providing the same effect as the packing. While the advantage of OTC systems is their smaller pressure drop along the column, they generally show an lower efficiency.
In order to have the present device working as a sensor in an analytical process environment, the decision was made to work at relatively low pressures (maximum 2 bars), thus pressure-driven flows could be obtained without resorting to the use of a high-pressure pump. This initial condition automatically lead to an OTC approach for the separation column.

2.2.3.1 Open-tubular separation column

Rectangular channels are a result of fabrication restrictions when going to miniaturization. Although integrated columns in silicon with cylindrical cross-sections have been presented (Tjerkstra *et al.*, 1997), rectangular cross-sections are generally preferred due to their relative ease of fabrication. If one considers figure 2.7, one can understand that from a intuitive point of view, a rectangular channel is a further simplification of multiple, parallel cylindrical channels. While this approximation is certainly correct from a fluidic point of view, it has to be relativized when looking at chromatographic columns.
Giddings *et al.* (1983) presented the fundamental theoretical basis for rectangular open channel reversed phase liquid chromatography, based on the work showed by Golay on open-tubular chromatography (1958) and on retention-less rectangular channels (1981). They called the rectangular columns *open parallel plates column* (OPPC) in contrast to the cylindrical OTC. The abbreviation OTC will be used in the present work

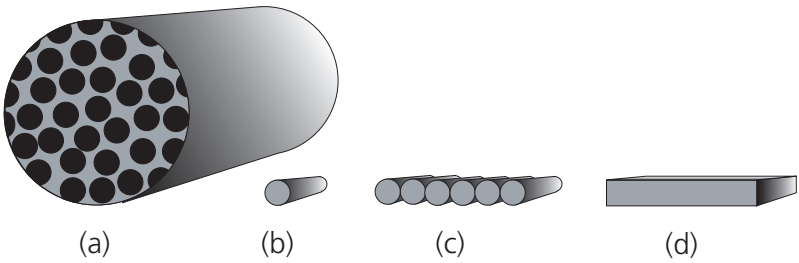

Figure 2.7: Schematic view (not to scale) of (a) standard packed HPLC column of serveral mm of diameter, (b) a open-tubular microcolumn of a diameter of typically $5-10\mu$m and thus in the same order of magnitude as the space in-between packing particles, (c) parallel open-tubular columns in order to reduce the back-pressure of the *entire* column, and (d) the corresponding, rectangular microfabricated column with similar behavior.

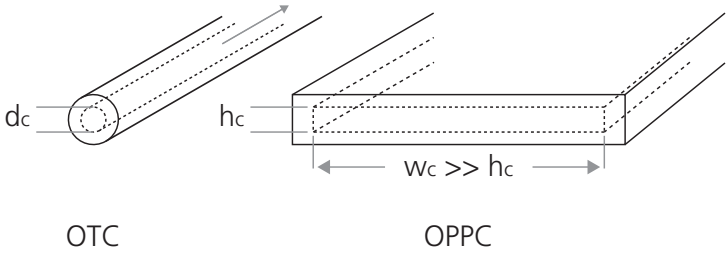

Figure 2.8: Open-tubular column (OTC) and open parallel plate column (OPPC) in comparison. The column height h_c can be reduced for rapid mass tranfer while the channel width w_c can be chosen to allow sufficient column volume and reduced pressure drop.

without differentiation (figure 2.8). The advantage of such rectangular columns of finite width (infinite widths serve for mathematical modeling only and are not of further practical use) is the possibility of enlarging only one dimension (w_c) while keeping the other (h_c). This results in a drop in the driving pressure needed without impairing, in a first approximation, the efficiency as the characteristic d_c length is still small (in this case $d_c = h_c$).

2.2.4 The chromatogram and its analysis

The eluted compounds are transported by the mobile phase to the detector and recorded as (ideally) bell-shaped, Gaussian curves. The signals are know as *peaks* and the set of peaks of one complete analysis of an analyte is called *chromatogram*. The peaks give qualitative and quantitative information about the analyte sample in question.

Retention factor k The chromatogram provides information on separation efficiency (figure 2.9): w is the peak width at the baseline, t_0 is the column dead time, which is equal to the retention time of an unretained solute. Hence the linear flow velocity u can be calculated from

the column length L_c and the column dead or hold–up time t_0 by:

$$u = \frac{L_c}{t_0} \tag{2.19}$$

The retention factor k is measured as the retention time of an analyte minus the retention time of an unretained peak divided by the retention time of the unretained peak. As explained by Neue and Fallah (1997) and Meyer (2004), this is a convenient way to normalize retention for comparison of different columns or the same column at different flow rates:

$$k = \frac{t'_R}{t_0} = \frac{t_R - t_0}{t_0} \tag{2.20}$$

Where t_R is the retention time and t'_R the net (or adjusted) retention time. According to Meyer, preferred values of k are between 1 and 10. Too low k-values mean insufficient separation (bad stationary phase and/or flow rate to high) and k-values above 10 stand for analysis times which are too long.

Plate number N and plate height H At this point it is important to introduce the concept of *plates* and the *theoretical plate number N*. This number is defined as the square of the relative standard deviation σ of the peak width at the end of the separation column. From a more practical point of view, N is the number of zones in the separation column where an equilibrium between stationary and mobile phase is reached. Martin and Synge (1941) introduced this idea in their pioneering work, where they modeled the chromatographic column like a distillation column. If one assumes Gaussian shape peaks, the *plate height H* can therefore be calculated using the overall length of the column, L_c:

$$\begin{aligned} N &= \sigma^2 \\ H &= \frac{\sigma^2}{L_c} \end{aligned} \tag{2.21}$$

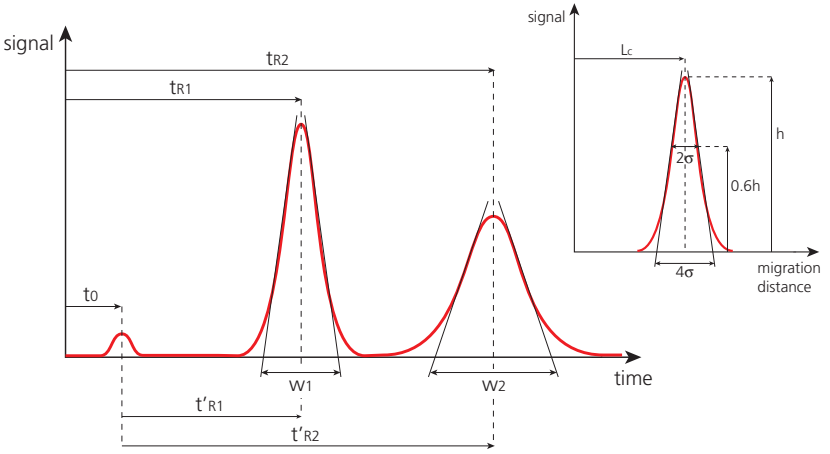

Figure 2.9: The chromatogram and its characteristic features.

From a more geometrical point of view, one can calculate the theoretical plate number N as follows (Figure 2.9):

$$N = 16\left(\frac{t_R}{w}\right)^2$$
$$N = 5.54\left(\frac{t_R}{w_{1/2}}\right)^2 \tag{2.22}$$

where w is the peak-width at the base-line and $w_{1/2}$ is the peak width at half-height. It is important to notice that the peak widths w and $w_{1/2}$ are calculated in the time domain and thus are rather times than distances, while the standard deviation σ presents a physical distance. It is therefore common to introduce the temporal standard deviation τ, with following relation:

$$\frac{\tau}{t_R} = \frac{\sigma}{L_c} \tag{2.23}$$

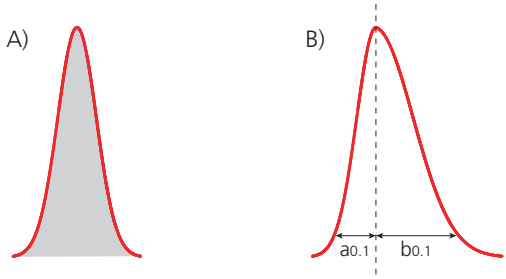

Figure 2.10: A) Shape of a theoretical Gaussian peak. B) Real shape peaks are rarely symmetric. The parameters $a_{0.1}$ and $b_{0.1}$ are used to describe the peak tailing.

Equations 2.21, 2.22 and 2.23 are only correct if the peak has a Gaussian shape: This is rarely the case with real-life chromatograms.

Tailing Small deviations from the ideal, gaussian peak form are insignificant (Meyer, 2004). However, large tailing (Figure 2.10 B) are to be taken into consideration. It has different reasons such as or poor quality of the stationary phase (packing or coating), extra column volumes, column overload (too much analyte injected) or incompatibility of the sample with the stationary or mobile phase. In the case of asymmetric peaks, correct values for N can be calculated by the momentum method, shown by Foley and Dorsey (1983) and Dyson (1998) and illustrated in figure 2.10, which results in the following equation:

$$N = 41.7 \frac{(t_R/w_{0.1})^2}{T_p + 1.25} \tag{2.24}$$

where $w_{0.1}$ is the peak width at 10% of the peak height and T_p is tailing $b_{0.1}/a_{0.1}$ at 10% of the peak height, $a_{0.1}$ and $b_{0.1}$ being the peak half-widths (see figure 2.10).

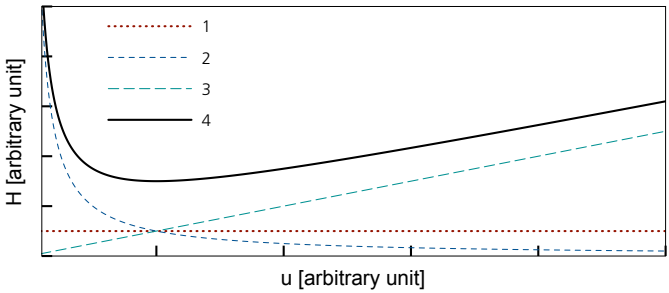

Figure 2.11: Van Deemter curve (H/u curve): 1 = eddy diffusion and flow distribution component due to different flow paths (= 0 in open tubular columns) 2 = longitudinal diffusion component; 3= mass transfer component; 4 = the resulting van Deemter H/u curve.

Band broadening The theoretical plate height H can be expressed as function of mobile phase flow velocity u through the equation by van Deemter *et al.* (1956), as illustrated in figure 2.11:

$$H = A' + \frac{B'}{u} + C' \cdot u \tag{2.25}$$

The A'-term is due to two phenomena: Eddy diffusion, caused by the different paths lengths of the sample molecules traveling trough a packed separation column, and flow distribution differences, as the mobile phase velocity is higher in the *channel* center than at the walls. *Channel* means the paths in-between the packing material or the entire column in case of OTC. The A'-term can be reduced by using packing material with a very small size distribution In the case of OTC, the A'-term is equal to 0 :

$$H_{OTC} = \frac{B'}{u} + C' \cdot u \tag{2.26}$$

The $\frac{B'}{u}$-term is due to Taylor dispersion of the analyte within the mobile phase. This problem can be reduced by choosing the mobile phase's mean

flow rate u as a function of the diffusion constant D_m of the sample in the mobile phase and the channels characteristic diameter or width d_c (compare to equation 2.12):

$$u \simeq \frac{2D_m}{d_c} \tag{2.27}$$

The $C' \cdot u$-term finally is due to mass transfer between mobile, 'stagnant mobile' and stationary phases. Sample molecules close to the stationary phase are not moving with the mobile phase anymore. The molecule either diffuses back to the mobile phase or interacts with the stationary phase; both mass transfer phenomena need time and hence contribute to the band broadening. The plate height in OTC is expressed by the extended Golay equation:

$$H = \frac{2D_m}{u_m} + \frac{d_c^2 u_m}{D_m} f_1(k) + \frac{d_f^2 u_m}{D_s} f_2(k) \tag{2.28}$$

with H = plate height, u_m the mean flow rate of the mobile phase, d_c = characteristic length, D_m = diffusion coefficient of solute in mobile phase, D_s = diffusion coefficient of solute in stationary phase, k = retention factor, d_f = layer thickness of stationary phase. For cylindrical columns, the functions $f_1(k)$ and $f_2(k)$ have the form:

$$\begin{aligned} f_1(k)_{cylindrical} &= \frac{(1 + 6k + 11k^2)}{96(1+k)^2} \\ f_2(k)_{cylindrical} &= \frac{2k}{3(1+k)^2} \end{aligned} \tag{2.29}$$

For OTC with a very thin column wall coating compared to the characteristic length d_c ($d_f \ll 1\,\mu$m for d_c between 5 and 10 μm), the term with $f_2(k)$ in equation 2.28 can be neglected:

$$H = \frac{2D_m}{u_m} + \frac{d_c^2 u_m}{D_m} \frac{(1 + 6k + 11k^2)}{96(1+k)^2} \tag{2.30}$$

that can be written as:

$$H = \frac{2D_m}{u_m} + \frac{d_c^2 u_m}{D_m} \frac{(A'' + B''k + C''k^2)}{N''(1+k)^2} \tag{2.31}$$

This equation is obviously equivalent to the van Deemter equation (2.25) without the term for plate height contributions due to different path lengths. Poppe proposed in 2002 modified coefficients A'', B'', C'' and N'' to account for the side-wall induced dispersion in high aspect ratio rectangular channels. For pressure-driven columns with stationary phase at all walls, Poppe calculated the factors as shown in table 2.1:

φ	A''	B''	C''
1	1.804	10.198	17.144
2	3.434	18.921	31.043
4	5.360	28.911	45.952
8	6.632	36.165	57.188
16	7.301	40.404	64.107

Table 2.1: Coefficient for f_1 of extended golay equation (2.30) with $N = 105$ and φ the channel aspect ratio w_c/h_c (Poppe, 2002).

The plate height H in function of the column shape is shown in figure 2.12, which illustrates that for a given set of parameters, the cylindrical column is always performing better than rectangular columns (Lower plate height H at higher flow velocity u).

Resolution R Figure 2.13 illustrates the term *resolution* R of two components. R measures the distance between the maxima of two (Gaussian shaped) peaks in function of the average standard deviation $\overline{\sigma} = (\sigma_1 + \sigma_2)/2$. For isocratic elution, the resolution of two peaks is dependent on the separation factor α, the number of theoretical plates N and

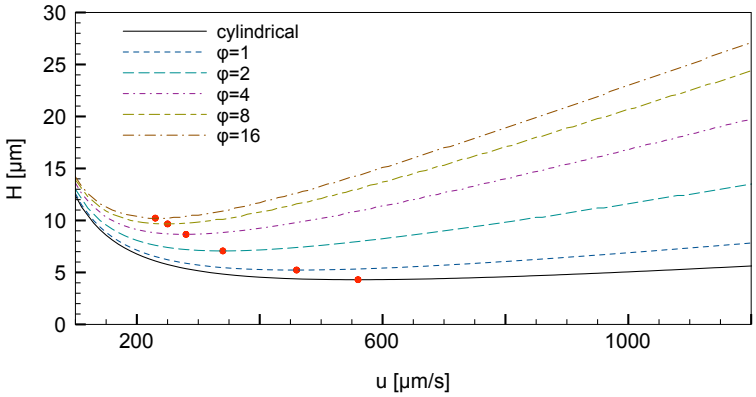

Figure 2.12: Golay-plots with modified coefficients by Poppe as shown in table 2.1: figure for various channel aspect ratios φ (width-to-height) and cylindrical channel for fixed $k = 1$. The characteristic length is $d_c = 7\,\mu$m and the solutes diffusion constant in the mobile phase $D_m = 6 \cdot 10^{-10}\,\mathrm{m^2\,s^{-1}}$. The dots indicate the optimum flow rate for a the minimum plate height.

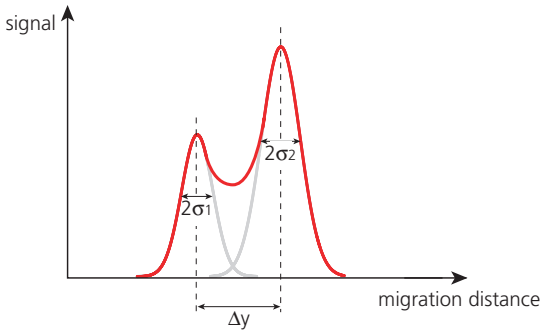

Figure 2.13: Resolution of two chromatographic peaks $R = \Delta y/\overline{\sigma}$.

the retention factor k:

$$\overline{k} = \frac{k_1 + k_2}{2} \tag{2.32}$$

$$\alpha = \frac{k_2}{k_1} \tag{2.33}$$

$$R = \frac{1}{4}(\alpha - 1)\sqrt{N}\left(\frac{k_1}{1+\overline{k}}\right) = \frac{1}{4}\frac{\alpha}{\alpha - 1}\sqrt{N}\left(\frac{k_2}{1+\overline{k}}\right) \tag{2.34}$$

together with 2.22, equation 2.34 can be expressed as follows:

$$R = 2\frac{t_{R2} - t_{R1}}{w_1 + w_2} = 1.18\frac{t_{R2} - t_{R1}}{w_{1/2_1} + w_{1/2_2}} \tag{2.35}$$

Base line resolution is obtained when $R = 1.5$. Analysis of equation 2.20 to 2.35 leads to table 2.2 that illustrates parameters influencing the enhancement of the chromatographic separation. This table shall be recalled when considering miniaturization in chapter 3.

To enhance separation	influencing parameters	
$N \Uparrow$	$t_r \Uparrow$	$w \Downarrow$
$H \Downarrow$	$L_c \Uparrow$	$N \Uparrow$
$R \Uparrow$	$\alpha \Uparrow$	$N \Uparrow$

Table 2.2: Factors to enhance chromatographic separation

2.3 Miniaturization aspects

2.3.1 Scaling laws

If one attempts to miniaturize macro-world devices, the so-called scaling laws are of utmost importance. Physical values are in relation with others and do scale differently with respect to their relation with the scale l. Table 2.3 gives an overview of scaling laws for typical values.

From a formal point of view, one has to differentiate between two types of l, as detailed by Tabeling (2003):

- isotropic objects: the object's dimensions are of the same order of magnitude in the three spacial directions. In this case, l simply represents the order of magnitude of the object's size.
- anisotropic objects: a microchannel's length can be much larger than its width or height. In this case l shall be the scale factor controlling all dimensions of the object, and maintaining the aspect ratios constant.

For some physical values, the scaling laws are obvious, as for example for an object's mass M:

$$m \sim V \sim l^3 \tag{2.36}$$

with V the volume of the object with size l. However the majority of scaling occurs where the relation between the value and the scale l introduces other values. Then there are two possibilites:

- intervening values are constants.
- intervening values are themselves dependent on l

parameter	scaling law
van der Waals force between molecules	l^{-7}
time	l^0
capillary force	l^1
distance	l^1
flow rate	l^1
diffusion time	l^2
volume	l^3
gravitational force	l^3

Table 2.3: Scaling laws for different parameters

When one considers miniaturization and looks at two values, the one with the lower exponent for l becomes more important the smaller the size; as an example shall serve the comparison between capillary force ($\sim l^1$) and gravitational force ($\sim l^3$) , where the latter becomes negligible at μm-scale. When it comes to separation devices, there are two approaches that are used for miniaturization, the dimensionless-parameter approach and the similarity approach (Janasek *et al.*, 2006). Dimensionless parameters are for example the Peclet number Pe or the Reynolds number Re. For the similarity approach, there is a difference to be made between time-constant systems and diffusion-related systems. In a time-constant system, miniaturization keeps the timescale constant (analysis time, elution time), while the flow rate u would decrease by a factor l, the volumic flow rate Q by a factor l^3 and Re by a factor l^2. However, the pressure-drop Δp necessary to keep the timescale constant would be unchanged during miniaturization.
Diffusion-related systems are considered when molecular diffusion or flow behavior is influencing the separation efficiency of the system. In this case the timescale is considered as a surface scaling with l^2 (Manz and Eijkel, 2001). This means that all dimension-less parameters such as Pe and Re, but also the plate number N remain constant during miniaturization.
Real systems are often a combination of both approaches, as miniaturized diffusion-related systems encounter practical problems as the required pressure-drop Δp scales with l^{-2} and thus rapidly reaches very high values.

2.3.2 Surface-to-volume ratio in separation columns

Considering a cylindrical column of radius r_c and length L_c. The surface-to-volume ratio χ can be expressed as:

$$\chi = \frac{A_c}{V_c} = \frac{2\pi r_c L_c}{\pi r_c^2 L_c} = \frac{2}{r_c} \tag{2.37}$$

with A_c being the column surface and V_c the column volume. For a rectangular column of width w_c, height h_c and length L_c, χ is:

$$\chi = \frac{A_c}{V_c} = \frac{2L_c(w_c + h_c)}{w_c h_c L_c} = \frac{2(w_c + h_c)}{w_c h_c} \tag{2.38}$$

which gives for a quadratic channel width side length $b_c = w_c = h_c$:

$$\chi = \frac{4}{b_c} \tag{2.39}$$

Now let's consider a column packed with spherical silica particles. These particles have a typical value of $100\,\mathrm{m^2\,g^{-1}}$ for the specific surface area, 30 nm for the pore diameter and $0.5\,\mathrm{g\,cm^{-3}}$ for the packing density (Meyer, 2004). In this case, χ is around $5 \cdot 10^7\,\mathrm{m^{-1}}$. In order to reach such numbers with an unpacked column, this leads to following values:

$$r_c = \frac{2}{\chi} = 40\,\mathrm{nm} \qquad \text{(cicular cross section)} \tag{2.40}$$

$$b_c = \frac{4}{\chi} = 80\,\mathrm{nm} \qquad \text{(rectangular cross section)} \tag{2.41}$$

When looking at chromatography, the following parameters are of interest:

diffusion time:	$t_D \sim l^2$
flow resistance:	$R_{fl} \sim l^{-3}$

It is evident that these two values, one rather performance oriented (t_d) and the other of rather practical interest (R_{fl}), are behaving strongly contrarily. It will therefore be a question of pondering when it comes to the design of the separation column.

2.4 Summary

In this chapter, the governing equations in microfluidics and chromatography have been introduced. The principles of chromatographic separations were shown, with an emphasis on open-tubular columns for liquid/solid chromatography. Furthermore the different scaling laws and miniaturization approaches have been detailed and explained.
This chapter will serve as theoretical framework for the following chapters.

Chapter 3

Miniaturized continuous sampling device

Summary The design criteria are detailed and the parameters for the chromatographic chip are calculated. Its fabrication is explained, as well as its operation modes and the surrounding setup.

3.1 Design

Microsystems often do not have less complexity than large systems. In most of the cases, and the present case is one of theses, there is nothing such as *the* single (solvable) differential equation describing the entire system. The engineering approach of such problems consists in defining initial conditions that describe the problem and narrow down the regions of interest of the governing parameters. Once a set of parameters is found that fulfill all requirements, there is to be proof that the chosen set is optimum or close to optimum. This section shall show the approach that led to the final device. Table 3.1 shows the requirements and the solutions chosen for the chip design.

parameter	requirements ⇒ *solution*
flow resistance	As low as possible in order to work at a convenient pressure drop of maximum 2 bar. ⇒ *Open-tubular separation column.*
liquid handling	capability of rapidly changing mobile phase and analyte, as well as possibility of column cleaning. ⇒ *Large flow-through channels implemented on the chip*
sample injection	robust and reliable technique for continuous repeatable injections. ⇒ *gated injection.*
detection	detection integrated on the chip. ⇒ *electrochemical (amperometric) detection by integrated Ti/Pt electrodes.*
materials	if possible use transparent materials (glass), to be able to visually control the microfluidic behavior. ⇒ *channels are etched in float glass or Pyrex®.*

Table 3.1: Initial requirements and proposed solutions

Plate number Chromatographic systems are usually characterized by their theoretical plate number N. There is room for discussion in order to find an agreement what plate number N shall be aimed for. Generally, when time is of no concern and higher analytical performance is preferred to rapid analysis time, values of several hundreds of thousands of plates are sought-after. However, numerous discussions with people from industry led to a value in the order of 10000 being sufficient for a *sensor-like* chromatographic system. In order to find the appropriate column length L_c, let's recall the van Deemter equation for open-tubular columns:

$$H_{OTC} = \frac{B'}{u} + C' \cdot u \tag{3.1}$$

The optimum speed u_{opt} for a minimum plate height is therefore:

$$u_{opt} = \sqrt{\frac{B'}{C'}} = \sqrt{\frac{2D_m^2}{d_c^2 f_1}} \tag{3.2}$$

with $f_1 = \frac{A''+B''k+C''k^2}{N''(1+k)^2}$. Putting 3.2 into 3.1, this yields:

$$H_{OTC} = 2D_m\sqrt{\frac{d_c^2 f_1}{2D_m^2}} + \frac{d_c^2 f_1}{D_m}\sqrt{\frac{2D_m^2}{d_c^2 f_1}} = \sqrt{2d_c^2 f_1} + \sqrt{2d_c^2 f_1} = 2\sqrt{2d_c^2 f_1} \tag{3.3}$$

Replacing the characteristic length d_c by the column height h_c, the plate number N can therefore be expressed as a function of the column length L_c and plate height h_c:

$$N = \frac{L_c}{H} = \frac{L_c}{2\sqrt{2h_c^2 f_1}} = \frac{L_c}{2\sqrt{2h_c^2\left(\frac{A''+B''k+C''k^2}{N''(1+k)^2}\right)}} \tag{3.4}$$

Putting in the modified coefficients according to Poppe (2002), and calculating for different retention factors from 1 (lowest acceptable) up to 10 (largest usable) yields Figure 3.1. For two arbitrarily chosen column heights: $h_c = 5\,\mu$m and $h_c = 3\,\mu$m, it illustrates the column length L_c necessary to achieve a plate number $N = 10000$ with different column aspect ratios φ, for different retention factors k.

Flow resistance Pressure-driven flow in microfluidic devices can typically be obtained by two means:

- Pumps, such as syringe pumps or, for low pressure applications, peristaltic pumps. This results in a flowrate control *volume/time*.
- Pressurized reservoirs: Rather than flowrate control, this method allows for a pressure drop Δp control.

There are a few reasons why, from an application point of view, pressurized reservoirs are to be preferred over pumps:

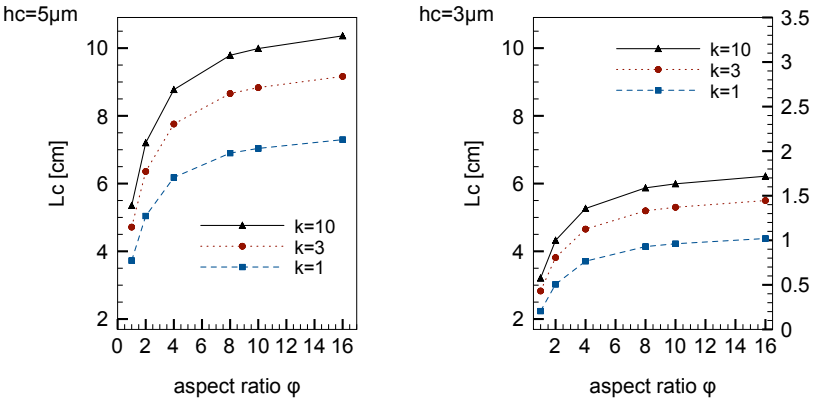

Figure 3.1: Column length L_c as a function of the column aspect ratios φ, for two different column heights h_c, with $N = 10000$ and three retention factors k.

- Reduction of dead-volumes inherent to the use of pumps.
- Possibility of rapid change in flowrates with great precision.
- No flowrate variations due to elasticity of tubing or other pump related parts.

Assuming $w_c \gg h_c$, the pressure drop Δp necessary to drive the system at the optimum flow rate u_{opt} can be calculated as follows:

$$\Delta p = Q \cdot R_{fl} = (u_{opt} \cdot w_c h_c) \frac{8\eta L_c (w_c + h_c)^2}{(w_c h_c)^3} = \frac{8\eta L_c u_{opt} (w_c + h_c)^2}{(w_c h_c)^2} \tag{3.5}$$

with Q being the volumic flow rate. Plugging in u_{opt} from equation 3.2 and L_c from equation 3.4, this leads to:

$$\Delta p = \frac{32 N \eta D_m (w_c + h_c)^2}{(w_c h_c)^2} \tag{3.6}$$

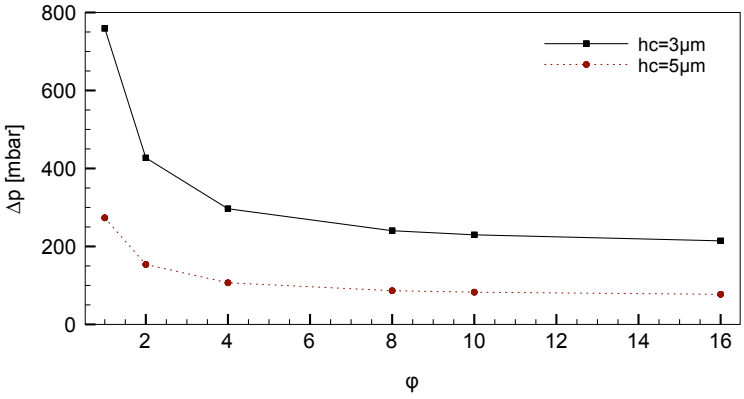

Figure 3.2: Pressure drop Δp at optimum flow rate u_{opt} and $N = 10000$ for different column aspect ratios φ.

Figure 3.2 shows the pressure drop needed as a function of the column aspect ratio φ for optimum conditions for $N = 10000$.

Starting point Following the relations established in the two previous paragraphs, a channel aspect ratio of $\varphi = 10$ was chosen, as higher aspect ratios do not show significant improvements for both, pressure-drop and minimum column length (Figures 3.1 and 3.2). This will allow to work at pressure drops below 1 bar, but with having the opportunity to run the chip at convenient flow rates u with pressure drops up to 1.5 bars for priming and washing cycles.
Table 3.2 summarizes the chosen parameters and the resulting chromatographic values, while figure 3.3 shows the plate height for the values in table 3.2.

Chip layout The layout was designed using CleWin® (WieWeb software). A footprint of 20 mm×20 mm was chosen. The separation column length L_c is 110 mm from sample injection cross to detector. Figure

parameter	value
plate number N	10000
channel height h_c	$5\,\mu$m
channel width w_c	$50\,\mu$m
column length L_c	10 cm
$\Rightarrow$ dead time t_0	295 s ($k = 1$)
	370 s ($k = 3$)
	415 s ($k = 10$)

Table 3.2: Parameters chosen for the chip for $N = 10000$ and the resulting dead times t_0 for different k-values at optimum flow rate u_{opt}.

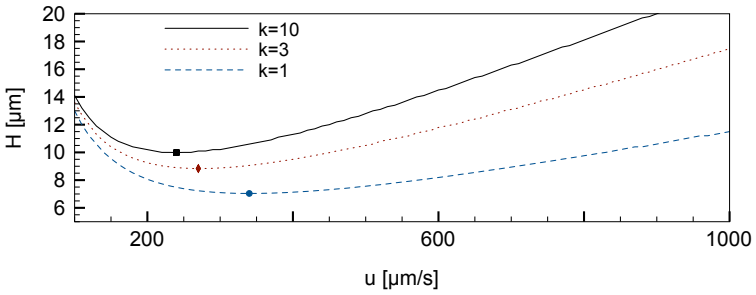

Figure 3.3: Plate height H as a function of the mobile phase velocity u for the parameters summarized in table 3.2. The dots indicate the optimum flow rate u_{opt} for minimum plate height H.

3.4 shows the chip design used for clean-room fabrication. The working principle will be explained in sections 3.4 through 3.8.

Band broadening induced by folded channels As the column length L_c is longer than a typical sidelength of a chip, the microfluidic channels will be folded into a serpentine-like arrangement in order to be integrated onto the chip (Figure 3.5). Such arrangements can yield

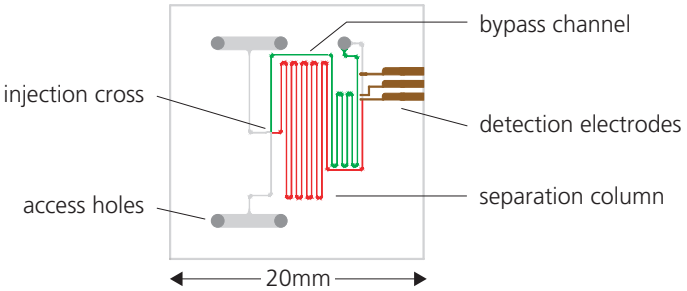

Figure 3.4: Schematic of the chip with sample injection cross, separation column, bypass channel and detection electrodes.

additional band broadening due to the different path length in the turns. Culbertson *et al.* (1998) and Griffiths and Nilson (2002) analyzed this dispersion for capillary electrophoresis and pressure-driven systems, and latter showed that for turn radii above certain minimum values, this additional band broadening reduces to a negligible amount with respect to total broadening. Considering the diffusion variance $(\sigma^2/w_c)^2$ for a straight segment of length L_s:

$$\sigma^2 = 2D_c t_D = 2\frac{L_s}{u} \Rightarrow \left(\frac{\sigma}{w_c}\right)^2 = \frac{2}{Pe}\frac{L_s}{w_c} = \frac{2L^*}{Pe} \tag{3.7}$$

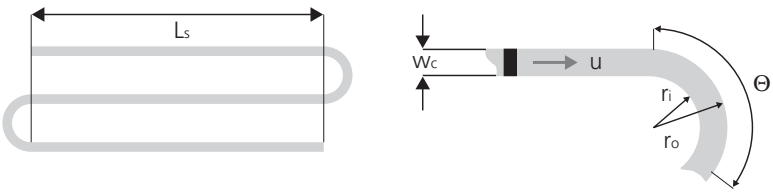

Figure 3.5: Schematic of a serpentine channel with straight segments and turns of angle Θ and constant radius.

where L^* is the straight segment length L_s normalized by the channel width w_c. The analogous expression for the variance in the turn is then:

$$\left(\frac{\sigma}{w_c}\right)^2 = \frac{2r^*\Theta}{Pe} \tag{3.8}$$

with r^* the normalized turn radius $\frac{(r_i+r_0)}{2w_c}$ and Θ the turn angle (See figure 3.5). The total increased variance due to diffusion in straight segment and turn can then be written as:

$$\left(\frac{\sigma}{w_c}\right)^2_{diffusion} = \frac{2}{Pe}(L^* + r^*\Theta) \tag{3.9}$$

The expression for the dispersion-induced variance in a turn such as proposed by Griffiths and Nilson is:

$$\left(\frac{\sigma}{w_c}\right)^2_{dispersion} = \frac{\Theta^2 Pe}{15r^*\Theta + 3Pe} \tag{3.10}$$

According to Griffiths and Nilson this expression is accurate to within ∼10% for all Peclet numbers, turns up to 180° and normalized turn radii $r^* \geq 1$.
Defining the dispersion induced variance being acceptable when being at least an order of magnitude smaller than the diffusion induced variance, this leads to the condition:

$$\frac{\Theta^2 Pe}{15r^*\Theta + 3Pe} \leq \frac{1}{10}\left[\frac{2}{Pe}(L^* + r^*\Theta)\right] \tag{3.11}$$

which can be rearranged in order to express the minimum, normalized turn radius r^* to fulfill the condition:

$$r^* \leq \frac{Pe + 5L^*}{10\Theta}\left[\sqrt{1 + \frac{20Pe(5\Theta^2 Pe - 3L^*)}{3(Pe + 5L^*)^2}} - 1\right] \tag{3.12}$$

In the case of low Peclet number Pe and large L^*, the term $(5\Theta^2 Pe - 3L^*)$ becomes negative and thus the square root as well. Practically a negative turn radius is of no interest, as the minimum normalized radius r^* is 0.5 (when the inner radius r_i vanishes completely). Hence for large enough L^* the turn-induced dispersion is not significantly contributing to the overall band broadening. Modified channel geometries to prevent turn-induced dispersion such as shown earlier by Griffiths and Nilson in 2001 are thus not necessary for L^* and r^* large enough. In the present device, the mean radius $\frac{r^i+r^0}{2}$ is 200 μm and the straight segment L_s 10.9 mm, which made the variance increase due to the turn-induce dispersion being below 1% of the total variance.

3.2 Fabrication

The microfabrication of the device used in all experiments presented in this thesis was carried out at the EPFL Center of MicroNanoTechnology, CMI. It is based on a four-step process using four masks, as illustrated in figure 3.6. The device is made up from two parts, bottom and top. Both are microfabricated on 4 inch float glass wafers of 525 μm thickness. Substrates were chosen to be float glass rather than Pyrex® for etching reasons.

On the bottom wafer, a 40 nm polysilicon layer is deposited that will later serve as ion barrier for the anodic bonding. With AZ 5214 negative photoresist etch mask, the separation column and bypass channel (whose function will be explained in section 3.5) are etched into the bottom substrate using plasma etching for the polysilicon layer and a hydrofluoric acid bath (HF(49%):H_2O, 1:5) for etching the glass (figure 3.6a). The available HF solutions in the cleanroom did not allow a sufficient verticality of the column walls in the case of Pyrex®, which led to the use of float glass. Concerns regarding the anodic bonding could be discarded as will be shown further down.

The Ti/Pt electrode layer for the amperometric peak detection is recessed. A second AZ 5214 layer is structured, and the underlying layers

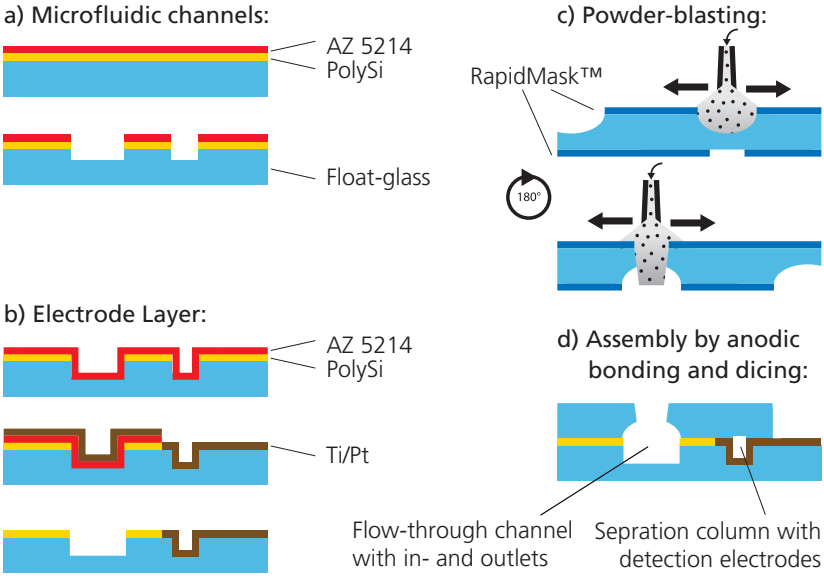

Figure 3.6: Schematic view of the four-mask microfabrication process of the glass substrates. Channels and electrodes are defined by HF-etching (a) and lift-off processing (b). Flow-through channels and access holes are powder-blasted through a laminated, photostructured mask (c). Finally the wafers are anodically bonded and diced (d). Detection electrodes access pads are liberated by partial dicing. Dimensions of the device are given in table 3.3.

recess-etched by plasma (polysilicon) and a 7% BHF bath (glass) and then covered by a 20 nm Ti layer followed by a 200 nm Pt layer by DC-sputtering. The Ti layer serves as adhesion layer below the Pt. The electrodes shape is then defined by a lift-off process (figure 3.6b).

The top substrate contains vertical through holes for liquid acces, as well as part of the *flow-through channels*, whose function will be further explained in section 3.5. Inspired by the work of Slikkerveer *et al.* (2000) and Schlautmann *et al.* (2001), it was decided to etch them through

channel width	[μm]	50
channel height	[μm]	7
flow-through channel height	[mm]	0.2
column length (injection cross to detector)	[mm]	111
column length (injection cross to outlet)	[mm]	116
bypass channel length	[mm]	54
wafer material		float glass
electrode material		Ti/Pt

Table 3.3: Device characteristics

powder-blasting To this end, a laminated dry resist specially designed for decorative sandblasting purposes (RapidMask^{TM}, Photoabrasive Systems, Duluth, MN, USA) was applied to both sides and exposed to uncollimated UV light through a transparency mask printed with a high-dpi inkjet printer. Powder blasting was then performed manually on both sides using 60 μm corundum grit. The flow-through channels were powder-blasted to a depth of roughly 200 μm. (figure 3.6c).
To close the channels, top and bottom glass wafers were anodically bonded, making use of the initially deposited polysilicon layer on the bottom substrate as an ion-barrier, according to procedures proposed by Berthold *et al.* (2000) and Lee *et al.* (2001). The procedures, although shown for Pyrex® substrates, worked without major adjustments for float glass. Substrate alignment was done manually. The bonding was achieved by applying 700 V at a temperature of 360 °C during 30 min in a muffle furnace under an ambient atmosphere.
Finally, the wafers were diced into single chips. Electrode access pads were liberated by half-through dicing such as illustrated in figure 3.6d.

3.3 Stationary phase coating of microcolumn

In order to achieve separations, the column must contain a stationary phase. As has been described in chapter 2, OTC have the advantage

of presenting a low pressure drop, paired with the inconvenience of the inherently low stationary phase capacity.
Numerous methods have been proposed to increase the column wall surface and thus the stationary phase capacity of OTC. Already back in 1979, Ishii *et al.* showed surface enhancement of open-tubular column surfaces by a treatment with a sodium hydroxide solution. While Tock *et al.* (1989) prepared OTC with porous silica layers, Pesek and Matyska (1996) increased the column surface through etching with saturated solution of ammonium hydrogen difluoride.
But column surface itself is not sufficient; it is the coating of that surface by attaching functional chemical groups that will yield chromatographic separations. The most commonly used coatings are silanols, such as octadecylsilanes, C_{18}, (Tsuda *et al.*, 1968) and octylsilanes, C_8, as briefly mentioned in section 2.2, citing Dolan and Snyder (1989).
All the methods of surface increase described before are therefore asking for a second step during which this retentive layer, the stationary phase, is fixed to the column surface.
A very elegant way of combining surface increase with stationary phase coating for open-tubular (OT) liquid chromatography as well as OT electrochromatography was shown by Guo and Colon (1995), Constantin and Freitag (2000) and Constantin *et al.* (2001). Their approach consists in using sol-gels. In theory, this technique allows for the coating of the column wall with a porous silica hybrid gel containing already the retentive functional groups. For the present device, two different methods for column surface coatings were used:

- Liquid-phase coating of C_8 or C_{18}
- Sol-gel technique yielding an increased surface with C_8 coating

3.3.1 Liquid phase C_8 or C_{18} coating

The procedure for the liquid phase coating C_8 or C_{18} was performed according to Kováts (2004). Chemicals were gratefully provided by Zeochem.

The column preparation was done by treating with 1 M NaOH solution for 1 h, then flushing with de-ionized water for 10 min and subsequently drying with argon for 15 min. This shall maximize the coverage of OH groups on the column surface. For the coating, the N-dimethylaminodimethyl-octadecylsilane/octylsilane solution was applied to the column and left to react for 10 min. The column was then dried with pressurized argon for 15 min, and then flushed with pure acetonitrile. The post-treatment consisted in drying at 35 °C and 20 mbar pressure for 2 h and then closing the in/outlets of the chip with silicon septa.

3.3.2 Sol-gel technique

The sol-gel process is a versatile technique for making ceramic and glass materials. Sol-gel processes involve the transition of a system from a liquid "sol" (mostly colloidal) into a solid "gel" phase. It is possible to fabricate ceramic or glass materials in a wide variety of forms: ultrafine or spherical shaped powders, thin film coatings (Shang *et al.*, 2005), ceramic fibers, micro porous inorganic membranes, monolithic ceramics and glasses, or extremely porous aerogel materials, as detailed by Brinker and Scherer (1990).
For the scope of this thesis, sol-gel is defined rather broadly as the preparation of ceramic materials by preparation of a sol[1], gelation of the sol and removal of the solvent. This section shall give a basic understanding of the sol-gel process, without going into the details of sol-gel science, including physics (fractal geometry and percolation theory), chemistry (mechanisms of hydrolysis and condensation) and ceramics (sintering and structural relaxation).

3.3.2.1 Theoretical aspects

Hydrolysis and condensation In the sol-gel process, as described by Constantin and Freitag (2000), precursors (starting compounds) for

[1] a sol is a colloidal suspension of solid particles in a liquid.

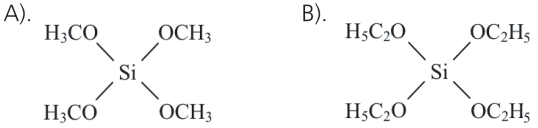

Figure 3.7: The most common used precursors: A) Tetramethoxysilane TMOS, B) Tetraethoxysilane TEOS

preparation of a colloid consist of a metal or metalloid element surrounded by various ligands (appendages not including another metal or metalloid atom (figure 3.7). In the sol–gel approach metalorganic monomers (often alkoxysilanes) are polymerized. At the functional group level, three reactions can be used to describe the process (figure 3.8). The first reaction corresponds to the hydrolysis of a liquid precursor (monomer), commonly an alkoxysilane. Alkoxy groups are replaced by hydroxyl groups and form silanol groups (SiOH) under release of alcohol. The silanol groups are highly reactive and condense readily with other alkoxysilanes (reaction 2) or with each other (reaction 3). As a result, a siloxane bond (Si–O–Si) is created and one molecule of alcohol respectively of water is released. Subsequent hydrolysis and condensation reactions form first a colloidal solution (sol) and finally a three-dimensional network (gel). This gel is nor longer fluid; however it shows elasticity when under mechanical stress.

Gelation The hydrolysis and condensation reactions discussed in the previous paragraph lead to growth of clusters that eventually link together into a gel. The simplest picture of gelation are clusters grown by condensation of polymers or aggregation of particles; links form between the clusters to produce a single giant cluster that is called gel. Progressively connecting clusters increase the stiffness of the gel. The sudden

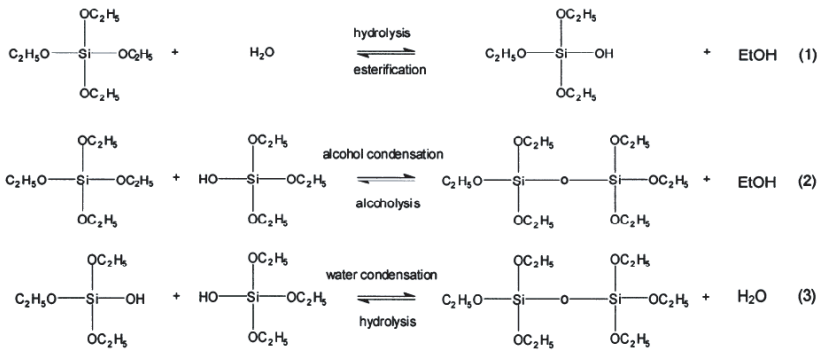

Figure 3.8: Reactions involved in forming a three-dimensional polymer network by the sol–gel technique (Constantin and Freitag, 2000)

change in the rheological behavior is generally used to identify the gel point in a basic way.

Aging Aging a gel before drying strengthens the network and thereby reduces the risk of fracture. This change during aging after gelation is categorized into *polymerization*, *coarsening* and *phase transformation*. Polymerization is the increase in connectivity of the network produced by condensation reactions, coarsening is the process of dissolution and reprecipitation, which is driven by differences in solubility between surfaces with different radii of curvature. This may result in a loss of surface area, and stiffening through growth of interparticle necks. Phase transformation includes phenomena such as separation of the solid phase from the liquid phase on a local scale, segregation of liquid into two or more phases or crystallization.

Drying Synersis is the shrinkage of the gel network resulting in expulsion of liquid from pores. The process of drying of porous material can be divided into two main stages. First the body shrinks by an amount

equal to the volume of the evaporating liquid, with the liquid-vapor interface remaining at the exterior surface of the body. The second stage starts when the body becomes too stiff to shrink and the liquid recedes into the interior, leaving air-filled pores near the surface.

3.3.2.2 Application of sol-gel technique

Different procedures corresponding to different sources (Constantin and Freitag, 2000; Constantin *et al.*, 2001; Guo and Colon, 1995) were tried. The basic components are shown in table 3.4. C_8-TEOS and TEOS were from Reactolab, all other chemicals from Fluka. De-ionized water is processed in-house.
The column was pre-treated with 1 M NaOH solution for 1 h, washed for 10 min with de-ionized water, and dried wtith argon for 15 min. Then C_8-TEOS (0.282 ml), TEOS (0.5 mL) and ethanol (0.177 ml) are mixed and briefly vortexed. Water (0.052 ml) and HCl (1 M, 0.053 ml) are added, the solution again vortexed for 1 min at 2500 rpm and allowed to react for additional 10 min. This sol-gel solution is pushed into the column and allowed to stay for 10 min. Then the column is flushed with argon

name	molecular formula and chemical structure
octyltriethoxysilane (C_8-TEOS)	$C_{14}H_{32}O_3Si$ 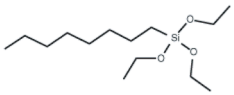
tetraethoxysilane (TEOS)	$C_8H_{20}O_4Si$ 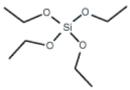

Table 3.4: Sol-gel coating precursors for C_8 stationary phase

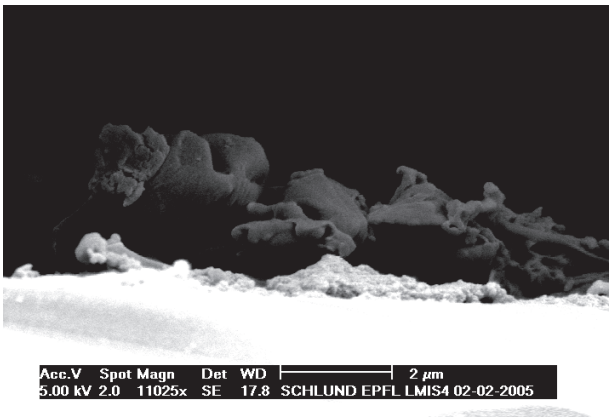

Figure 3.9: SEM picture taken with a tilt of a sol-gel coated column wall. The average sol-gel layer thickness was estimated to be around 0.3 μm.

for 5 min at 5 bar. The chips are dried at 35 °C at 20 mbar during 2 h and subsequently flushed with acetonitrile (5 min) and NaOH (10 min). The final drying step was again 2 h at 35 °C and 20 mbar.
The results of the coating in terms of separation power of the column are discussed in chapter 4. Figure 3.9 shows a SEM (scanning electrode microscopy) picture of a coated column wall.

3.4 Connectivity and actuation

A crucial aspect of microfluidic setups is the interconnection between the chip, electronics and fluidics, which are frequently cumbersome and the starting point of a large number of problems related to the lab-on-a-chip technology. Conventional tubing and interconnection techniques, as well as valves and pumps, often present dead volumes that are orders of magnitude larger than the total volume of the microfluidic channels on the chip itself. Two main strategies tend to minimize those dead vol-

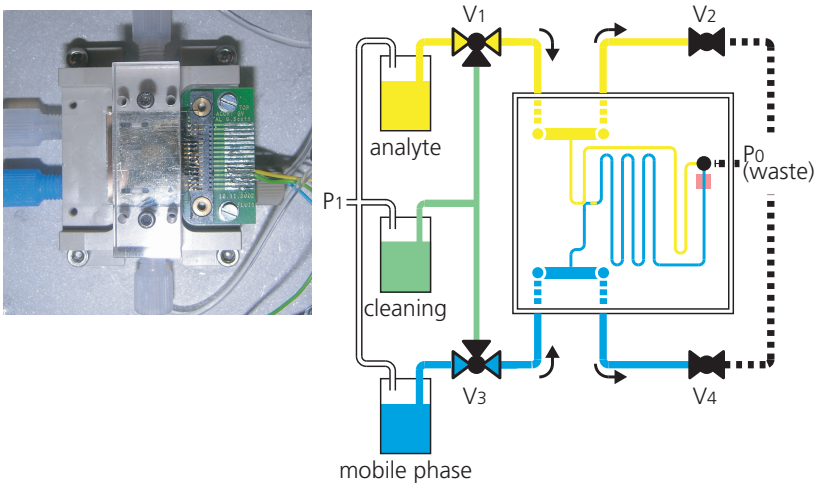

Figure 3.10: Image and schematic view showing the PEEK chip holder with the printed circuit board for signal acquisition and the ETFE flangeless fittings providing liquids from the bottom through o-ring sealed interconnections. Visual access to the chip is guaranteed through the plexiglass covering fixation part.

umes. A first approach consists of integrating on the microfluidic chip those parts responsible for dead volumes, as for example check valves. The inconvenience of a maximized integration is an important increase in fabrication complexity, as illustrates the complicated on-chip monolithic polymer check valves shown by Unger *et al.* (2000) or Hasselbrink *et al.* (2002).

Because controlled fluid pressures rather than flow rate, were essential for proper operation of the experimental set-up, it was more efficient to use pressurized reservoirs for both sample and mobile phase delivery, providing precise pressure control as opposed to pumps (figure 3.10). Sample and mobile phase were contained in separate 100 ml glass bottles using fluid distribution caps with threaded flat-bottom ports (Bohlender).

The liquid pressure was controlled by varying the pressure in the headspace over the liquids using pressurized air, with control of the gas pressure assured by a manual high-precision pressure regulator and precision gauge over a range of $0 - 1.5$ bar (Marsh Bellofram). For most experiments, the system was operated between 300mbar and 1500 mbar, with 500 mbar to 1000 mbar being typical. The precision was of 1 mbar controlled by a digital pressure indicator. In the present setup this is equivalent to a flow velocity precision of $1\,\mu m\,s^{-1}$.
Fluid delivery lines and connectors, Teflon® tubing and ETFE flangeless fittings, respectively, were obtained from Upchurch Scientific. Fluid flow was controlled by normally closed solenoid isolation valves (Bio-Chem Valve /Omnifit). The valves were actuated using solid state relays controlled by logic signals emanating from the data acquisition board (PCI-DAS6014 D/A-A/D-DIO board, Measurement Computing). For data acquisition and system control, a LabVIEW® virtual instrument (VI) manager was written using the appropriate drivers for the data acquisition board as supplied by the manufacturer.

3.5 Sampling method

An adequate injection technique that is fully integrated and reliable, not requiring a syringe pump to load the chip, is of highest importance to a device that is meant to accomplish multiple, subsequent samplings. Furthermore a robust sampling method from a macroscopic flow is required. In reference to the first point, on-chip injection methods in pressure driven systems that have been reported in the literature have used a double-T junction type microfluidic design that emulates the usual HPLC injector loop, that also has been subject to optimization efforts (Chervet and Ursem, 1996; Vissers *et al.*, 1996). In this design, an injection plug of fixed volume is contained in the main channel segment between the two side branches. This requires the use of syringe pumps or a standard HPLC injection valve, as for example shown by Manz *et al.* (1990b), McEnery *et al.* (2000a) or O'Neill *et al.* (2001).

Verheggen *et al.* (1988) introduced the T-injection which allows for fixed-volume pressure-driven plug injections. This has been extended and studied for electrokinetic plug injections (Ocvirk *et al.*, 2000), with double and triple T-injection (Fu *et al.*, 2002; Sinton *et al.*, 2003b). However, it is difficult to assure repeatability using this technique, as the confining segment is easily overflowed, and the extremely low flow rates for sample loading are difficult to obtain. An improvement in terms of injection plug control is the so-called pressure-pinched injection, where the continuous analyte flow is compressed at the injection cross from either side by side streams of mobile phase, in order to minimize the volume while at the same time obtaining reproducible injection plugs, as shown by Bai *et al.* (2002b) and Sinton *et al.* (2003a). This design relies on very delicate balancing of flow rates to work properly. A variation on this theme was the pressure pinched injection devised by Vahey *et al.* (2000), where the flow scheme allows a variable plug length to be injected into the separation channel, and electrokinetic focusing shown by Fu *et al.* (2003) and Ren *et al.* (2003). Again, a delicate flow rate balance must be maintained. Another interesting method is the so-called pressure-pulse injection developed for electrophoretic microchips by Solignac and Gijs (2003) or the impulse-based nanoinjector with a solenoid-based micropump presented by Gorbounov *et al.* (2003). Lee *et al.* (2003) presented a microinjector based on a fused glass microneedle and a PDMS-based microvalve.

A peculiarity of all these systems is, that, before and after plug injection, the flow of the analyte is stopped. This may lead to different, hardly controllable phenomena such as diffusion related concentration changes or even precipitation of the analyte under certain conditions.

The injection method introduced here is very simple but nonetheless robust, based on continuously flowing analyte and mobile phase streams. A gated injection approach is proposed, whereby the confluence of two laminar flows at an injection cross can be made to exclude the analyte from entering the separation column by the mobile phase stream, which exclusively flows in this channel, until an intentional perturbation in the

flow rate of the latter allows the former to enter. This technique has been employed in plug formation on electroosmotically driven microfluidic chips, where voltage switching is used to gate the injection, and is a well known injection method for chip-based electrophoretic separations, as shown by Jacobson *et al.* (1994, 1999) and Ermakov *et al.* (2000), and as well as by Rocklin *et al.* (2000), Slentz *et al.* (2002) or Fu and Lin (2003), who called it double-L injection.

In the present thesis, perturbation of driving pressures is used to create repeatable injections with injection volumes dependent on the duration of the pressure change and the flow velocity.

A further point to be addressed is representative sampling. Rapid renewal as well as purging of sample inlet lines to the chip is of paramount importance for obtaining representative samples in on-line analysis of microreactors and macro-scale reactors, and to eliminate cross-talk between samples. In order to accomplish this, it is necessary to design the system so that meso-scale flow rates (tens of microliters to milliliters per minute) of fresh sample liquid can pass by the inlet leading to the on-chip injector, where fresh aliquots can be drawn from the stream. To this end, a flow-through strategy for sample and mobile phase introduction was conceived, permitting continuous or intermittent flow of fresh sample stream on to the chip, with injection of an aliquot of the sample stream executed in a periodic or random fashion. Large flow-through channels ($200\,\mu\text{m} \times 1\,\text{mm} \times 5\,\text{mm}$) permit sample and mobile phase streams to flow either separately or simultaneously on the chip. This sampling approach has found precedent in microfabricated electrophoretic devices, in the work by Lin *et al.* (2001), Chen *et al.* (2002), Wang *et al.* (2005) and Büttgenbach and Wilke (2005), but has not been attempted for chip-based LC.

The design principle of the injection system calls for sample and mobile phase inlet channels to intersect orthogonally, with the sample inlet channel continuing as the separation channel after the intersection. Figure 3.11 shows a schematic of the device. Large-bore flow-through inlets (A, M) are connected to reservoirs with applied pressure P_1, containing

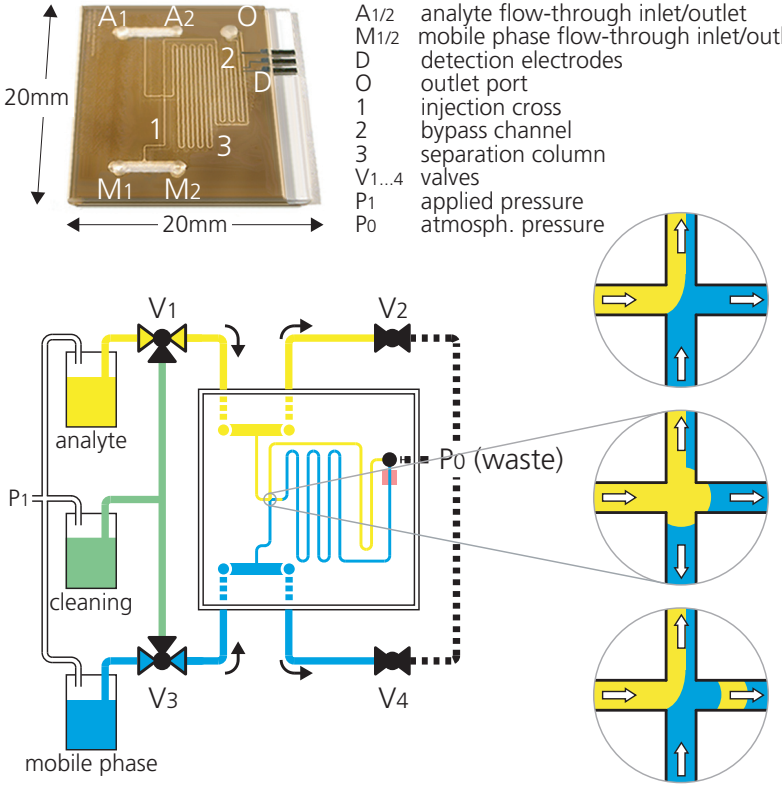

Figure 3.11: Photo of a finished chip showing large flow-through channels flanking the bypass and separation channels, with electrical contact pads deployed on the right side of the chip. Schematic of the chip showing salient features of microfluidic network. The inset shows flow separation of the analyte streams (from left) and mobile phase streams (from bottom) in the injection cross, making possible gated injection.

analyte and mobile phase respectively, while outlet (O) of the microfluidic manifold is connected to atmospheric pressure. Segment 3 is the separation column while segment 2 is the analyte bypass channel. These channels intersect with the flow-through inlets A and M, and access fluids flowing through them. The liquids are driven by the resulting pressure drop from the point of intersection with A and M to the outlet O. A higher flow resistance in the separation column compared to that of the bypass channel causes the analyte flow to divert into the bypass channel, while the mobile phase is forced to flow into the separation channel due to the inability of streamlines to cross in laminar flow. Mobile phase can also flow into the bypass channel, and the ratio of analyte to mobile phase flowing in this branch is controlled by the fluid pressures. A continuous flow of part of the mobile phase into the bypass channel screens the separation column from the analyte, thus preventing analyte from flowing unintentionally into the separation column, either by diffusion into the mobile phase at the injection cross or by small pressure variations at the inlets (Figure 3.11, inset).
Pressure variations in either stream will result in a change in the flow rate ratio. To engender plug injection into the separation channel, a reduction of the mobile phase flow rate by intentional momentary release of the pressure, or by constriction of the flow, will allow analyte stream to begin flowing into the separation channel. Conversely, a higher overpressure in the analyte stream can cause the mobile phase to recede and overtake its flow down the separation channel. The duration of the pressure perturbations will define the injected plug length and thus its volume.
Two different methods were used to accomplish this and are further explained in the two following sections:

- Opening of an isolation valve (V_4) connected to the flow-through tubing downstream of the chip, releasing hydrostatic pressure in the mobile phase line.

- Local heating in the analyte or mobile phase stream in order to generate a bubble that momentarily changes the pressure distribution.

Simultaneous opening of both isolation valves V_2 and V_4 is used for the optional washing cycles. If one wishes to change analytes or mobile phases, the pressurized reservoirs are simply disconnected and exchanged via the manual switching valves (V_1 and V_3). When the new reservoirs are connected, a washing cycle can be carried out. This takes from a few seconds (only analyte change) up to a few minutes (analyte and mobile phase), depending on the chosen flow rate.
This method for continuous pressure-driven analysis on a chip, using a bypass channel and gated injection by momentary flow pattern variations, has been patented, in collaboration with Scott E. Gilbert, founder and president of Crystal Vision Microsystems LLC. (Schlund and Gilbert, 2004).
The following sections will show two implementations of this sampling method.

3.6 Thermal plug injection

In order to generate a momentary pressure distribution change in the microfluidic system, a mechanism for local heating and bubble generation, thus thermal plug injection, is integrated onto some of the devices developed, and has been characterized in the frame of the present work. To this end, a thin-film platinum resistance (heater) is deposited by lift-off during the same processing step as the detection electrodes. Heating at sufficient rate shall then generate a bubble that modifies the flow behavior. Figure 3.12 shows the basic principle of this plug injection technique. To obtain such behavior, one has to look further into bubble growth mechanisms.

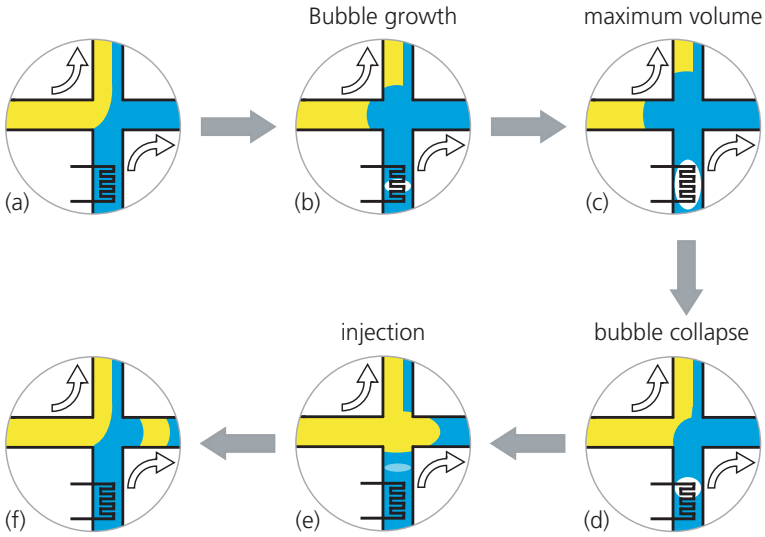

Figure 3.12: Schematic view of the injection cross during thermal injection. (a) normal flow pattern, (b) beginning of the current pulse: nucleation of a bubble, (c) the bubble has expanded to its maximum size, (d) the bubble starts to collapse, (e) during bubble collapsing the analyte starts to inject into the separation column, (f) the bubble has completely collapsed and the normal flow pattern is resumed.

3.6.1 Bubble growth mecanisms and heater element

Homogeneous and heterogeneous nucleation Bubble growth can occur either by heterogeneous nucleation or by homogeneous nucleation, as illustrated in Viisanen *et al.* (1993). One one hand, heterogeneous nucleation occurs when a bubble is formed from a pre-existing nucleus on the surface. It is difficult to know the characteristics of such nuclei, and thus this process is complicated to predict. On the other hand, evaporation in the interior of the liquid is called homogeneous nucleation. This appears when the liquid is heated at very fast rate (Deng *et al.*, 2003) give a value of $6 \times 10^6\,^{\circ}\mathrm{K\,s^{-1}}$). To reach homogeneous nucleation,

the liquid goes through supercritical fluid state and nucleates around 270 °C (Deng *et al.*).

Required power The bubble volume depends on numerous parameters, in particular on the channel geometry. With channel dimensions of 50 μm (width) $\times$5 μm (height), initial tests showed a typical maximum bubble volume of around $3 \times 10^5\,\mu\text{m}^3$. Assuming the conditions proposed by Deng *et al.* and applying them to the present channel geometry, the bubble generation time as well as the required power can be calculated. Taking the law of perfect gases and knowing that the bubble's maximum expansion is at $T_{maxvol} = 75\,°\text{C}$ and the pressure of the bubble, $p_{bubble} = 1\,\text{bar}$, one can determine the liquid's mass of the bubble volume:

$$m_{bubble} = M_{liquid}\frac{p_{bubble}V_{bubble}}{R_{gc}T_{maxvol}} \tag{3.13}$$

With M_{liquid} = molar mass, V_{bubble} = bubble volume and R_{gc} = gaz constant. As first approximation, the liquid considered is pure water, knowing that the mobile phase used for the chromatographic separations will contain an important amount of water. Hence the required energy for bubble generation is given by:

$$E_{25\rightarrow 270°\text{C}} = (c_{p,water}\cdot\Delta T + L_{h,water})\cdot m_{bubble}$$

$$\begin{aligned} \Delta T &= 245°\text{C} \quad \text{(temperature difference)} \\ c_{p,water} &= 4.1\cdot 10^3\,\text{J}\,\text{kg}^{-1}\,\text{K}^{-1} \quad \text{(specific heat capacity)} \\ L_{h,water} &= 2.26\cdot 10^6\,\text{J}\,\text{kg}^{-1} \quad \text{(latent vapor heat)} \end{aligned} \tag{3.14}$$

Together with the minimum rate necessary to reach homogeneous nucleation, one obtains following numbers:

$$t_{25\rightarrow 270°\text{C}} = \frac{\Delta T}{6\cdot 10^6} = 41\mu\text{s} \tag{3.15}$$

and thus the required power:

$$P_{bubble} = \frac{E_{25\rightarrow 270^\circ\mathrm{C}}}{t_{25\rightarrow 270^\circ\mathrm{C}}} = 0.015\,\mathrm{W} \tag{3.16}$$

Efficiency factor The applied power only marginally transfers into the bubble, while the major part is dissipated in heating the surrounding liquid and the chip. This is taken into account by the efficiency factor $K_e < 1$. Experimental and theoretical studies by Hong *et al.* (2004) with a similar setup as presented here showed that only a very small fraction of about 6 % of the energy transmitted to the liquid is actually used for the evaporation. This value will be considered for further calculations. The second limitation to the actual energy transmission is the absorption by the sourrounding substrate, as the heater element is deposited on the bottom part of the microfluidic channel. Taking into account the thermal conductivity of the liquid (water) and the substrate (glass), one can assume that around $\frac{2}{3}$ of the dissipated energy flows into the substrate and only $\frac{1}{3}$ is directly absorbed by the liquid.

$$\begin{aligned} P_{bubble} = K_e \cdot \frac{1}{3} \cdot P_{liquid} &= 0.015\,\mathrm{W} \\ \Rightarrow P_{liquid} &= 0.75\,\mathrm{W} \end{aligned} \tag{3.17}$$

In order to have some reserve, a power of 1 W was considered for the heater design. Assuming a total DC bias of 30 V and maximum current of 100 mA, together with the applied power of 1 W, the heater's electrical resistance has to reach a value of 100 Ω to dissipate the desired amount of heat. For fabrication reason, the heater element's parameters were chosen as shown in table 3.5.

Maximum temperature It is important to note that, once the liquid is evaporated, almost all the heat still dissipated by the heater element will flow into the substrate, as the thermal conductivity of water vapor is approximately 1000 times lower than for liquid water. Hence one should consider a maximum current pulse length in order to not overheat the

parameter	value
material	Ti/Pt (20 nm/200 nm), same as the detection electrodes.
feature size	width 5 μm (photolithography limits) and length therefore 500 μm, as the Pt sheet resistance is approximately 1 $\Omega/\square$.
implementation	the total length of the heater was folded into a serpentine-like element.

Table 3.5: heater element characteristics

substrate. This can be calculated by solving the heat equation according to Widder (1975):

$$\frac{dT}{dt} = \frac{\kappa}{\rho c_p}\frac{dT}{dx^2} \tag{3.18}$$

With κ the thermal conductivity, ρ the density and c_p the specific heat capacity. In a semi-infinite solid initially at a temperature $T = T_0$ with a constant power applied on the surface at $x = 0$ and from time $t = 0$ on, equation 3.18 has following boundary conditions:

$$\begin{aligned} T(x,0) &= T_0 \\ \frac{dT(x,t)}{dt} &= \frac{1}{\kappa}\cdot\frac{P_{tot}}{A} \\ \text{with: } &\frac{P_{tot}}{A}\text{power per unit surface} \end{aligned} \tag{3.19}$$

which yields the following solution:

$$\begin{aligned} T(x,t) = &\frac{2P_{tot}\cdot\sqrt{\frac{\alpha t}{\pi}}}{\kappa A}\cdot exp\left(-\frac{x^2}{4\alpha t}\right) \\ &- \frac{P_{tot}\cdot x}{\kappa\cdot A}\left(1 - erf\frac{x}{2\sqrt{\alpha t}}\right) + T_0 \end{aligned} \tag{3.20}$$

Where $erf(x)$ is the Gauss error function given by:

$$erf(x) = \frac{2}{\sqrt{\pi}} \int_0^x e^{-t^2} dt \tag{3.21}$$

Hence the maximum temperature T_{max} is given by:

$$T_{max} = T(x,t)|_{x=0} = \frac{2P_{tot} \cdot \sqrt{\frac{\alpha t}{\pi}}}{\kappa \cdot A} + T_0 \tag{3.22}$$

Putting in the numbers yields the maximum pulse length allowed before the substrate overheats:

$$A_{heater} = 7.71 \cdot 10^{-4} \frac{\sqrt{t}}{T_g - 25} \quad \Rightarrow \quad t_{pulse,maximum} = 20\,\mu\text{s} \tag{3.23}$$

With T_g the glass transition temperature of the substrate.

3.6.2 Electrical driving circuit

In order to obtain sufficient power on the heater element, a push-pull circuit was used to amplify the current of a function generator signal. An AC signal is applied in order to prevent eventual electrolysis and fouling of the heater element which could occur in the case of a DC bias. This circuit is a class-B amplifier: only one transistor conducts at a time while the other is blocked. When the input voltage is high, the NPN transistor conducts while the PNP is blocked and vice-versa (Figure 3.13). The advantage of the circuit is that when there is no input signal, no transistor conducts and there is no power dissipation. The two diodes are used to eliminate crossover distortion. The resistances are used as current source and to improve the output linearity.

3.6.3 Bubble volume

As described above, the volume of the bubble is related to the energy dissipated in the heater. However, if nucleation occurs before the end

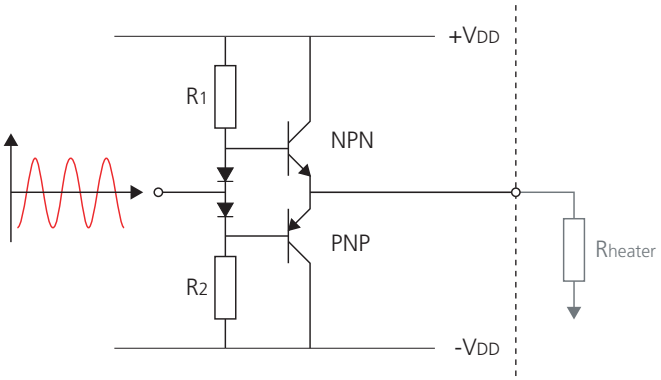

Figure 3.13: A push-pull circuit is used as power amplifier. The circuit is a class-B amplifier, each transistor conducts half of the time while the other is blocked. It consists of one NPN and one PNP transistor and two diodes for base-emitter bias compensation. The two resistances limit the signal distortion.

of the current pulse, the volume reaches a maximum expansion, as the heat transfer is nearly stopped at the bubble nucleation due to the very low thermal conductivity of the vapor.
In order to predict this volume, it is necessary to know the dissipated power in the liquid given the applied voltage $\hat{U}$, the total electric resistance R_{tot} and the heater resistance R_h:

$$P_{liquid} = \frac{A_{heater}}{A_{tot}} \frac{\kappa_{liquid}}{\kappa_{liquid} + \kappa_{substrate}} \frac{\left(\frac{R_h}{R_{tot}} \frac{\hat{U}}{\sqrt{2}}\right)^2}{R_{heater}} \tag{3.24}$$

with $\frac{A_{heater}}{A_{total}}$ being the fraction of the surface covered by the bubble and the effective heater surface. Finally one can calculate the bubble's mass and volume, knowing the energy and using the perfect gas law:

$$m_{bubble} = \frac{E_{bubble}}{(T_{nucl} - T_{amb}) \cdot c_{p,liquid} + L_{h,water}} \tag{3.25}$$

$$V_{bubble} = \frac{m_{bubble}}{M_{liquid}} \cdot R_{gc} \cdot \ T_{maxV} \cdot \frac{1}{P_{atm}} \tag{3.26}$$

with c_p the specific heat capacity, $L_{h,liquid}$ the latent vaporization heat, R the gas constant, M_{liquid} the liquid molar weight and P_{atm} the atmospheric pressure. Putting the numerical values $\hat{U} = 10\,V, \kappa = 0.063, A_{tot} = 3200\,\mu\text{m}^2, A_{heater} = 1200\,\mu\text{m}^2$ yields:

$$V_{bubble} = 6.55 \cdot 10^5\,\mu\text{m}^3 \tag{3.27}$$

3.6.4 Experimental results

For the characterization of the thermal plug injection, a prototype chip was fabricated using a Pyrex®. substrate with Ti/Pt electrodes (20 nm/ 200 nm thickness) and channels patterned in a overlaying, 10 μm thick SU-8 layer. The channels were then sealed by clamping a PDMS (polydimethyl siloxane) layer onto the top of the chip. Plug length and thus plug volume was characterized as a function of the fluidic and electric parameters. The repeatability of the injected plug's length and therefore size on one chip was excellent, but differed significantly from one chip to another, due to fabrication tolerances. For all characterizations, plug length was measured rather than plug volume, knowing that they are linearly dependent.

3.6.4.1 Bubble behavior

During the experiments, the bubble behavior matched theoretical predictions. The growth and collapse occurred in times in the range of a microsecond. However, instead of a fast and complete collapse, it was observed that a thin bubble remained for a much longer time (hundreds of milliseconds) and blocked the flow (Figure 3.14). The duration of this

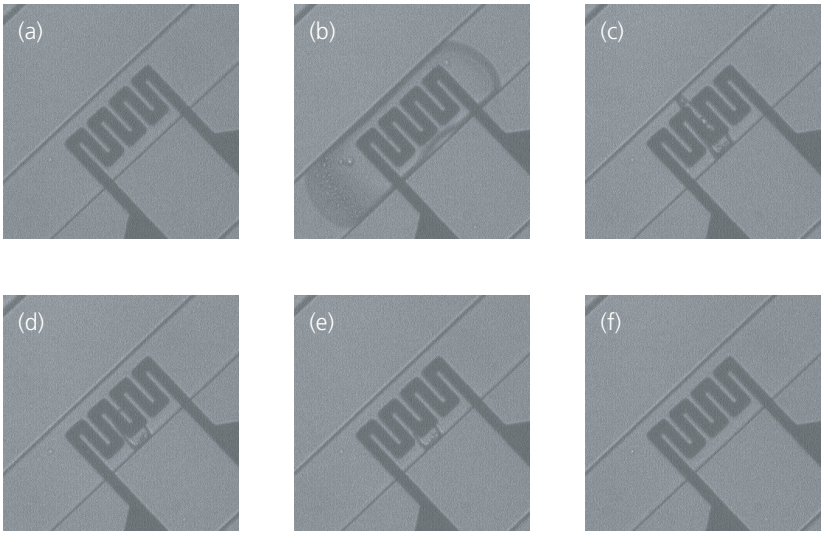

Figure 3.14: Bubble growth and collapse: (a) no current through the heater, (b) several μs after the pulse beginning, the bubble is at its maximum volume, (c) at $t = 200\,\mathrm{ms}$, (d) at $t = 600\,\mathrm{ms}$, (e) at $t = 1\,\mathrm{s}$, (f) at $t = 5\,\mathrm{s}$. Channel dimensions are $50\,\mu\mathrm{m}$ width and $10\,\mu\mathrm{m}$ height.

phenomenon depends on the liquid pressure, thus related to the flow rate, and the dissipated power, which therefore allows a controllable plug injection.
The bubble length at maximum expansion was found to be around $150\mu\mathrm{m}$ and thus the bubble volume around $7.5 \cdot 10^5\,\mu\mathrm{m}^3$, which is in good agreement with the theoretical values found above.

3.6.4.2 Dryout

Normally a thin layer of liquid always separates the bubble from the wall. However, when the heat flux between a heated surface and a liquid is larger than a critical value (critical heat flux), the liquid cannot recover

the surface. If dryout takes place, a fraction of the vapor contained in the bubble will be directly in contact with the channel wall.
When the bubble then collapses, it does not have sufficient energy to break the surface of the meniscus and the complete collapse can only be assured by cooling down and subsequent condensation of the vapor. It was observed that the dryout occurs on all wall surfaces near the heater, so that the remaining bubble obstructed the channel momentarily and thus generated the plug injection. This phenomenon is indeed the key to this injection method. The meniscus formed is strongly attached to the surface, a phenomenon strongly related to the surface's roughness. Figure 3.15 illustrates the dryout phenomenon, the difference of collapse between a situation where dryout does not occur and when there is dryout. One can see that when dryout occurs, a thin plug of vapor remains. This remains in the channel for several hundreds of milliseconds (cf. figure 3.14c) and generates the plug injection.

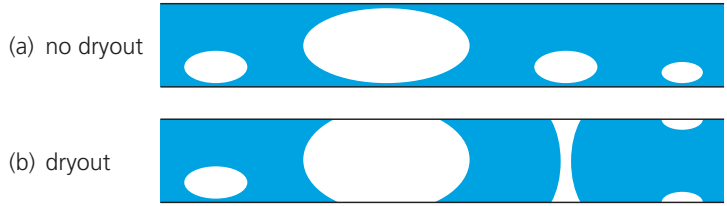

Figure 3.15: Dryout phenomenon. Due to the shockwave and the extreme heat flux, the thin liquid layer between the bubble and the channel walls evaporates and the vapor is directly in contact with the walls. (a) and (b) show the difference of collapse between a bubble without dryout (a) and a bubble with dryout (b). When there is dryout, a meniscus is formed and a thin vapor bubble remains for a several hundreds of miliseconds before complete collapse.

3.6.4.3 Plug injection

The injection process was studied by optical and fluorescence microscopy. The injection technique worked finely and was conform to the theoretical predictions. Plugs were injected controllably and the generated bubble always collapsed. The smallest plugs created were approximately $10^5\,\mu m^3$ or 100 pl (cf. paragraph 3.6.4.5), which is less than 0.2 % of the total separation column volume. A fluorescence microscopy of one plug injection sequence is shown in figure 3.16.

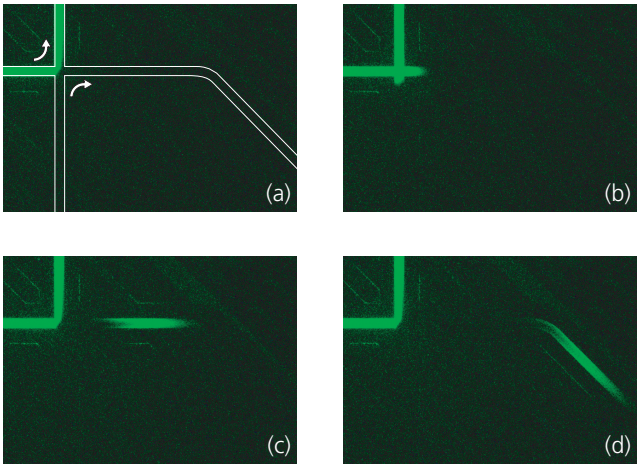

Figure 3.16: Fluorescence microscopy of a plug injection at the injection cross. The analyte is a saturated fluorescein solution, the mobile phase de-ionized water and not visible. (a) normal flow pattern, (b) the bubble has formed and is already collapsing, the analyte flows into the separation column, (c) the bubble has completely collapsed, the normal flow pattern is resumed and (d) the plug flows through the separation column. The column depth is 10 μm and width is 50 μm.

3.6.4.4 Heater damage

In other systems using thermal bubble generation, such as thermal inkjet printers, the heater element is covered by a protection layer (generally tantalum) conceived to protect the metal from cavitation damage. Cavitation occurs when bubbles rapidly collapse. It may cause severe damage to the surrounding components as a result of shockwaves. This process typically happens in large scale pumps or propellers when the liquid pressure falls below the liquid's vapor pressure. In the case of the heater, a similar phenomenon due to the rapid collapse of the bubble is observed. High temperature and heating rate during short lapse of time also cause the platinum to be damaged. The damage is highly dependent on the pulse's electrical power and duration. The experiments showed nevertheless that the heater can support several hundred pulses before the lead is interrupted.

3.6.4.5 Influence of power density and pulse duration

Serpentine-shaped heaters with 4 and 8 turns (cf. figure 3.14 for a 4-turn heater) were tested under different conditions. Their respective electrical resistances were measured as being:

$$\text{4-turn heater + access pads: } R_{4-turn} = 71\,\Omega$$
$$\text{8-turn heater + access pads: } R_{8-turn} = 108\,\Omega$$

Without considering the access pads, the 8-turn heater resistance should be exactly twice the one of the 4-turn heater. Therefore, one can estimate an access pad resistance of 34Ω, and thus resistances of 37 Ω and 74 Ω for the 4-turn and the 8-turn heaters respectively. Consequently, the power density is 4 times more important in the small heater than in the larger at same applied voltage.
This difference in power density has an influence on the heating rate. Therefore, homogeneous nucleation is more likely to occur on the small heater, which was experimentally observed. These observations addi-

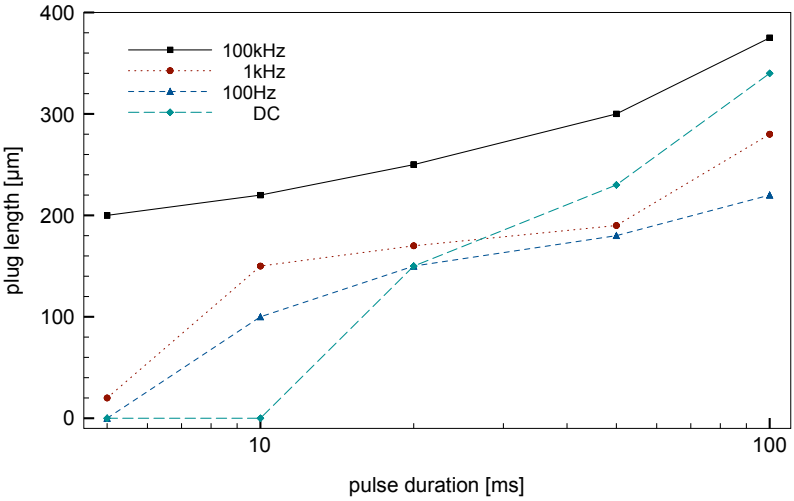

Figure 3.17: Plug length as a function of pulse duration, and various frequencies.

tionally confirm the advantageous character of homogeneous vs. heterogeneous nucleation. The bubble growth was less regular and controllable on the large heater and bubble did not collapse completely, yielding unreliable injections.

3.6.4.6 Influence of frequency

The driving voltage of the heater element is an AC signal in order to avoid hydrolysis and fouling. Numerous experiments were run to study the influence of signal frequency on the bubble length and thus volume. Frequency ranged from pure DC up to 100 kHz, while the pulse duration was maintained at a constant value. On figure 3.17 one observes that the frequency has a complex influence on bubble length:

- Frequency does not significantly change the length of the bubble, the effect is minor and the general trend remains the same for all the curves.
- High frequencies increase the bubble size, whereas a low frequency creates shorter bubbles. This is attributed to the fact, that at higher frequency the heater element cannot *cool* down between the pulses as much as at lower frequencies.
- However, DC signal also seems to increase the length of the generated bubble. This is most probably due to additional bubble volume formed by electrolysis.

3.6.4.7 Influence of flow rate

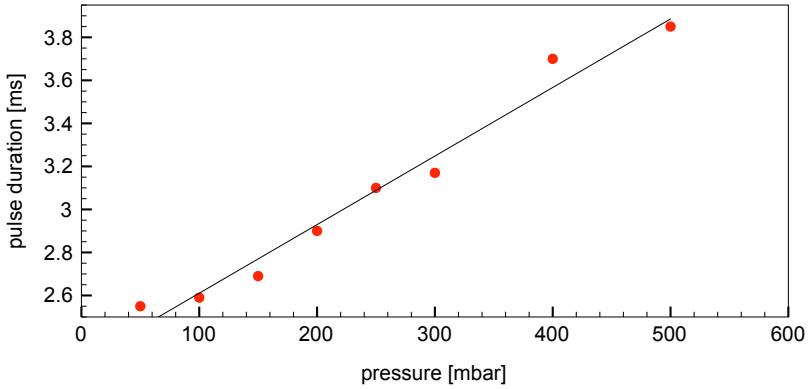

Figure 3.18: Minimum pulse duration to start injection as a function of pressure (and thus flow rate)

If the hydraulic resistance remains constant, pressure is proportional to flow rate. Thus the length of the plug increases linearly with pressure for a constant voltage and pulse duration. However, high pressure (=

high flow rate) tends to compress the bubble and therefore accelerates its collapse. During experiments, it was observed that a higher pressure increased the minimal pulse duration to inject a plug.
The results shown in figure 3.18 indicate that flow rate has a linear influence on plug length. Moreover, one can observe that compression on the bubble surface has indeed little influence on its breakup. This indicates that the collapse of the bubble is rather influenced by surface roughness or temperature/pressure gradient than by pressure.

3.6.5 Conclusions

Plug injection by bubble nucleation is working fine. Experiments showed the importance of working at sufficiently high heat rates of above $6 \times 10^6\,^{\circ}\mathrm{K\,s^{-1}}$ to reach homogeneous nucleation.
The bubbles always completely collapsed at homogenous nucleation, whereas in the case of heterogeneous nucleation, numerous problems yielded unrepeatable injections. Furthermore, the bubble collapse and the dryout phenomenon were in agreement with the theoretical predictions. Characterization showed that the plug volume can be reliably varied by controlling the pressure and by modifying the pulse duration and/or the power. Finally, plugs as small as $10^5\,\mu\mathrm{m}^3$ (100 pl) were injected in the separation column. However, the drawback of this method is the heater element damage and the overall heating of the device which, depending on the application, may not be desirable. Heater damage could be solved by adding a supplementary protection layer such as tantalum. However, it would require additional fabrication steps which raises complexity and cost. Moreover this method is very dependent on fabrication tolerances of the column height and the electrode heater element, and showed important differences of the repeatability between different devices.

3.7 Pressure-drop plug injection

Gated plug injection by heat generated bubbles may work correctly, it nevertheless presents inherent disadvantages such as long-term instability and heating of the device. The pressure-drop method presented in this chapter takes advantage of the entire system with its four valves, of which two are electrically actuated.

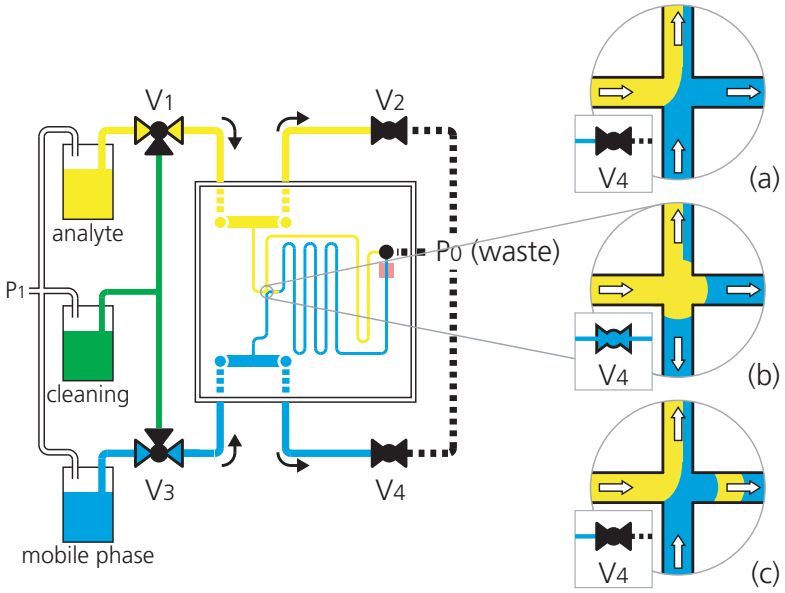

Figure 3.19: Schematic view of the injection cross during pressure-drop plug injection, the inset shows the three phases during the plug injection(a) normal flow pattern, (b) isolation valve V_4 is open and analyte is flowing into both, separation column and mobile phase inlet channel, (c) V_4 is closed again and normal flow pattern is reestablished. Simultaneous opening of isolation valves V_2 and V_4 is used for purging of the flow-trough channels.

Figure 3.19 shows the scheme of the pressure-drop injection setup. By opening the isolation valve V_4 after the flow-through channel of the mobile phase ($V_3 \rightarrow V_4$), the fluidic pressure in the mobile phase inlet is dropping, and therefore changing the flow pattern in a way to allow the analyte flowing in both the separation column as well as backwards into the mobile phase inlet, creating the later injected plug. Reestablishing the initial flow pattern by closing again the isolation valve V_4 pushes the analyte plug into the separation column. This mechanism has the advantage of not altering the temperature on the chip and of being highly repeatable.

3.7.1 Plug injection

The entire system turned out to be very robust and simple to handle. Flow injection tests were carried out *a priori* with two liquids containing different food dyes in order to visualize the functionality of the design. For quantization of injection repeatability, two methods have been used, optical measurements using fluorescent dye for the analyte and amperometric detection using phenol as analyte.

3.7.1.1 Optical measurements

Plug injection reproducibility as a function of injection time and applied pressure (or mean flow velocity) was measured using a CCD camera and fluorescent analyte (saturated fluorescein solution at pH = 9.0). Visual observation is shown in the sequence of fluorescence micrographs presented in figure 3.20.
Integration of the fluorescence intensity allowed to determine the quantity of the injected analyte. In order to have sufficient analyte intensity, fluorescence and subsequent amperometric measurements were carried out using chips with microchannels of 10 μm depth and 50 μm width. These measurements showed a relatively good repeatability and a linear

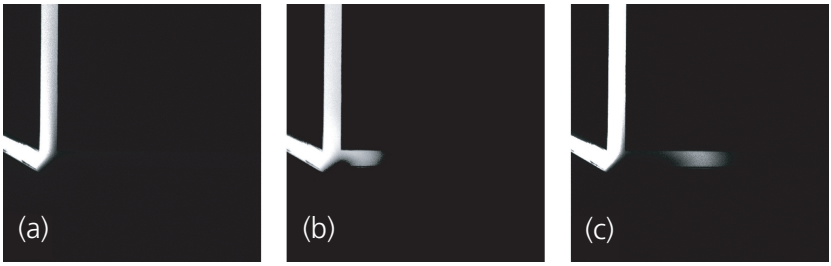

Figure 3.20: Fluorescence micrograph sequence of pressure-driven gated injection: (a) fluorescing sample stream diverted into bypass channel; (b) pressure release on mobile phase stream causes retreat of the latter, allowing sample stream to flow into the separation channel (towards the right); (c) detachment of the sample plug when the mobile phase stream flow is re-established after the pressure perturbation. The column depth is $10\mu m$ and width is $50\mu m$

behavior of the plug volume vs. the injection time. Nevertheless, as one camera pixel corresponds to $4.1\,\mu\mathrm{m}^2$, this is a major source of error.

3.7.1.2 Amperometric measurements

For verification of the fluorescence measurements, amperometric detection of single component analytes were analyzed (Amperometric detection is further explained in section 3.8). Peak areas of 5 consecutive samples with 4 different injection times each were analyzed and confirmed the fluorescence data. For visualization reasons, figure 3.21 only shows the peaks of three consecutive plug injections of 5mM phenol and illustrates the repeatability of the plug injection. The valve was opened for 1000 ms at each injection. Figure 3.22 shows the linear trend of the plug volume vs. the applied pressure drop (flow rate) confirms the observations made during fluorescence measurements. Repeated injections of analyte and its detection showed volume variations of less than 5%, which finally resulted in peak area reproducibility error of less than 1%

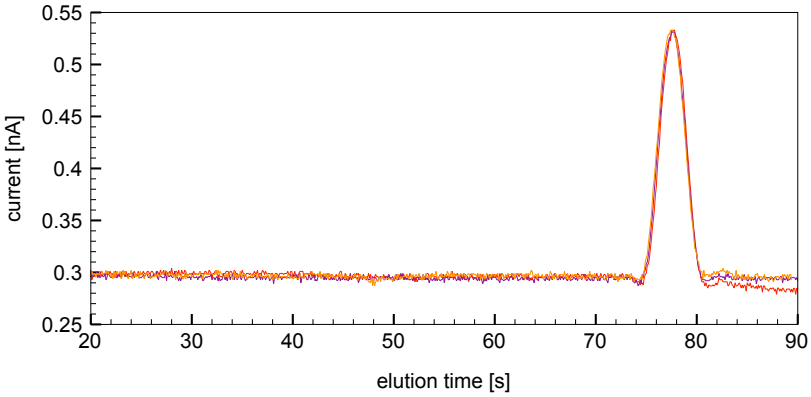

Figure 3.21: Comparison of 3 samples by amperometric detection. Stationary phase: Sol-Gel C_8. Mobile phase: H_2O and acetonitrile (ACN) (70:30, v/v). Analyte: 5mM phenol. The injection time was always 1000ms and the pressure drop across the setup was 1000 mbar.

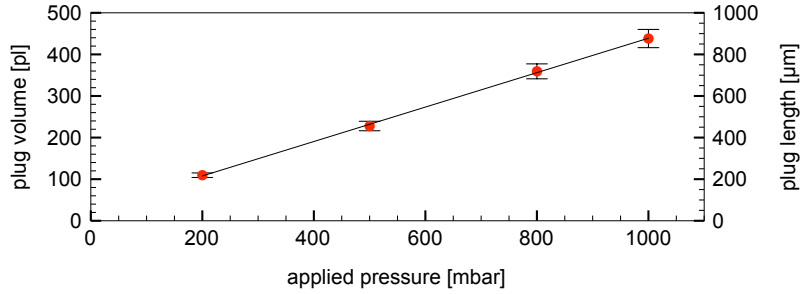

Figure 3.22: Plug volume as a function of the applied pressure drop (flow rate). The data is from 5 samples with 4 different injection times each. The reproducibility error is lower than 5% (error bars). Channel depth is 10 μm, width is 50 μm

standard deviation. This is comparable to electrokinetic gated injection, where errors of 0.5% standard deviation has been shown (Jacobson *et al.*, 1999)

3.7.2 Fluid dynamics of pressure-drop plug injection

To measure the influence of injection time on plug volume, phenol was injected at a concentration of 5mM into a mobile phase stream consisting of H_2O/acetonitrile (ACN) (90:10,v/v). Peaks were recorded for various injection volumes of 200, 500, 1000 and 1500 ms corresponding to 70, 175, 350 and 525 pl. An overlay of the single peak chromatograms recorded for each injection volume is shown in figure 3.23. Reasonably Gaussian peak shapes are evident, with increasing tailing for larger plug volumes.

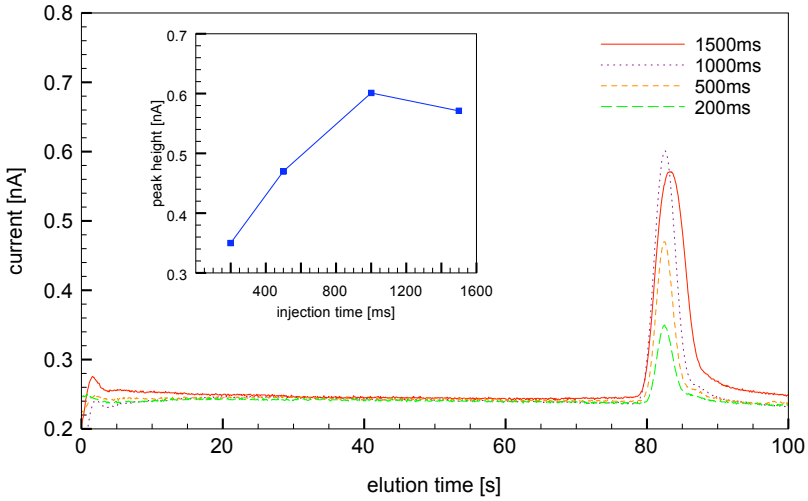

Figure 3.23: Example of different injection times. Stationary phase: Sol-Gel C_8. Mobile phase: H_2O and ACN (90:10, v/v). The pressure drop was 1000 mbar. Analyte: 5 mM phenol. 4 injections with different injection times are compared.

This point is addressed in chapter 4. For injection times up to 1000 ms (350 pl), the peak heights increased linearly. Above 350 pl, peak heights appear to quickly reach a steady value in this system. This can be attributed to two phenomena:

- Purely physical zone dispersion behavior, as observed in non-chromatographic flow injection systems. In such systems, the peak maximum follows a linear dependence on sample volume up to a point, then approaches a constant value asymptotically following an exponential law, as shown by Ruzicka and Hansen (1981).
- Flow pattern disturbance, as the pressure distribution on the entire fluidic network is changed during the plug injection, resulting in a reduction of flow rate.

These two phenomena add up and finally lead to the approach of a constant value of the plug volume.

3.7.3 Conclusions

Both injection methods, thermal as well as pressure-drop, proved to be reliable and usable over a long period of time. However, heater electrode damage and overall device heating in the case of thermal plug injection turn out to be reasons to prefer pressure-drop injections. In the case of pressure-drop injection, there is no improvement on the chip level with respect to fabrication complexity , but the surrounding setup is simplified, as this method uses the already present isolation valves. Pressure-drop plug injection was thus used for all further experiments with chromatographic separations.

3.8 Detection

For on-chip separation devices, one can distinguish between two fundamental approaches of detection; on-chip and off-chip detection; The first method has the advantage of being integrated on the device and it thus

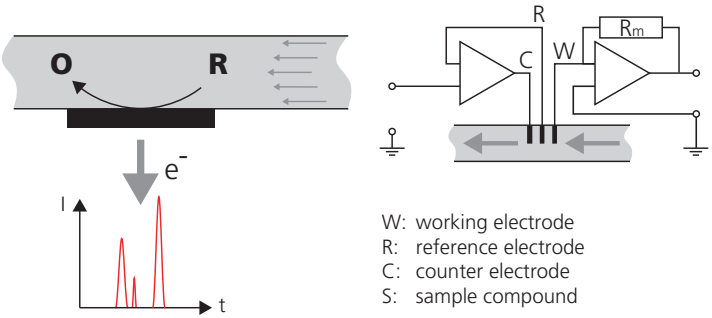

Figure 3.24: Amperometric detection: On the left, a schematic view of electron transfer at the surface of a thin-layer electrode. The analyte passes over the electrode in the thin-layer zone containing reduced analyte R. Oxidation to O at the electrode surface releases electrons to the electrode surfaces. This current is subsequently recorded to produce the chromatogram. On the right, the measurement principle of an amperometric detector.

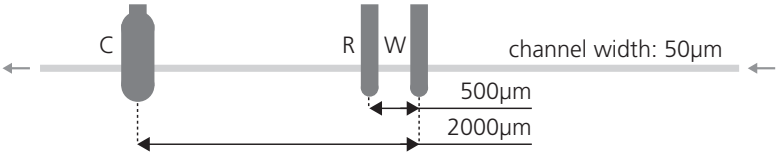

Figure 3.25: Amperometric detector as implemented on chip. Electrode widths are 100 μm for working (W) and reference (R) electrodes and 200 μm for the counter (C) electrode.

does not add to the entire setup volume. Off-chip detection methods are often derived from *macro*-world detectors and hence are much larger instruments. Table 3.6 illustrates the different detection methods and their implementation for on-chip separation devices.
Electrochemical detection has inherent advantages for being integrated onto a chip, as shown by Parriott (1993). As it is a surface sensitive technique rather than being volume sensitive as is optical detection, it is strictly dependent on the analyte concentration rather than on the number of molecules present in the detector volume (Toth *et al.*, 2004). Thus, the detection volume can be made arbitrarily small. Especially when considering absorbance detection the short pathlengths limit the sensitivity. However, this can be circumvented by using multireflection cells to increase the optical pathlength, or by using the thermal lens approach, where the refractive index change due to heating during the light absorption is measured, as detailed by Schwarz and Hauser (2001). For the present device, amperometric detection was chosen for its ease of integrability on to the chip. It is typically used in HPLC for the analysis of organic compound separation (Girault, 2001). In contrast to electrophoretic separation devices, for pressure-driven separation columns there is no need of electrical decoupling of the driving voltage and the measurement cell, such as shown by Osbourn and Lunte (2003) or Lai *et al.* (2004).
DC amperometric electrochemical detection was accomplished using a BioAnalytical Systems 4B-LC HPLC electrochemical detector, with the output signal conditioned using the unit's internal analogue low pass filter set at a 0.3 Hz cutoff to remove mostly 50 Hz noise. The output signal measured the electrochemical current as a function of time, and peak heights in the chromatographic data are given in units of nanoamperes (nA). Platinum working, pseudo-reference and counter electrodes were deposited directly in the separation channel near the exit, with the working electrode upstream of the others. Working and reference electrodes were 100 μm wide, while the counter electrode's width was chosen to be 200 μm in order to allow sufficient current injection. The electrodes

Method	Detector	Implemenation
Spectroscopic	fluorescence	on/off-chip
	absorbance	on/off-chip
	chemiluminescence	on/off-chip
	mass spectroscopy	on/off-chip
Electrochemical	amperometry	on-chip
	conductometry	on-chip
	potentiometry	on-chip

Table 3.6: detection methods for on-chip chromatography

were spaced as shown in figure 3.25. The detection volume can be taken as the space immediately surrounding the working electrode, and consists of a volume of approximately 35 pl, or 0.1% of the total column volume of 35 nl. Additionally this volume is also sufficiently small in comparison to the un-dispersed minimum plug size of 100 pl, achieved by pressure-drop injection.

Electrode fouling When working with DC voltages on detection electrodes, their surface is subject to fouling. In order to overcome this problem, pulsed amperometric detection (PAD) is the method of choice (Girault, 2001). With PAD the detection potential is interspersed with a cleaning and a regeneration potential with cycle periods of around 1 second. As the BioAnalytical Systems unit had no pulsed detection capability, the applied potential was inverted after each separation for 5 subsequent periods of 5 seconds. This sequence, arbitrarily chosen, proved to efficiently prevent the detection electrodes from fouling.

3.9 Summary

The design and fabrication of the liquid/solid chromatography chip was described. A novel method of plug sampling was described allowing for

continuous sampling from flowing analyte streams. The introduction of the bypass channel avoids any stagnant fluid in the microchannels, and thus prevents the chromatographic separation from any difficulties through clogging or precipitating analyte due to slowly or not moving liquids. Two different plug injection methods (thermal and pressure-drop) were described and characterized. The overall system, including aliquot sampling, electrochemical (amperometric) detection and pressure control was presented. The entire system comprising chip and chip holder allows for a rapid cycle time for multiple analyses, exchange of analyte and mobile phase in less than a minute, and complete cleaning cycles within a few seconds only. Chip exchange is performed in less than a minute by the opening and closing two screws on the chip holder.

Chapter 4

Liquid/solid chromatography measurements

Summary Chromatographic test separations are shown and the separation column's performance is characterized and discussed. Vitamin separations are shown as a possible application of the system.

4.1 Materials and Methods

Chemicals The mobile phase chosen for the experiments was a mixture of de-ionized water and HPLC-grade acetonitrile (Reactolab). Table 4.1 gives an overview of the chemical compounds used for the chromatographic test separations. All compounds belong to the family of phenols. In reversed phase chromatography, that is with a hydrophobic stationary phase, a molecule's retention increases with its number of C-H groups. For the compunds shown in table 4.1, the elution order is therefore first uracil (unretained), phenol, dimethylphenol, trimethylphenol and finally pentylphenol. All chemicals were from Acros Organics. For analyte preparation, the phenols were diluted in the mobile phase used for the separation. Prior to injection into the device, the analyte

was vortexed for one minute and then filtered through a 0.2 μm pore-size Teflon® filter in order to remove agglomerates and impurities.

name	molecular formula	chemical structure
uracil	$C_4H_4N_2O_2$	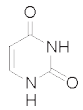
phenol	C_6H_6O	
2,6 dimethylphenol (DMP)	$C_8H_{10}O$	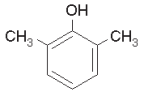
2,3,5 trimethylphenol (TMP)	$C_9H_{12}O$	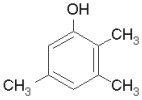
4 pentylphenol (PP)	$C_{11}H_{16}O$	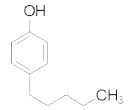

Table 4.1: Phenolic compounds used for the chromatographic separatios. The unretained Uracil was used to determine the column's dead time t_0 .

Separation column Liquid phase coating of the column, as opposed to sol-gel coatings, did not show sufficient separation power. Hence all experiments shown in this chapter are performed in sol-gel coated column. SEM observation of the C_8 sol-gel coated column showed that the actual column height is rather 7μm than the original $5\,\mu$m. This is to be attributed to the NaOH pretreatment of the column. For consistency in the experiments comparing uncoated with coated columns, the uncoated columns did also undergo the NaOH treatment to equate the column geometry.

Mobile phase As discussed in paragraph 2.2.2.3, the mobile phase is a mixture of H_2O and a solvent. In order to minimize the flow resistance, acetonitrile (ACN) was chosen to be the solvent for all measurements shown in this chapter. The mobile phase was prepared using HPLC-grade ACN (Fluka) and de-ionized H_2O (CMI, EPFL). Prior to use, the mobile phase was degassed for 1 h and filtered through a $0.2\,\mu$m pore-size Teflon® filter.

Amperometric detection In order to work at the maximum signal strength, cyclic voltametry was carried out to find maximum oxidation/reduction currents of phenol and DMP solutions were carried out using a Potentionstat / Galvanostat 263A from Princeton Applied Research and a saturated calomel reference electrode. These led to the use of a voltage of 1 V for the amperometric detection.

Data analysis and representation As briefly mentioned in section 3.4, the data acquisition was performed with data acquisition board and with a LabVIEW ® virtual instrument (VI). The obtained data in textfile form was then analyzed by algorithms programmed in Matlab®. All separations shown in this chapter are performed by isocratic elution. The chromatograms have undergone corrections as follows: the base-line offset of the current signal is put to zero and any drift of the base-line is corrected with a linear function calculated based on the slope of the

base-line between the plug injection and the first peak. However, for all chromatograms shown in this chapter, drift always stabilized after a few minutes of running time, and was always below 0.01 mV/min.
Signal disturbance due to the plug injection and voltage inversion for measurement electrode cleaning has been removed from the final chromatograms. The elution time's zero is put at the end of the plug injection procedure.

4.2 Uncoated vs. coated column

In order to characterize the stationary phase, un-coated columns were compared to sol-gel (TEOS/TEOS-C_8) coated column under identical chromatographic conditions. A phenolic test solution with 2.5mM phenol/DMP with a mobile phase of H_2O and ACN (90:10, v/v) was used.

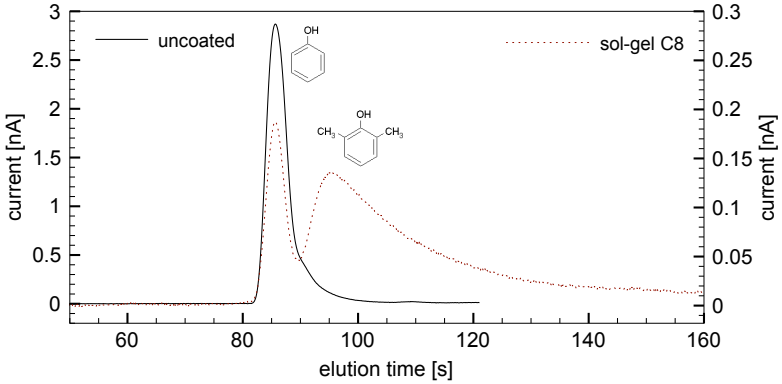

Figure 4.1: Comparison between an uncoated column and a sol-gel C_8 coated column. The injection volume was around 440 pl and the flow rate, u, 1.3 mm/s. The analyte was composed of 2.5mM phenol and 2.5 mM DMP. The mobile phase used was H_2O and ACN (90:10, v/v).

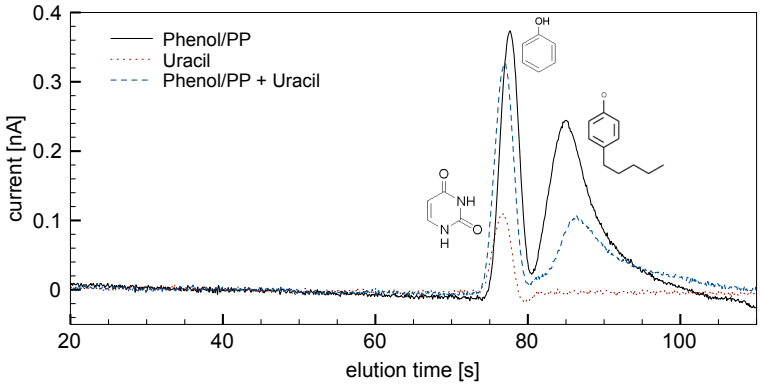

Figure 4.2: Comparison between the unretained uracil and 2.5mM phenol/PP in a mobile phase with H_2O/ACN (90:10, v/v). The plug volume was around 300 pl. Flow rate, u, was 1.3 mm/s.

Figure 4.1 shows the two chromatograms. As both separations were undertaken in the same conditions, this shows that the phenol compound is unretained in both cases, as its retention time t_r is almost identical. It is to be mentioned that the sensitivity of the electrodes in the coated column is diminished by a factor of 10, likely due to the partial sol-gel covering of their surface. Although the separation was undertaken at non-ideal conditions with the flow rate u being above the ideal value (cf. figure 4.5) , it still illustrates the separation efficiency increase due to the sol-gel coating.

In order to estimate the values of the separation factors k, uracil was added to the analyte as a marker for unretained analyte. Figure 4.2 shows a chromatogram of a separation of uracil, phenol and PP (2.5 mM) in a mobile phase of H_2O and ACN (90:10, v/v). Obviously the peaks of uracil and phenol are not sufficiently resolved, which confirms the extremely low retention of phenol in the separation column. For the shown chromatogram in figure 4.2, the retention factors k can be calcu-

lated as being 0.02 for phenol and 0.11 for PP. For all measurements, the retention factors of phenol varied from 0.02 up to 0.07 and for PP from 0.11 up to 0.12. This is typically one to two orders of magnitude lower than the values obtained with conventional reversed phase HPLC systems (Cledera-Castro *et al.*, 2005, 2007)

4.3 Multi-component mixtures

This section shall investigate the chromatographic power of the system in terms of resolution, detection limits and optimum parameter set for operation. For this purpose, multi-component phenolic analytes are separated and their chromatograms analyzed. As an example of application, vitamin separations are shown.

4.3.1 Mobile phase strength influence on retention time

A crucial aspect of chromatographic systems is the mobile phase. In reversed-phase chromatography, a strong solvent decreases retention, while a weak solvent increases it. That means, the larger the volume fraction of H_2O in the mobile phase, the larger the retention for a retained sample, as the column walls are coated with hydrophobic molecules, and H_2O is a weak solvent of the analytes.
Figure 4.3 shows two chromatograms with an H_2O/ACN mobile phase with volume fractions of 30% and 10% of ACN. Identical samples were injected with both mobile phases under the same conditions, one by one, so the peaks are not masking each other. The samples are phenol, DMP and TMP and the flow rate, u, was 1.3 mm/s. The figure clearly illustrates that sufficient separation of the compounds is only achieved at very low strong solvent content (10%). This can be attributed to a insufficient retention through the stationary phase, which thus necessitates a mobile phase of very low solvent strength, as explained in section 2.2.4.

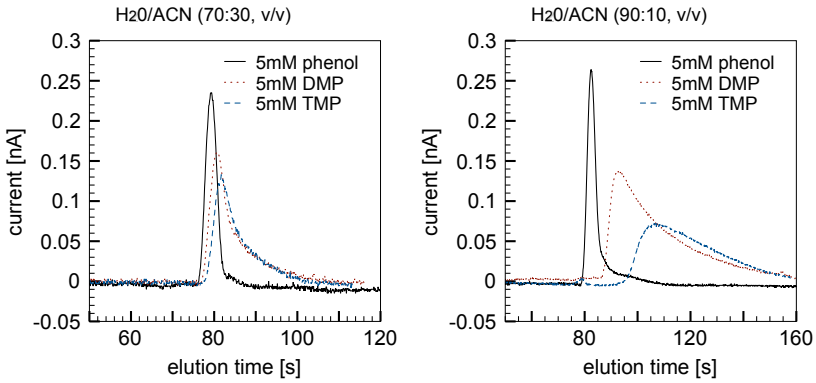

Figure 4.3: Influence of the mobile phase strength on retention time. Stationary phase was sol-Gel C_8 and mobile phase composition H_2O/ACN (70:30, v/v) (left) and H_2O/ACN (90:10, v/v) (right). Injection plug volume was around 300 pl and flow rate, u, was 1.3 mm/s

Furthermore, one can also observe the increasing of the tailing with the number of C-H groups of the compounds.

4.3.2 Flow rate influence

Figure 4.4 illustrates the influence of the flow rate u (linearly proportional to the applied pressure drop Δp) on the separation efficiency. Four separations of a two component analyte (2.5 mM phenol/DMP) are compared at different flow rates (2.0, 1.3, 1.0 and 0.7 mm/s). Lower flow-rates tend to baseline resolution of the two peaks, what is to be expected, as theoretical optimum speed is to be found around 0.2 to 0.4 mm/s, while at the same time the tailing of the peaks is increasing. The Golay plot in figure 4.5 clearly illustrates that flow rates below 1.35 mm/s do not significantly reduce the plate height H and thus do not contribute to an improvement of the separation power. This is in-

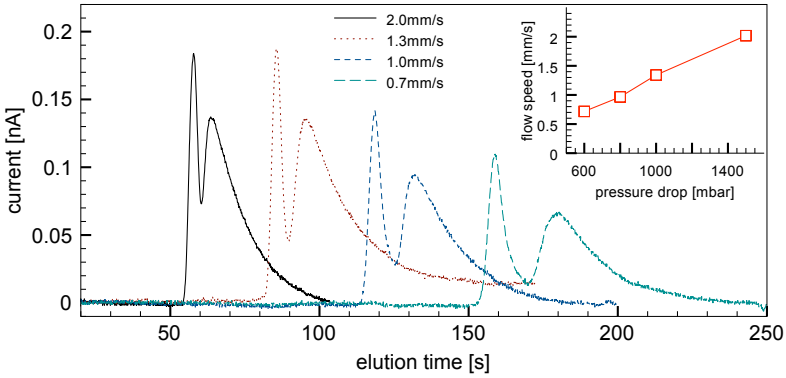

Figure 4.4: Flow rate influence on separation efficiency. The stationary phase is sol-gel C_8 and the mobile phase H_2O and ACN (90:10, v/v). The analyte is 2.5 mM phenol/DMP. The injection volume was around 300 pl.

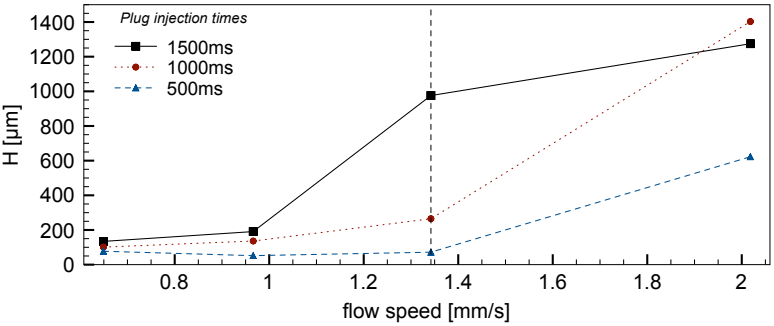

Figure 4.5: Golay plot of chromatograms of 5 mM phenol/DMP analyte in 90:10 (v/v) H_2O/ACN mobile phase for different plug injection times.

deed very promising, as this means that the system, in the case of the phenolic separations, can be run at a much larger flow rate u as calculated for unretained compounds in section 3.1. This gives a large band of operation in which the system's performance is rather independent of u. However it also shows that the plate heights H are two magnitudes larger than calculated. This can be attributed to various parameters, such as poor stationary phase coating, and additional hydrodynamic dispersion induced by the column cross-section not being entirely rectangular.

4.3.3 Continuous separations

One of the most important aspects of the present work from a practical perspective, is the capability of the device to perform consecutive separations in a continuous manner. Figure 4.6 shows a series of 4 chromatograms performed consecutively on the same chip. Between the plug injections, the electrodes were cleaned by inverting the applied potential as described in section 3.8. For the sake of better readability of the chromatogram, the signal disturbances due to injection and voltage inversion were removed.
Besides separation number 3, all separations show baseline resolution. The presented device is capable of doing subsequent separation, with or without washing cycles between. Under the conditions shown in figure 4.6, up to 24 separations/h were achieved, with an injecton every 2 min. If a washing cycle between two consecutive separations is preferred, e.g. for changing analyte or mobile phase, the system can perform up to 10 injections/h with an injection every 6 min.

4.3.4 Reproducibility

Consecutive analysis of the same analyte under the same conditions, such as presented in the former paragraph, shall yield the same results. While in typical reports about lab-on-a-chip devices such concerns are not discussed in particular, the scope of this thesis expressly addresses this issue.

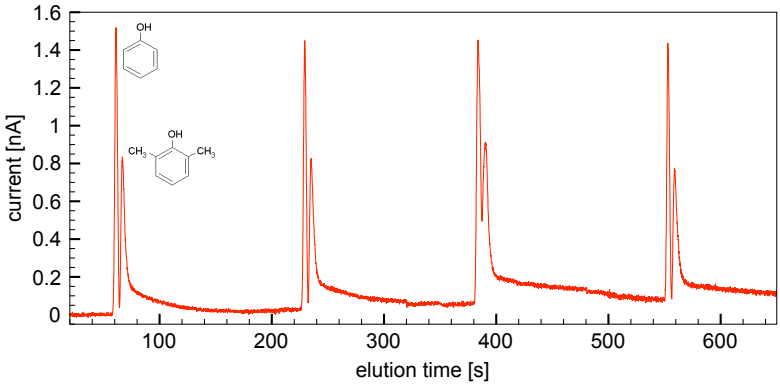

Figure 4.6: Chromatogram of four subsequent injections of 5mM phenol/DMP analyte with 90:10 (v/v) H_2O/ACN mobile phase. Flow rate, u, was 1.3 mm/s and the plug volume 240 pl.

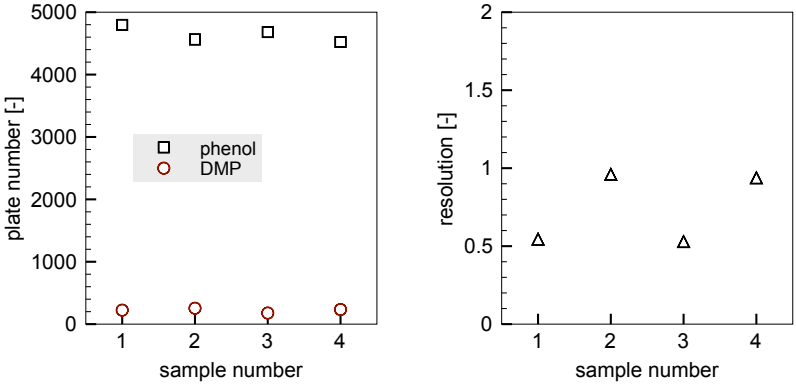

Figure 4.7: Analysis of the four consecutive chromatograms shown in figure 4.6. The figure to the left shows the plate number N, the figure to the right the resolution R. The variation of N (phenol) is less than 5%.

Figure 4.7 shows the chromatographic analysis of the separations shown in figure 4.6. The variation of the phenol peak volume and thus of the plate number N of the phenol compound is less than 5% (typical values around $N = 4500$), while N of the dimethyl varies by about 35% (typical values around $N = 220$). This variation is to a large extent due to a difficult estimation of the actual peak width due to significant tailing. With respect to a saturated uracil solution, the retention factors k obtained are 0.07 for phenol and 0.18 for DMP, whereas the separation factor α is $\simeq 2.3$.

4.3.5 Maximum separation power and detection limits

All precedent chromatograms shown were obtained with a mobile phase of 90:10 (v/v) H_2O/ACN. If the solvent content is lower than 10%, the stationary phase's silanol groups fold to the surface and retention is drastically reduced. This phenomenon is known as *hydrophobic collapse* (Meyer, 2004).

A 2.5 mM phenol/PP solution was separated to show the influence of mobile phase strength. In contrast to DMP and TMP, the PP molecule presents a C_5 alkyl chain attached at the fourth carbon atom of the aromatic ring (see table 4.1), which strongly interacts with the stationary phase. This allowed to separate the analyte at solvent (ACN) concetrations of 30% and 20% respectively. Figure 4.8 (left) illustrates the rise in retention and tailing by decreasing the solvent content. At the same time, as illustrates figure 4.8 (right), plug volume only marginally influences the resolution of the peaks. Plug volume reduction results in a decrease of the signal strength. This can be attributed to the analyte plug that is diluting through diffusion within the mobile phase during the elution time.

In fact, the longitudinal diffusion length is much larger than the plug lengths. Assuming the diffusion constant of phenol in a mobile phase of 90:10 (v/v) H_2O/ACN to be close to the one in pure H_2O, $0.89{\cdot}10^{-9}\,m^2/s$

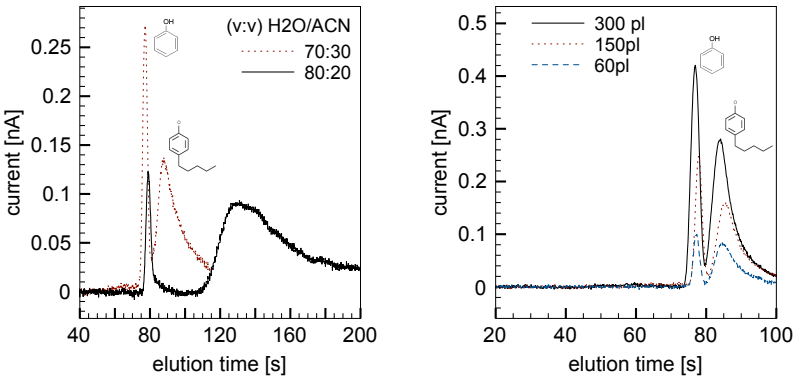

Figure 4.8: Flow rate, u, was 1.3 mm/s. Analyte is 2.5mM phenol and PP: Influence of the mobile phase strength on resolution on the left (plug volume is 300 pl) and plug volume influence on signal strength on the right (mobile phase is 70:30 (v/v) H_2O/ACN).

(Lyde, 2007), and setting the diffusion time t_D equal to the dead time t_0, the plug length increase is given by $2\sqrt{D_c t_D}$. For the chromatograms shown in figure 4.8, right), the dead time t_0 is 75 s and thus the plug length increase is $\simeq$ 5 mm. Comparing that value to the initial plug length of $\simeq$ 1 mm for an injection time of 1 s, this leads to the conclusions that reducing the plug injection time does not improve the separation power of the system, but rather simply reduces the signal strength. At the detector, smaller plug volumes of higher initial concentration can therefore be compared to large plug volumes of lower initial concentration. For doing this, one has to consider the background noise level of the amperometric signal. According to Katz *et al.* (1998), the limit of detection (LOD) for a certain analyte is defined as the analyte concentration that gives a signal (peak) that will be recognized with a probability of 50%. In the present case of liquid/solid chromatography, the LOD can be related to the peak height and the noise on the baseline

(signal-to-noise-ratio SNR). The LOD of the detector can be expressed as:

$$LOD = 2\frac{N_s}{S_i} \tag{4.1}$$

with N_s the noise of the signal and S_i the sensitivity with respect to compound i, defined as:

$$S_i = \frac{dI_{meas}}{dc_{mobile,i}} \tag{4.2}$$

where I_{meas} is the current measured at the detector, and $c_{mobile,i}$ is the concentration of compound i in the mobile phase.
The base-line average noise level of the amperometric detector was estimated to be around 0.005 nA, which thus yields a LOD for phenol of 0.2 mM in 90:10 (v/v) H_2O/ACN mobile phase as illustrated in figure 4.9. Typical values for HPLC are in the pM range (Jin *et al.*, 2002; Sarrion *et al.*, 2002).

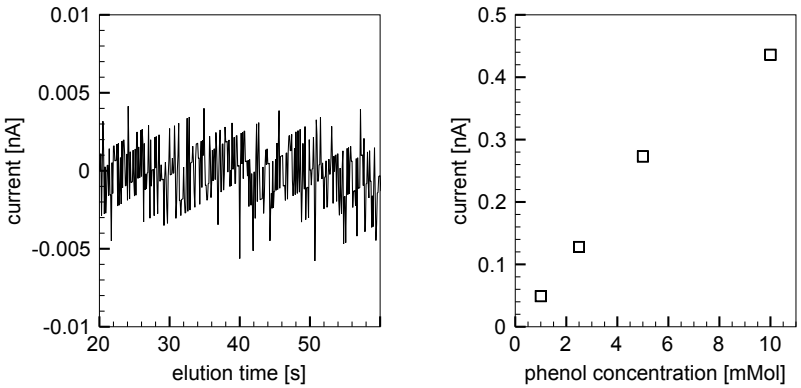

Figure 4.9: Limit of detection (LOD): Noise level of baseline on the left and current response of phenol concentrations in 90:10 (v/v) H_2O/ACN) mobile phase on the right.

4.4 Fields of application

The present device with its reversed-phase, non-polar stationary phase is suitable for any chromatographic separation of relatively non-polar compounds that can either be oxidized or reduced at the amperometric detector, including amines and peptides (Reichmuth *et al.*, 2005), or even petrochemical compounds (Meyer, 2004).
As application example of the present device, multicompound phenol separation for water analysis and vitamin separations are shown.

4.4.1 Multicompound phenolic separations

Medium concentrations of phenols in water can be successfully reduced by biological cleavage. However, very large concentration, where the cleavage is too slow, or very low concentration, where the cleavage is not working, present serious problems for wastewater treatment. One possible solution of the wastewater purification process for samples containing phenols is the adsorption of these phenols onto polymeric adsorbents or ion exchangers, as explained by Azanova and Hradil (1999). A rapid assessment of the phenol concentration in the wastewater would help to optimize the process time of the adsorption process.
Figure 4.10 shows a chromatogram of a separation of three phenolic compounds. Each compound was analyzed separately before they were mixed together for the separation. Figure 4.10 indicates the best performance possible of the present device in terms of resolution. If the compound's concentration is increased, the signal strength increases, but so does tailing. If flow rate, u, was decreased, resolution of DMP and TMP peaks slightly increases, however they do not reach baseline resolution. But with u decreasing, the signal strength is diminished due to the higher longitudinal peak broadening and peak detection of DMP and TMP become difficult.
The chromatogram again shows high tailing for compounds with stronger retention, which illustrates the rather poor separation power of the column.

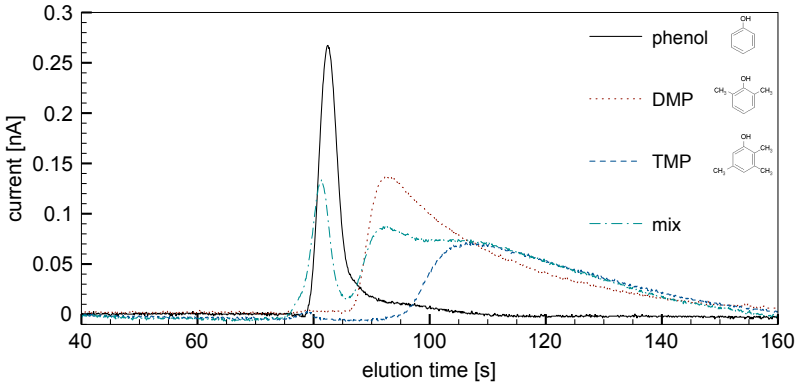

Figure 4.10: Analysis of a phenol, DMP, TMP (5mM each). Each component was first analyzed separately and then mixed together for the separation (mix). While phenol and dimethlyphenol are separated almost to the baseline, the trimethylphenol is only visible as a shoulder. The mobile phase was 90:10 (v/v) H_2O/ACN mobile phase and the flow rate, u, was 1.3 mm/s.

4.4.2 Vitamin separations

After discussion with chromatography experts about interesting applications for the present device, the idea of vitamin separation was investigated. Apparently there is an interest in food and health industry to be able to separated rapidly different vitamin solutions. The decision was made to use liposoluble acetates of vitamin A and E by FLUKA, as shown in table 4.2.

The vitamin acetates were dissolved in 100% ACN before H_2O was added to reach the same solvent concentration as in the moblile phase (90:10 (v/v) H_2O/ACN). The vitamin acetates' concentration was 1 mM, as higher concentrations were problematic in terms of clogging and inconsistent results. Prior to injection into the device, the analyte was vortexted for one minute and then filtered through a 0.2 μm pore-size Teflon® fil-

name	molecular formula and chemical structure
vitamin A acetate	$C_{22}H_{32}O_2$ 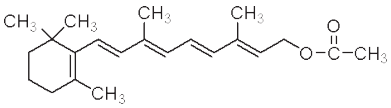
vitamin E acetate	$C_{31}H_{50}O_2$ 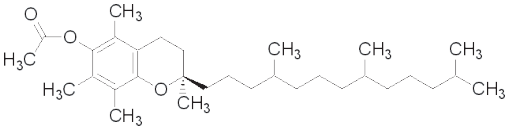

Table 4.2: Vitamin A and E acetates for separation application.

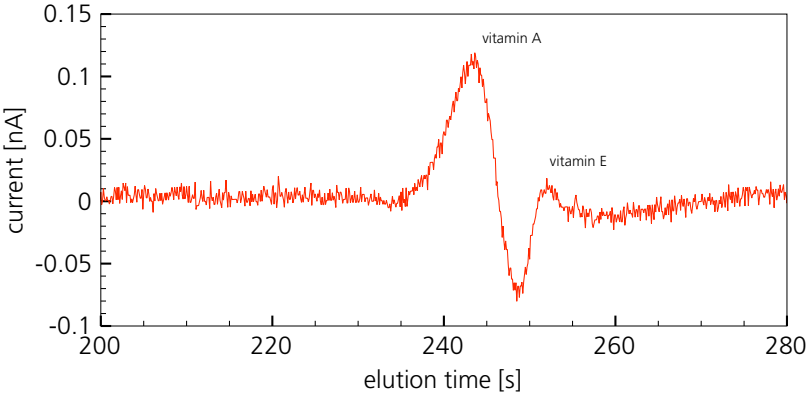

Figure 4.11: Chromatogram of a vitamin solution containing 1mM vitamin A acetate and 1 mM vitamin E acetate in 90:10 (v/v) H_2O/ACN mobile phase. Flow rate is 0.5 mm/s and plug volume is 100 pl. Amperometric detection with an applied voltage of 1 V.

ter in order to remove agglomerates and impurities. Figure 4.11 shows the separation of the vitamin A and E acetate. Vitamin A elutes before E, as its chemical structure let expect, having less free C-H groups that will interact with the stationary phase. The separation factor α with respect to the unretained uracil is only 1.3, compared to those of the penol separations generally above 2. However, the device was run at a flow rate$u$ of around 0.5 mm/s This was possible due to the apparent lower diffusion coefficient of the vitamin acetates in the mobile phase and thus the lower concentration decrease due to longitudinal diffusion of the plug.
The sensitivity is reduced compared to the phenol separations, which can be attributed to the relatively low analyte concentrations used for the separation, as described earlier.

4.5 Concluding remarks and summary

The aim of this thesis is to implement pressure-driven chromatography as a fast sensor for continuous analysis. This perspective has to be kept in mind when analyzing the results presented in this chapter. Successful separations of phenolic analytes and vitamin acetates have been shown. The microfluidic concept with pressure-drop gated injection, bypass channel and aliquoting from meso-scale flows proved to be very reliable for sequent plug injection. The systems robustness allowed for up to 24 analyses per hour.
Consecutive analysis of identical analyte showed less that 5% variation of the plate number N. Integrating large flow-through channels into the chip while having the actuating valves outside of the device proved to be an advantageous solution for both, fabrication complexity and rapid cycle times of analyte and mobile phase. During the experimental phase it was indeed greatly appreciable to be able to change liquids within seconds and to clean the separation column within a few minutes only.
The detection limit LOD of the amperometric electrodes was measured to be 0.2 mM for the phenolic analytes. Theoretical plate numbers N of

up to 4500 could be achieved. However, the measured separation factors k were extremely low, in-between 0.07 for phenol and 0.7 for PP. For the sake of comparison, the k-values presented in this chapter are smaller as those reported by Manz *et al.* (1990b), $k = 3.3$, who used smaller and longer columns with much higher pressure drops to achieve the desired flow rates, but larger as those shown by McEnery *et al.* (2000a,b).
To our dismay, from a purely chromatographic point of view, our values of k do not meet the theoretical limits $1 < k < 10$, detailed in paragraph 2.2.4. Although a thorough preparation of the sol-gel stationary phase yielded an order of magnitude improvement for k compared to the first series of chips, the separation power remained unsatisfying. This can be attributed to the fact, that, altough the sol-gel approach yields a higher surface area as conventional liquid-phase coating with silanol groups, there is no control of the density of the C_8 molecules at the surface of the sol-gel. And although the column preparation with NaOH before the application of the sol-gel shall yield a high density of OH groups at the column wall surface to promote the adhesion of the sol-gel, it has to be assumed that the effective sol-gel covering is indeed very low.
However, despite these drawbacks the system proved to be very reliable in terms of repeatability and its robustness, although at a very basic performance. The use in the field of water analysis for phenols and for vitamin separations illustrates the potential application fields of the system.

Chapter 5

Size-exclusion enhanced hydrodynamic chromatography

Summary This chapter introduces the concept of a porous column wall that enhances hydrodynamic separation in pressure-driven columns. The fabrication method is detailed and experimental verifications of the theoretical predictions are shown and discussed.

5.1 Introduction

Pressure-driven flows have the disadvantage of a parabolic flow profile within the channel. While this phenomena in general contributes to the reduction of the separation power in case of liquid/solid chromatography such as presented in the previous chapter, it can be made use of, as a separation mechanism based on the size of the compounds to separate. Figure 5.1 shows the hydrodynamic chromatography (HDC) principle. For geometrical reasons, large molecules cannot approach the column walls as close as smaller molecules, and are therefore moving at a larger average flow rate u. Hence the larger molecules elute before the smaller.

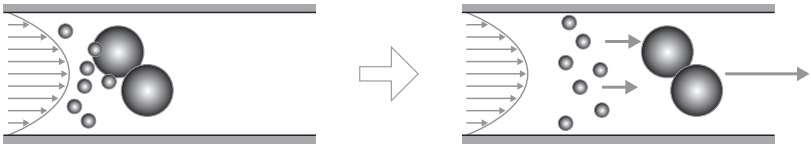

Figure 5.1: Principle of hydrodynamic chromatography (HDC): Compound separation in a pressure driven flow with parabolic flow profile, as result of different mean flow rates u for different particle sizes.

Dimarzio and Guttman (1971) were first to theoretically express this phenomena, but it was Small *et al.* in 1974 and 1976 who demonstrated practically the application of hydrodynamic separation to colloidal dispersions of particles in packed beds with solid, non-porous polymer beads. Tijssen *et al.* (1983, 1986) showed the application of hydrodynamic separation of polystyrene beads in open-tubular capillaries, showing good accordance with theoretical predictions. Hydrodynamic separation in a rectangular, chip-based column was shown by Chmela *et al.* (2002) and Blom *et al.* (2002) and it was again Blom *et al.* (2003) that performed hydrodynamic separations of fluorescent nanoparticles and biomolecules with UV absorption detection on chip.

Size-exclusion chromatography (SEC) is, as well as HDC, different from all other chromatographic methods, by separating compounds simply based on their size, rather than by chemical interactions with a stationary phase. In SEC, the separation column typically contains a porous packing material of defined pore size. Compounds with molecule sizes larger than the pore size are *excluded* and thus elute faster from the column than compounds that are retained, as their molecules are small enough to diffuse into the pores containing stagnant mobile phase. SEC's typical application fields are analysis for polymer synthesis and proteomics, where differently folded species are eluting at different flow rates due to their steric differences (Nguyen, 1998). SEC is as well used in ad-

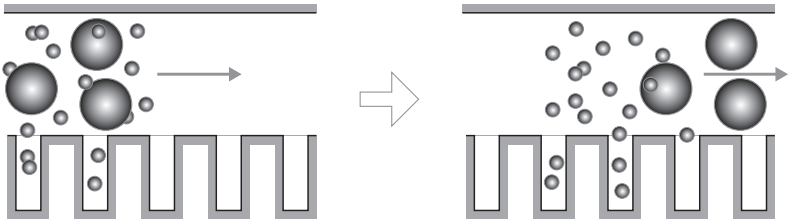

Figure 5.2: Principle of size-exclusion chromatography (SEC): compounds with molecule size larger than the pore size are *excluded* and thus eluting faster as compounds with molecules small enough to have access to the pore volume.

dition to HPLC, especially for compounds with molar mass differences of over 10% (Meyer, 2004).

A particular form of entropic separation, where obstacles in the form of pillars or other structures are placed in the column, was first shown by He *et al.* (1998). It was further developed by other groups such as Chou *et al.* (1999) who showed sorting by diffusion in a pillar-packed setup, Costa *et al.* (2005), who used porous glass channels, or Eeltink *et al.* (2006), who showed the performance limits of such devices. An interesting method of entropic separation was shown by Han and Craighead (2000, 2002) for separating large DNA molecules by entropic barriers made of deep and shallow column regions.

The inherent problem of this sieving approach is the easy clogging of the column; the column allows the smaller molecules to pass, while retaining the larger ones. This problem is overcome with SEC using porous layers on the column walls rather than packed columns. Sano *et al.* (2003) showed the application of a porous layer of anodic alumina with electrophoresis as a driving force to separate DNA molecules in a chip. Porous layers on one side of the column are well-known from the shear-driven chromatography (SDC) theoretically introduced by Desmet and Baron in 1999 and experimentally demonstrated by Desmet *et al.* (2001)

and Clicq *et al.* (2002). It was Clicq *et al.* in 2004 that showed SDC with a porous silicon layer.
While combination of HDS and SEC is not new, as e.g. Stegeman *et al.* (1991) showed polymer separations with that technique, it has to our knowledge always been performed in columns packed with porous particles. This chapter will show the combination in a open-tubular, pressure-driven column: HDC separation is enhanced by SEC through a porous silicon layer on one column wall, hereafter referred to as SOHS (Size-exclusion enhanced, open-tubular hydrodynamic separation).

5.2 Column design and experimental setup

The chip for SOHS chromatography is based on a silicon substrate containing the separation column with dimensions of 1 μm×100 μm×33 mm, T-intersection for sample injection, and a covering Pyrex® wafer containing powder-blasted holes. It is placed in a chip holder made from PEEK, providing fluidic access through sealing with o-rings, analogous to

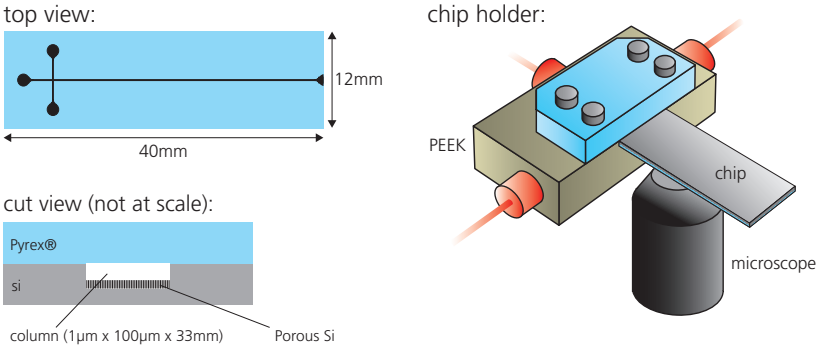

Figure 5.3: Schematic of the SOHS chip with the separation column, and the setup allowing high-pressure fluidic connections and optical detection.

the setup shown in chapter 3. The chip holder is connected through fused silica tubing and ETFE flangeless fittings (Upchurch Scientific) to a high-pressure piston pump (Hitachi L6200) providing the necessary pressure up to 100 bars. Optical detection is performed using an inverted microscope (Zeiss Axiovert S100 TV) wtih two Zeiss objectives: A-Plan 10×, NA 0.25, and Achroplan, 40×, NA 0.8, water immersion. For illumination, a 100 W mercury vapor lamp and a band-pass filter for fluorescein (400 nm to 550 nm) were installed. Data acquisition was performed with a CCD camera (Andor Luca^{EM}) with a typical frame rate of 10 fps and recorded with Andor Solis. The chip holder is constructed such as to allow detection between 15 mm and 33 mm of the column length. Figure 5.3 illustrates schematically the chip layout and the chip holder with the microscope for the optical detection.
For the purpose of the experiments presented in this chapter, the sample injection is performed using an external, two-position valve (Cheminert®, Valco Instruments). The sample injection method is illustrated in figure 5.4. The sample liquid is filled into the tubing in-between valve-entry #4 and the chip, and then injected using the high-pressure-pump. The pump is programmed to maintain the system under a constant pressure rather than to deliver a constant flow. This approach, similar to the one introduced for the device shown in chapter 3, proved to be very reliable. The end of the separation column is connected to atmospheric pressure and covered with a drop of the mobile phase in order not to let the column dry out from the end. The plug volume is defined by the volume of the injection cross (10 pl), although the real plug volume is larger due to the overflow of the analyte into the separation column during injection. For an injection time of 1 s, a mean flow rate, u, of 1 mm/s and taking into account the flow resistance ratio of the separation column over the analyte waste line of 0.07, one can estimate the effective plug volume to be around 20 pl.

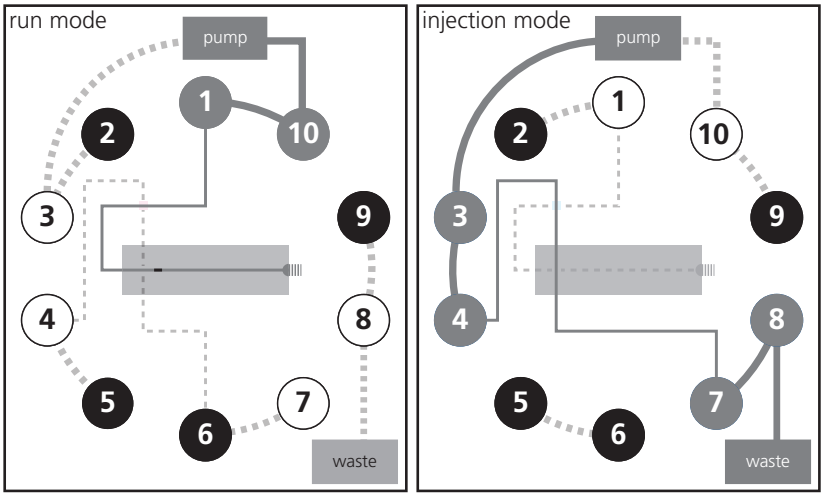

Figure 5.4: Schematic of the sample injection mechanism for the SOHS chip. Entries # 2,5,6, and 9 are blocked on the valve. Full lines are free-flowing and pressurized, while dashed lines are symbolizing blocked or open lines.

5.3 Fabrication

The fabrication is illustrated in figure 5.5. The device is based on a p-doped silicon wafer covered with a 200 nm layer of silicon nitride (Si_3N_4), which will act as an etching mask for both column etching and column wall porosification. The silicon nitride is structured using a thick layer AZ92xx photoresist. The separation column and the other microfluidic channels are etched with dry-etch processing in an Alcatel AMS 200 DSE plasma etcher using carbon-fluoride chemistry (figure 5.5a). Hereafter, the entire microfluidic channels, that is the separation column, as well as the access channels to the T-intersection, are porosified on the bottom. It was Uhlir (1956) who discovered that cleaning attempts of silicon through electrochemical etching in HF was only possible with a

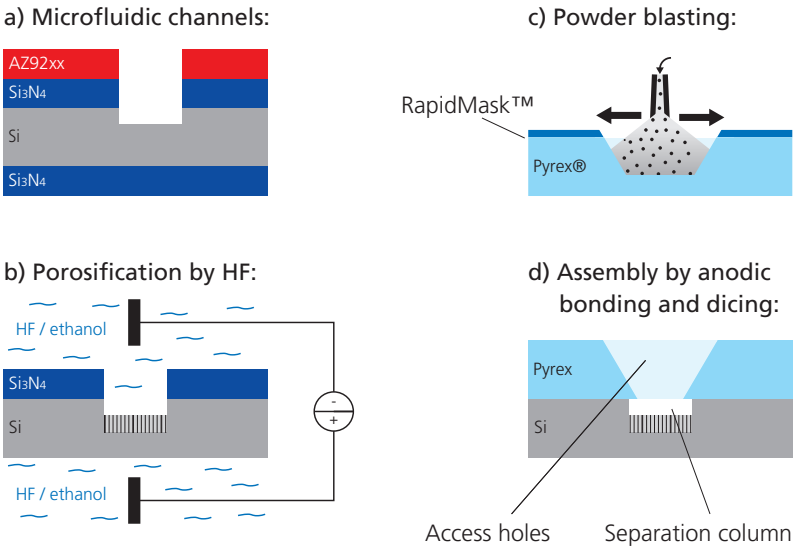

Figure 5.5: Fabrication steps for the SOHS device.

current density above a certain threshold value. Below that threshold, the etching yielded black surfaces, that have taken until 1972 to be described by Theunissen as being porous silicon.
The chemical reactions of the porosification of the silicon can be described as follows:

$$SiH_2 + 2\,F + 2\,H^+ \rightarrow SiF_2 + H_2$$
$$SiF_2 + 4\,HF \rightarrow 2\,H^+ + {SiF_6}^{2-} + H_2$$

According to Lehmann *et al.* (2000), the current density has to be below 600 mA/cm^2 for porosification of silicon in a 1:1 HF(50%wt)/ethanol etching bath. Ethanolic solutions are generally preferred to aqueous solutions for their better wetting properties, which is particularly important

in the case of etching very deep pores. They also observed an increase of the porosity with pore depth; pores become wider with round tips at the bottom, while they are narrow with sharp tips close to the surface of the substrate. This is attributed to the reduction of the electrolyte concentration with pore depth, caused by a limited diffusion at the pore entry. However, this effect can be circumvented by current densities lower than $300\,\mathrm{mA/cm^2}$ and etching times not exceeding one minute.
The boron doping of the p-type $< 100 >$ silicon substrate with a resistivity ranging from 0.01 to $0.02\,\Omega\,\mathrm{cm}^{-1}$ from SILTRONIX, is porosified using an applied electrical potential across the substrate placed in an 1:1 HF(50%wt)/ethanol etching bath. The setup and the parameters are chosen following the indications of Lehmann *et al.* (2000) about mesopore formation in silicon and the procedures described and developed by Lammel (2001). Etch test with various current densities and etch times were carried out in order to adjust the parameters for the separation column. For the present device, the current density was set to $250\,\mathrm{mA/cm^2}$ and the etching time was adjusted to 10 s, in order to obtain vertical pores with diameters of around 20 nm, a porosity of 50%, and a pore depth of around $1\,\mu$m. After the pore-etching, the substrate was left in the HF solution during 1 h in order to remove the Si_3N_4 etch mask. Extensive flushing with de-ionized water was used to remove residues on the surface in order to not compromise the final bonding step.
The top substrate's vertical access holes were sandblasted and then the two substrates anodically bonded and finally diced into chips, making use of the processes already described in section 3.2. However, there was no need of an additional ion-barrier as the silicon substrate is acting as such. The diced chips were immediately stored in de-ionized water containing a surfactant, as will be further detailed in section 5.5.1.
Figure 5.6 shows SEM pictures of the final chip. The images show a very uniform, porous silicon layer on the column bottom and the excellent verticality of the column side walls through the plasma etching. The mean pore size has been estimated to be around 20 nm and the overall

porosity at the surface was evaluated through SEM observation to be at around 50%.

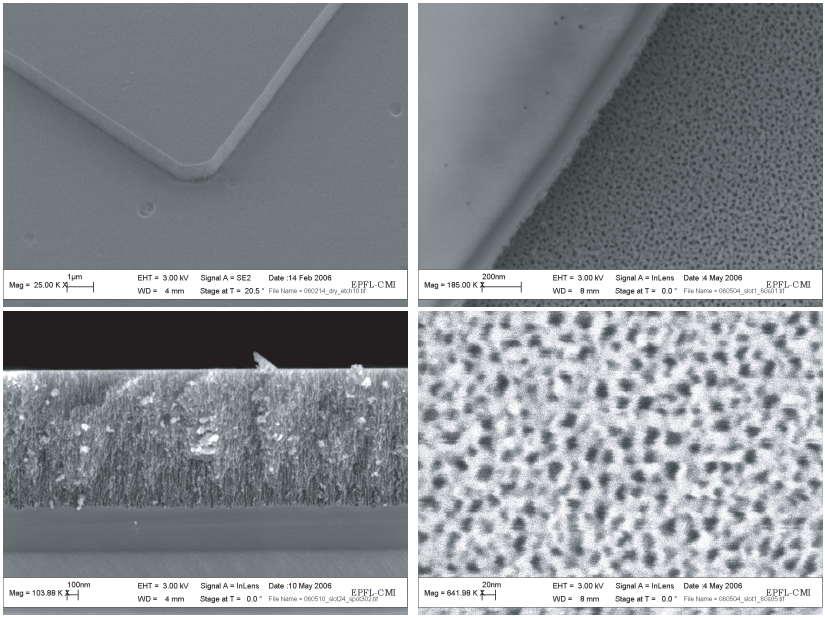

Figure 5.6: SOHS column after dry-etch (top left) and with porous silicon layer on the bottom wall (top right). Close-up of the porous layer with pore depth of around 1 μm (bottom left) and pore size of 20 nm and porosity of 50% (bottom right).

5.4 Theoretical aspects

5.4.1 Hydrodynamic separation

In a column with pressure-driven flow and thus a parabolic flow profile, larger molecules cannot approach the walls as closely as smaller molecules. This results in a difference in the mean flow rate u for different molecule sizes. According to Tijssen *et al.* (1986) and Stegeman *et al.* (1994), this can be expressed for circular columns as follows.
The local flow rate u for a stream line in the mobile phase at the radial position r is:

$$u(r) = 2u_m \left[1 - \frac{r}{r_c}\right] \tag{5.1}$$

with r_c the column radius and u_m the mean flow rate for the point-size molecules exchanging between the entire column diameter $0 < r < r_c$:

$$u_m = \frac{2}{r_c^2} \int_0^{r_c} r \cdot u(r) dr \tag{5.2}$$

For spherical molecules i of radius $r_{eff,i}$, the mean flow velocity $u_{m,i}$ becomes then:

$$u_{m,i} = \frac{2}{(r_c - r_{eff,i})^2} \int_0^{r_c - r_{eff,i}} r \cdot u(r) dr \tag{5.3}$$

which leads, together with equation 5.1, to

$$\begin{aligned} &u_{m,i} = u_m(1 + 2\lambda_i - \lambda_i^2) \\ &\text{with } \lambda_i = \frac{r_{eff,i}}{r_c} \text{ the aspect ratio of molecule } i \end{aligned} \tag{5.4}$$

The relative retention time $t_{R,rel,i}$ of a molecule i is thus given by:

$$t_{Rel,i} = \frac{t_{R,rel,i}}{t_0} = \frac{1}{1 + \lambda_i - \lambda_i^2} \tag{5.5}$$

with t_0 the dead time or the elution time of the unretained mobile phase. For rectangular columns with height h_c much smaller than the column width w_c, such as presented here, equation 5.5 can be adapted by expressing λ_i by:

$$\lambda_i = \frac{2r_{eff,i}}{h_c} \tag{5.6}$$

In order to estimate the peak dispersion, one can safely use the expression of the plate height H for infinite parallel plates introduced by Golay (1958):

$$H = \frac{2D_c}{u_m} + \frac{h_c^2}{105D_c}u_m \tag{5.7}$$

With typical diffusion constants D_c of the order of $10^{-10}\,\mathrm{m}^2/\mathrm{s}$, a separation column of $1\,\mu$m depth and 33 mm length has therefore more than 100 000 theoretical plates, for a column length of 15 mm still over 50 000 plates.

5.4.2 Size-exclusion separation

Size-exclusion chromatography (SEC) is one of the most intuitive approaches to compound separation: A sample is injected in a separation column containing pores of a defined size. Molecules that are larger than the pore size simply elute in the interstitial volume V_0 of the column, while smaller molecules that can diffuse into the pores are seeing a total elution volume V_t which is raised by the total pore volume V_{pores} (Katz *et al.*, 1998):

$$V_{tot} = V_0 + V_{pores} \tag{5.8}$$

The elution volume of a compound i, V_i, can then be expressed in terms of the SEC exclusion coefficient K_{SEC}:

$$V_i = V_0 + K_{SEC,i}V_{pores} \tag{5.9}$$

where K_iV_{pores} is the pore volume accessible by compound i with K_i ranging from 0 for a totally excluded compound to unity for a to-

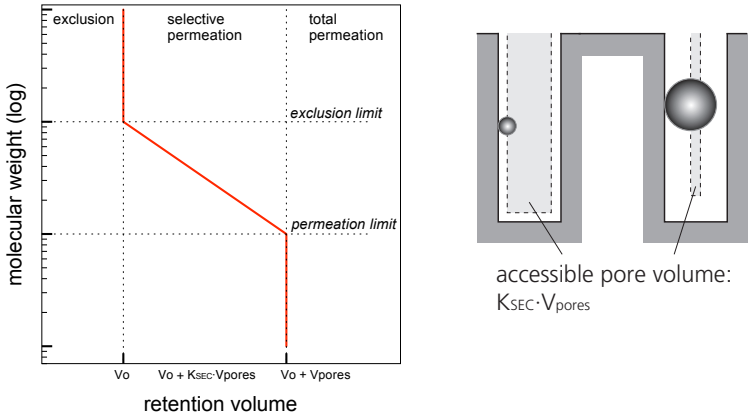

Figure 5.7: Calibration curve for size-exclusion chromatography. Molecules larger than the exclusion limit are completely excluded while molecules smaller than the permeation limit are completely permeated. The volume accessible by the molecules, $K_{SEC,i} \cdot V_{pores}$, is called the working volume of the column.

tally permeated compound. Molecules with sizes in between the exclusion/permeation limits are partially excluded, as they can only access a part of the pore volume, depending on their effective size (figure 5.7). Especially in the case of DNA or polymer separation, where the molecules can fold, the configuration of the folding influences the molecule size and thus the exclusion factor K_{SEC}.

5.5 Experimental results

5.5.1 Materials and methods

After the fabrication, the chips were put into degassed, de-ionized H_2O containing a surfactant, put into vacuum for 1 day and then let stay for at least two additional days in order to prime the column and to absorb

air bubbles present in the separation column. Prior to any separation experiment, the chips were run with pure H_2O at pressures ranging up to 100 bars in order to flush any remaining bubble out of the column. Separation experiments were carried out using a solution of fluorescein (FLUKA) and fluorescent polystyrene latex beads of different diameters (carboxylate modified, from SIGMA and MOLECULAR PROBES, hereafter referred to as *beads*). Optical detection was performed as described in section 5.2.

5.5.2 Results

Figure 5.8 shows the separation of fluorescein (2mM) and beads of 0.1 μm diameter (1% wt). The microscope was placed after 15 mm of the column length. The flow rate was set close to the optimum flow rate calculated from equation 5.7 being of the order of 1.4 mm/s. The fluorescence

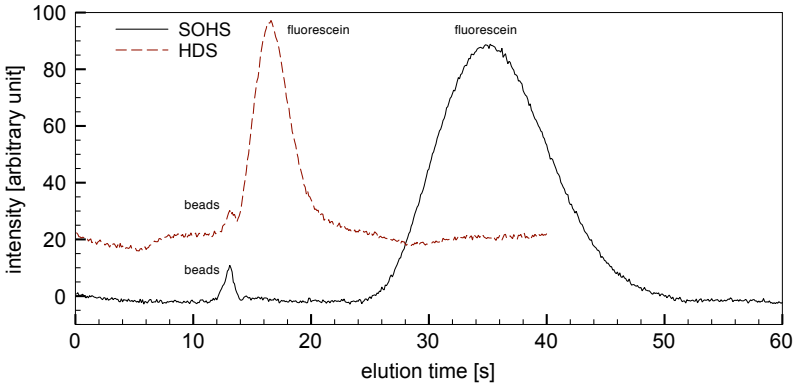

Figure 5.8: Comparison between pure hydrodynamic separation (HDS) in a non-porous column and size-exclusion enhanced hydrodynamic separation (SOHS) in a column with a porous bottom wall and optical detection after 15 mm column length. The graphs are separated vertically for better readability.

	HDS		SOHS	
	t_{Rel} (normalized) th./exp.	N	t_{Rel} (normalized) th./exp.	N
fluorescein	1.00/1.00	64	1.00/1.00	35
0.1 μm beads	0.91/0.70	1500	- /0.37	1000

Table 5.1: Relative elution times t_{Rel} normalized with respect to fluorescein elution (theoretical estimation and experimental data), and plate number N of the data shown in figure 5.8.

intensity of the fluorescein is much larger than for the beads which is easily understandable when looking at the effective fluorescent content in the column. Within the column height h_c, only a few beads are present at once, while the entire volume can be filled out with fluorescein. It was preferred to use a sufficiently high fluorescein concentration in order to observe the peak dispersion.

For the purpose of estimating the influence of the porous bottom wall on the overall separation power, a chip with an untreated column wall (hereafter referred to as non-porous column) was compared to a chip with a porous column wall. By application of equations 5.5 and 5.6, one finds $t_{Rel,beads} = 0.95$ and $t_{Rel,fluorescein} = 1.00$. The additional pore volume accessible to the fluorescein molecules can be estimated to be around 50% of the interstitial volume, according to the fabrication parameters. Table 5.1 shows the relative retention times t_{Rel} and the plate number N for the data shown in figure 5.8.

By applying equation 2.35, one can calculate the resolution of the two peaks for HDS and SOHS respectively:

$$R_{HDS} = 1.01$$
$$R_{SOHS} = 1.73$$

This illustrates the additional separation power through the porous silicon layer.

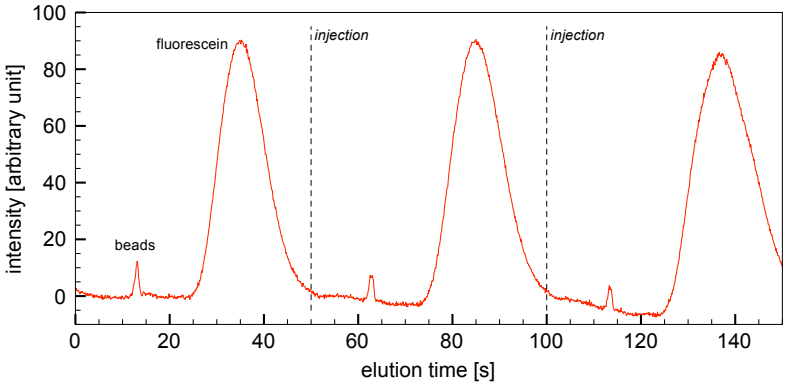

Figure 5.9: Repeated separations of 0.1 μm beads and fluorescein. Sample injections are performed at 0 s, 50 s and 100 s. Peak volume variations of less than 4% are observed.

The repeatability of the separation method is illustrated in figure 5.9. The sample was injected at 0 s, 50 s and 100 s. Peak volume analysis showed less than 4% variation in-between the subsequent injections.

5.5.3 Discussion

The separation power increase due to the addition of a porous silicon layer is clearly demonstrated. However, the absolute value of the resolution for the SOHS might seem small compared to the distinct separation of the two peaks. This is mainly due to the higher peak broadening induced by the SEC which is directly influencing the resolution.
The discrepancy between theory and experimental results for HDS can be explained by two phenomena: First, there are stagnant layers on the side walls, that retain sample and mass transfer from one side to the other is very slow (channel width $w_c = 100\,\mu$m), thus adding dispersion to the peaks. Numerous studies have treated that phenomena, as

for example Doshi *et al.* (1978) and Dutta and Leighton (2001). The other contribution are interactions between the fluorescein and the column surface. At the neutral pH of the mobile phase, the surfaces of both, Pyrex® and silicon (due to partial oxidation), have a majority of SiO^- groups compared to the SiOH surface and have thus a negative potential. This leads to a positively charged double layer on the pore surface which attracts the negatively charged fluorescein to the surface and thus increases its retention.

5.6 Concluding remarks and outlook

The SOHS setup proved to be very difficult in terms of column preparation and fluidic handling. The priming of the column is time consuming and takes several days. As the presence of any bubbles in the separation column greatly interfere with the flow rate and the peak measurement, it had to be assured that no bubble was present in the column. Furthermore the fluorescent beads are subject to formation of agglomerates when not moving rapidly enough, which proved to be a major source of problems during the experiments.
However, once the system was setup, and all bubbles flushed out of the column, it proved to be very reliable in terms of repeatability of the measurements. The chip holder and its o-rings were able to withstand pressures up to 100 bars for several minutes.
The design of the chip and the chip holder did not permit to take measurements at column lengths under 15 mm. Due to dispersion the separation of beads with diameters lower than 0.1 μm could not be reliably recorded as the fluorescence intensity of the beads was too low. It would therefore be interesting to design a chip that will allow to observe the separation from the t-injection cross on in order to visualize the separation directly from the beginning. An interesting feature could be to have two parallel columns next to each other, one with a porous layer on the bottom wall and one without, in order to observe the difference in separation behavior. In order to enlarge the application range, the pore

size should be extendable up to several hundreds of nm. The wafers and procedures that were used for the present device did not allow to reach pore sizes larger than 20 nm.
From the application point of view the present device is very promising for DNA as well as polymer separations. The advantage of the SOHS approach is the insensibility to clogging when compared to devices with an entropical separation approach based on confined column regions, as it is the larger molecules that are not retained and elute first.

Chapter 6

Conclusion and outlook

Summary This chapter summarizes this thesis. The methods and results presented in the former chapters are recapitulated and brought into relation with the objectives defined in section 1.4. It concludes with an outlook on the impact of the results and gives recommendations for future research.

6.1 Summary of results

The aim of this thesis was to develop new concepts for the application of pressure- driven chromatography as a fast sensor for continuous analysis. To do so, following achievements were made:

Chip design A novel concept of microfluidic chip design for continuous sampling was introduced. By making use of the gated injection principle combined with a column bypass channel, a setup with continuously flowing analyte stream was obtained. The use of only one outlet and one pressure source for all liquids streams proved to be a robust approach, and the overall chip design led to the filing of a PCT (Schlund and Gilbert, 2004)

Chip fabrication and setup Cleanroom fabrication using planar technologies was performed to manufacture the chip. The bottom glass wafer with numerous chips containing a separation column of 11 mm length, and Ti/Pt electrodes for amperometric plug detection, was anodically bonded to its top glass counterpart incorporating powder-blasted, vertical fluidic access holes and large bore flow-through channels, before being diced into single chips of 20 mm×20 mm footprint.

Stationary phase coating Sol-gel coating of the column walls with TEOS/TEOS-C_8 was successfully implemented in order to increase the chromatographic retention of the integrated separation column and to obtain a hydro-phobic stationary phase for reversed phase liquid/solid chromatography. It proved to be very superior to conventional liquid phase coatings of C_8 or C_{18}, mainly because of the surface increase generated by the sol-gel technique. The sol-gel coating step however turned out to be the largest source of separation power variations in-between different chips. It was of extreme importance to carefully pursue the protocols found in literature and to precisely control every processing parameter for the production of reproducible chips.

Sample plug injection of variable volume Two methods for repeatable sample plug injection have been introduced; thermal plug injection and pressure-drop plug injection. The former consists in generating a bubble through homogeneous nucleation by local heating, while the latter creates a pressure-drop through the short opening of a check valve outside of the chip. Both methods aim to momentarily change the liquid's pressure distribution in the microfluidic network to allow sampling by gated injection.
Both approaches have been successfully tested and implemented on chip and presented excellent results for continuous flow injection analysis. However the experiments with thermal plug injection demonstrated a certain number of disadvantages compared to the pressure-drop plug injection, such as damage of the heating element under long-term ap-

plications, as well as a the chip heating through heat dissipation in the substrate. Hence pressure-drop plug injection was chosen for all experiments of liquid/solid chromatography.

Liquid/solid chromatography Isocratic separations of phenolic multi-compound analytes as well as vitamins have been shown in order to characterize the performance and the application possibilities of our chip. Excellent results were obtained in terms of repeatability of subsequent analysis during long-term sampling, showing variations of less than 5% of the plate number N, which reached values up to 4500. Up to 24 analyses per hour could be performed in the case of the phenol separations. This illustrates the devices ability of being used as a reliable apparatus for continuous flow injection analysis.
The detection limit (LOD) of the amperometric electrodes was measured to be 0.2 mM for phenol. However, the obtained separation factors k were extremely low, in-between 0.07 for phenol and 0.7 for PP. From a purely chromatographic point of view this is clearly insufficient compared to the calculated theoretical limits, but the robustness of the entire system is very promising for future applications.

Size-exclusion enhanced, open-tubular hydrodynamic chromatography The last chapter introduced the concept of an open-tubular separation column for size-exclusion enhanced hydrodynamic chromatography (SOHS). The column was integrated in a silicon substrate, with the lower column wall containing a porous silicon layer made by galvanostatic etching in an HF bath, and anodically bonded to a Pyrex® cover containing powder-blasted fluidic access holes.
Fluorescence detection through a CCD camera coupled to an inverted microscope illustrated the potential of this approach. Analytes containing fluorescein and fluorescent beads of 0.1 μm in diameter were separated within tens of seconds, using the described device and compared to separations carried out in a device without the porous layer. The results

showing the superiority of the SOHS method were very promising for further applications in DNA or polymer separations.

6.2 Contribution to knowledge and discussion

The purpose of a thesis is to make an original contribution to science. Based on what is documented in literature, the author believes that following points are the most important addition to scientific knowledge:

- Showing that minaturized liquid/solid chromatography can be successfully used as sensor for continuous flow injection analyis.
- Developing a robust and reliable plug injection method with continuously flowing analyte and mobile phase streams, allowing aliquoting from meso-scale flows.
- Combining size-exclusion and hydrodynamic chromatography in an open-tubular column (SOHS) on chip for rapid separations within tens of seconds.

Finally this thesis contains ample information about fabrication technology that can be easily adapted for various devices in the field of microsystems, and microfluidics in particular.

6.3 Outlook

LSC The use of the LSC chip as a sensor for continuous flow injection analysis is an ideal tool for various applications in different fields. Proteomics and pharmaceutical manufacturing are fields of potential interest for such a device. When rapid and continuous sample analysis is being preferred to slower but more precise laboratory analysis, the present LSC chip can be the tool of choice.
Improvements of the device shall mainly focus on the stationary phase

coating and the fabrication technology. The sol-gel coating is an interesting approach to a high-surface area open-tubular chromatograph. If it could be combined with even higher surface area the performance of the device could dramatically improve. Such surfaces could be attained by making use of porous silicon or glass column walls already shown for electrokinetic separations (Costa *et al.*, 2005).
The introduction of plasma etching of glass substrates in nowadays cleanrooms allow for more precise etching of columns in glass substrates and eliminate concerns about not fully vertical column walls obtained through conventional HF wet etching. Making use of this new technology will further enhance the chromatographic separations in the open-tubular column.

SOHC The SOHC approach shall be investigated for polymer and DNA separation. The advantage of having a device that is less susceptible to clogging than conventional entropic separation columns is very promising and leaves a considerable potential for pressure-driven chromatography in these fields.
From a microfabrication point of view it is important to be able to generate porous column walls with pore sizes ranging from tens of nm up to several hundreds of nm in order to be able to adjust the column porosity to the sample composition. Finally it would certainly be interesting to combine the injection technique proposed for the LSC chip with the SOHC column, and connect the separation column outlet to subsequent analysis and/or receptive devices.

Bibliography

Azanova VV and Hradil J, 1999: *Sorption properties of macroporous and hypercrosslinked copolymers*. Reactive and Functional Polymers, *vol. 41*(1-3): 163–175. 100

Bai X, Josserand J, Jensen H, Rossier JS and Girault HH, 2002a: *Finite Element Simulation of Pinched Pressure-Driven Flow Injection in Microchannels*. Analytical Chemistry, *vol. 74*(24): 6205 –6215. 5

Bai X, Lee H, Rossier J, Reymond F, Schafer H, Wossner M and Girault H, 2002b: *Pressure pinched injection of nanolitre volumes in planar micro-analytical devices*. Lab on a chip, *vol. 2002*(1): 45–49. 5, 58

Bart SF, Tavrow LS, Mehregany M and Lang JH, 1990: *Microfabricated electrohydrodynamic pumps*. Sensors and Actuators A: Physical, *vol. 21*(1-3): 193–197. 6

Berthold A, Nicola L, Sarro P and Vellekoop M, 2000: *Glass-to-glass anodic bonding with standard IC technology thin films as intermediate layers*. Sensors and Actuators A:Physical, *vol. 82*: 224–228. 49

Bidlingmeyer BA, 1987: *Preparative liquid chromatography* (Elsevier, Amsterdam). 16

Blom MT, Chmela E, Gardeniers JGE, Tijssen R, Elwenspoek M and van den Berg A, 2002: *Design and fabrication of a hydrodynamic chro-*

matography chip. Sensors and Actuators B-Chemical, *vol. 82*(1): 111–116. 106

Blom MT, Chmela E, Oosterbroek RE, Tijssen R and van den Berg A, 2003: *On-Chip Hydrodynamic Chromatography Separation and Detection of Nanoparticles and Biomolecules.* Analytical Chemistry, *vol. ASAP Article.* 106

Brinker CJ and Scherer GW, 1990: *Sol-gel science the physics and chemistry of sol-gel processing* (Academic Press, Boston). 51

Brody JP, Yager P, Goldstein R and Austin RH, 1996: *Biotechnology at low Reynolds numbers.* Biophys J, *vol. 71*(6): 3430–3441. 13

Büttgenbach S and Wilke R, 2005: *A capillary electrophoresis chip with hydrodynamic sample injection for measurements from a continuous sample flow.* Anal Bioanal Chem, *vol. 383*: 733–737. 59

Chen S, Lin YH, Wang LY, Lin CC and Lee GB, 2002: *Flow-Through Sampling for Electrophoresis-Based Microchips and Their Applications for Protein Analysis.* Analytical Chemistry, *vol. 74*: 5146–5153. 59

Chervet JP and Ursem M, 1996: *Instrumental Requirements for Nanoscale Liquid Chromatography.* Analytical Chemistry, *vol. 68*(9): 1507 –1512. 57

Chmela E, Tijssen R, Blom MT, Gardeniers HJGE and van den Berg A, 2002: *A chip system for size separation of macromolecules and particles by hydrodynamic chromatography.* Analytical Chemistry, *vol. 74*(14): 3470–3475. 106

Chou CF, Bakajin O, Turner SW, Duke TA, Chan SS, Cox EC, Craighead HG and Austin RH, 1999: *Sorting by diffusion: an asymmetric obstacle course for continuous molecular separation.* Proceedings Of The National Academy Of Sciences Of The United States Of America, *vol. 96*(24): 13762–13765. 107

Cledera-Castro M, Santos-Montes A and Izquierdo-Hornillos R, 2005: *Comparison of the performance of conventional microparticulates and monolithic reversed-phase columns for liquid chromatography separation of eleven pollutant phenols.* Journal of Chromatography A, *vol. 1087*(1-2): 57–63. 92

Cledera-Castro M, Santos-Montes A, Izquierdo-Hornillos R and Gonzalo-Lumbreras R, 2007: *Comparison of the performance of different reversed-phase columns for liquid chromatography separation of 11 pollutant phenols.* Journal of Separation Science, *vol. 30*(5): 699–707. 92

Clicq D, Vervoort N, Vounckx R, Ottevaere H, Buijs J, Gooijer C, Ariese F, Baron GV and Desmet G, 2002: *Sub-second liquid chromatographic separations by means of shear-driven chromatography.* Journal of Chromatography A, *vol. 979*(1-2): 33–42. 108

Clicq D, Tjerkstra RW, Gardeniers JGE, van den Berg A, Baron GV and Desmet G, 2004: *Porous silicon as a stationary phase for shear-driven chromatography.* Journal of Chromatography, *vol. 1032*(1-2): 185–191. 108

Constantin S and Freitag R, 2000: *Preparation of stationary phases for open-tubular capillary electrochromatography using the sol-gel method.* Journal Of Chromatography A, *vol. 887*(1-2): 253–263. 50, 51, 53, 54

Constantin S, Freitag R, Solignac D, Sayah A and Gijs MAM, 2001: *Utilization of the sol-gel technique for the development of novel stationary phases for capillary electrochromatography on a chip.* Sensors and Actuators B: Chemical, *vol. 78*(1-3): 267–272. 50, 54

Costa RCDA, Mogensen KB and Kutter JP, 2005: *Microfabricated porous glass channels for electrokinetic separation devices.* Lab on a Chip, *vol. 5*(11): 1310–1314. 107, 127

Culbertson CT, Jacobson SC and Ramsey JM, 1998: *Dispersion Sources for Compact Geometries on Microchips.* Analytical Chemistry, *vol. 70*(18): 3781–3789. 45

Culbertson CT, Jacobson SC and Ramsey JM, 2000: *Microchip Devices for High-Efficiency Separations.* Analytical Chemistry, *vol. 72*(23): 5814 –5819. 4

Deng P, Lee YK and Cheng P, 2003: *The growth and collapse of a microbubble under pulse heating.* International Journal of Heat and Mass Transfer, *vol. 46*(21 SU -): 4041–4050. 63, 64

Desmet G and Baron GV, 1999: *On the possibility of shear-driven chromatography:; a theoretical performance analysis.* Journal of Chromatography A, *vol. 855*(1): 57–70. 107

Desmet G, Vervoort N, Clicq D and Baron GV, 2001: *Experimental demonstration of the possibility to perform shear-driven chromatographic separations in micro-channels.* Journal of Chromatography A, *vol. 924*(1-2): 111–122. 107

Dimarzio EA and Guttman CM, 1971: *Separation by flow and its application to gel permeation chromatography.* Journal of Chromatography A, *vol. 55*(1): 83–97. 2, 106

Dolan JW and Snyder LR, 1989: *Troubleshooting LC systems a comprehensive approach to troubleshooting LC equipment and separations* (Humana Press, Clifton, New Jersey). 20, 21, 50

Doshi MR, Daiya PM and Gill WN, 1978: *Three dimensional laminar dispersion in open and closed rectangular conduits.* Chemical Engineering Science, *vol. 33*(7): 795–804. 120

Dutta D and Leighton DT, 2001: *Dispersion reduction in pressure driven flow through microetched channels.* Analytical Chemistry, *vol. 73*(3): 504–513. 120

Dutta P and Beskok A, 2001: *Analytical solution of combined electroosmotic/pressure driven flows in two-dimensional straight channels: finite Debye layer effects.* Analytical Chemistry, *vol. 73*(9): 1979–1986. 5

Dyson N, 1998: *Chromatographic integration methods.* Second ed. (The Royal Society of Chemistry, Cambridge). 29

Eeltink S, Desmet G, Vivo-Truyols G, Rozing GP, Schoenmakers PJ and Kok WT, 2006: *Performance limits of monolithic and packed capillary columns in high-performance liquid chromatography and capillary electrochromatography.* Journal of Chromatography A, *vol. 1104*(1-2): 256–262. 107

Ermakov S, Jacobson SC and Ramsey JM, 2000: *Computer Simulations of Electrokinetic Injection Techniques in Microfluidic Devices.* Analytical Chemistry, *vol. 72*(15): 3512–3517. 59

Foley J J P Foley and Dorsey JG, 1983: *Equations for Calculation of Chromatographic Figures of Merit for Ideal and Skewed Peaks.* Analytical Chemistry, *vol. 55*(4): 730–737. 29

Fu LM and Lin CH, 2003: *Numerical analysis and experimental estimation of a low-leakage injection technique for capillary electrophoresis.* Analytical Chemistry, *vol. 75*(21): 5790–5796. 59

Fu LM, Yang RJ, Lee GB and Liu HH, 2002: *Electrokinetic Injection Techniques in Microfluidic Chips.* Analytical Chemistry, *vol. 74*(19): 5084–5091. 58

Fu LM, Yang RJ and Lee GB, 2003: *Electrokinetic Focusing Injection Methods on Microfluidic Devices Microfluidic Devices.* Analytical Chemistry, *vol. 78*(8): 1905 –1910. 58

Ganetsos G, 1993: *Preparative and production scale chromatography* (Dekker, New York). 16

Giddings JC, 1989: *Field-flow fractionation of macromolecules.* Journal of Chromatography A, *vol. 470*(2): 327–335. 2

Giddings JC, Chang JP, Myers MN, Davis JM and Caldwell KD, 1983: *Capillary liquid chromatography in field flow fractionation-type channels.* Journal of Chromatography A, *vol. 255*: 359–379. 5, 25

Girault H, 2001: *Electrochimie physique et analytique* (Presses Polytechniques et Universitaires Romandes). 84, 85

Goedecke N, Eijkel J and Manz A, 2002: *Evaporation driven pumping for chromatography application.* Lab on a chip, *vol. 2002*(4): 219 – 223. 6

Golay MJE, 1958: *Theory of Chromatography in Open and Coated Tubular Columns with Round and Rectangular Cross-sections.* DH Desty (Ed), Gas Chromatography, p. 36. 25, 31, 115

Golay MJE, 1981: *The height equivalent to a theoretical plate of retentionless rectangular tubes.* Journal of Chromatography A, *vol. 216*(1): 1–8. 5, 25

Gorbounov V, Kuban P, Dasgupta PK and Temkin H, 2003: *A Nanoinjector for Microanalysis.* Analytical Chemistry, *vol. ASAP*(ASAP). 58

Griffiths SK and Nilson RH, 2001: *Low-dispersion turns and junctions for microchannel systems.* Analytical Chemistry, *vol. 73*(2): 272–278. 47

Griffiths SK and Nilson RH, 2002: *Design and Analysis of Folded Channels for Chip-Based Separations.* Analytical Chemistry, *vol. 74*(13): 2960–2967. 45, 46

Guo Y and Colon LA, 1995: *A Stationary Phase for Open-Tubular Liquid-Chromatography and Electrochromatography Using Sol-Gel Technology.* Analytical Chemistry, *vol. 67*(15): 2511–2516. 50, 54

Han J and Craighead HG, 2000: *Separation of long DNA molecules in a microfabricated entropic trap array.* Science, *vol. 288*(5468): 1026–1029. 107

Han JY and Craighead HG, 2002: *Characterization and optimization of an entropic trap for DNA separation.* Analytical Chemistry, *vol. 74*(2): 394–401. 107

Harrison DJ, Manz A, Fan Z, Luedi H and Widmer HM, 1992: *Capillary electrophoresis and sample injection systems integrated on a planar glass chip.* Analytical Chemistry, *vol. 64*(17): 1926 – 1932. 4

Hasselbrink EF, Sheppod TJ and Rehm JE, 2002: *High-Pressure Microfluidic Control in Lab-on-a-Chip Devices Using Mobile Polymer Monoliths.* Analytical Chemistry, *vol. 74*(19): 4913 –4918. 5, 56

He B, Tait N and Regnier F, 1998: *Fabrication of nanocolumns for liquid chromatography.* Analytical Chemistry, *vol. 70*(18): 3790–3797. 107

Ho W, Stuart B and Prichard E, 2003: *High performance liquid chromatography* (Royal Society of Chemistry, Cambridge). 18

Hong Y, Ashgriz N, Andrews J and Parizi H, 2004: *Numerical Simulation of growth and collapse of a bubble induced by a pulsed microheater.* Journal of Microelectromechanical Systems, *vol. 13*(5): 857– 869. 65

Huang X, Quesada M and Mathies R, 1992: *DNA sequencing using capillary array electrophoresis.* Analytical Chemistry, *vol. 64*(18): 2149 – 2154. 2

Ishii D, Tsuda T and Takeuchi T, 1979: *Studies of open-tubular microcapillary liquid chromatography : IV. Soda-lime glass columns treated with alkaline solution.* Journal of Chromatography, *vol. 185*: 73–78. 50

Jacobson SC, Koutny LB, Hergenroeder R, Moore AW and Ramsey JM, 1994: *Microchip Capillary Electrophoresis with an Integrated Postcolumn Reactor.* Analytical Chemistry, *vol. 66*(20): 3472 – 3476. 59

Jacobson SC, Ermakov S and Ramsey JM, 1999: *Minimizing the Number of Voltage Sources and Fluid Reservoirs for Electrokinetic Valving in Microfluidic Devices.* Analytical Chemistry, *vol. 71*(15): 3273–3276. 59, 81

Janasek D, Franzke J and Manz A, 2006: *Scaling and the design of miniaturized chemical-analysis systems.* Nature, *vol. 442*(7101): 374–380. 36

Jang J and Lee SS, 2000: *Theoretical and experimental study of MHD (magnetohydrodynamic) micropump.* Sensors and Actuators A: Physical, *vol. 80*(1): 84–89. 6

Jin J, Hiroi T, Sato K, Miwa T and Takeuchi T, 2002: *Use of Disposable GRC Electrodes for the Detection of Phenol and Chlorophenols in Liquid Chromatography.* Analytical Sciences, *vol. 18*(5): 549. 99

Jinno K and Sawada H, 2000: *Recent trends in open-tubular capillary electrochromatography.* TrAC Trends in Analytical Chemistry, *vol. 19*(11): 664–675. 7

Katz E, Eksteen R, Schoenmaker P and Miller N, 1998: *Handbook of HPLC* (Dekker). 23, 98, 115

Kirby BJ, Shepodd TJ and Hasselbrink EF Jr, 2002: *Voltage-addressable on/off microvalves for high-pressure microchip separations.* Journal of Chromatography A, *vol. 979*(1-2): 147–154. 5

Kovacs GT, 2000: *Micromachined Transducers Sourcebook* (McGraw-Hill). 11

Kováts E, 2004: *Private communications.* Ecole Polytechnique Fédérale de Lausanne, EPFL. 50

Kricka LJ, 1998: *Miniaturization of analytical systems.* Clinical Chemistry, *vol. 44*(9): 2008–2014. 7

Lai J, Chi-Chung, Chen Ch and Ko FH, 2004: *In-channel dual-electrode amperometric detection in electrophoretic chips with a palladium film decoupler.* Journal of Chromatography A, *vol. 1023*(1): 143–150. 84

Lammel G, 2001: *New micromachining technologies using porous silicon.* Ph.D. thesis, EPFL, no 2387. 112

Lee DJ, Lee YH, Jang J and Ju BK, 2001: *Glass-to-glass electrostatic bonding with intermediate amorphous silicon film for vacuum packaging of microelectronics and its application.* Sensors and Actuators A:Physical, *vol. 89*: 43–48. 49

Lee S, Jeong W and Beebe DJ, 2003: *Microfluidic valve with cored glass microneedle for microinjection.* Lab on a chip, *vol. 3*(3): 164 – 167. 58

Lehmann V, Stengl R and Luigart A, 2000: *On the morphology and the electrochemical formation mechanism of mesoporous silicon.* Materials Science and Engineering B, *vol. 69-70*: 11–22. 111, 112

Li D, 2001: *Electro-viscous effects on pressure-driven liquid flow in microchannels.* Colloids and Surfaces A: Physicochemical and Engineering Aspects, *vol. 195*(1-3): 35–57. 5

Lin YH, Lee GB, Li CW, Huang GR and Chen S, 2001: *Flow-through sampling for electrophoresis-based microfluidic chips using hydrodynamic pumping.* Journal of Chromatography A, *vol. 937*(1-2): 115–125. 6, 59

Lyde DR (ed.) 2007: *CRC Handbook of Chemistry and Physics.* 87 ed. (CRC Press). 98

Manz A and Eijkel JCT, 2001: *Miniaturization and chip technology. What can we expect.* Pure and Applied Chemistry, *vol. 73*(10): 1555–1561. 36

Manz A, Graber N and Widmer HM, 1990a: *Miniaturized total chemical analysis systems: A novel concept for chemical sensing.* Sensors and Actuators B: Chemical, *vol. 1*(1-6): 244–248. 2

Manz A, Miyahara Y, Miura J, Watanabe Y, Miyagi H and Sato K, 1990b: *Design of an open-tubular column liquid chromatograph using silicon chip technology.* Sensors and Actuators B: Chemical, *vol. 1*(1-6): 249–255. 4, 57, 104

Manz A, Harrison DJ, Verpoorte EMJ, Fettinger JC, Paulus A, Ludi H and Widmer HM, 1992: *Planar chips technology for miniaturization and integration of separation techniques into monitoring systems ; Capillary electrophoresis on a chip.* Journal of Chromatography A, *vol. 593*(1-2): 253–258. 3, 4

Manz A, Effenhauser C, Burggraf N, Harrison DJ, Seiler K and Fluri K, 1994: *Electroosmotic Pumping and Electrophoretic Separations for Miniaturized Chemical-Analysis Systems.* Journal of Micromechanics and Miroengineering, *vol. 4*(4): 257,Äì265. 3

Martin AJP and Synge RLM, 1941: *A new form of chromatogram employing two liquid phases.* Biochemical Journal, *vol. 35*: 1358–1368. 17, 27

McEnery MM, Aimin T, Alderman J, Patterson J, OMathuna C and Glennon JD, 2000a: *Liquid chromatography on-chip: progression towards a μ-total analysis system.* The Analyst, *vol. 125*(1): 25–27. 4, 57, 104

McEnery MM, Glennon JD, Alderman J and O'Mathuna SC, 2000b: *Liquid chromatography on-chip.* Biomedical Chromatography: BMC, *vol. 14*(1): 44–46. 104

Meyer V, 2004: *Practical High-Performance Liquid Chromatography*, vol. 4th edition (John Wiley & Sons, Chichester). 21, 23, 27, 29, 37, 97, 100, 107

Moore AW, Jacobson SC and Ramsey JM, 1995: *Microchip Separations of Neutral Species via Micellar Electrokinetic Capillary Chromatography.* Analytical Chemistry, *vol. 67*: 4184–4189. 7

Neue UD and Fallah MZE, 1997: *HPLC columns theory, technology, and practice* (Wiley, New York). 18, 20, 27

Nguyen T, 1998: *Chromatographie en phase liquide des polymères synthétiques: principes et applications.* Analusis magazine (EDP Sciences, Wiley-VCH), *vol. 26*(2): M35–M41. 106

Ocvirk G, Verpoorte E, Manz A, Grasserbauer M and Widmer HM, 1995: *High Performance Liquid Chromatography Partially Integrated onto a Silicon Chip.* Analytical Methods and Instrumentation, *vol. 2*(2): 74–82. 4

Ocvirk G, Munroe M, Tang T, Oleschuk R, Westra K and Harrison DJ, 2000: *Electrokinetic control of fluid flow in native poly(dimethylsiloxane) capillary electrophoresis devices.* Electrophoresis, *vol. 21*(1): 107 – 115. 58

O'Neill AP, O'Brien P, Alderman J, Hoffman D, McEnery M, Murrihy J and Glennon JD, 2001: *On-chip definition of picolitre sample injection plugs for miniaturised liquid chromatography.* Journal of Chromatography A, *vol. 924*(1-2): 259–263. 57

Osbourn DM and Lunte CE, 2003: *On-Column Electrochemical Detection for Microchip Capillary Electrophoresis.* Analytical Chemistry, *vol. 75*(11): 2710 –2714. 84

Parriott D, 1993: *A Practical Guide to HPLC Detection* (Academic Press. New York). 84

Pesek JJ and Matyska MT, 1996: *Electrochromatography in chemically modified etched fused-silica capillaries.* Journal of Chromatography A, *vol. 736*(1-2): 255–264. 50

Poole CF, 2003: *The essence of chromatography* (Elsevier, Amsterdam). 17, 22

Poppe H, 2002: *Mass transfer in rectangular chromatographic channels.* Journal of Chromatography A, *vol. 025948*(1-2): 3–17. 5, 32, 33, 41

Qiao R and Aluru NR, 2002: *A compact model for electroosmotic flows in microfluidic devices.* Journal of Micromechanics and Microengineering, *vol. 12*(5): 625,Äì635. 5

Reichmuth DS, Shepodd TJ and Kirby BJ, 2005: *Microchip HPLC of peptides and proteins.* Analytical Chemistry, *vol. 77*(9): 2997–3000. 100

Ren L, Sinton D and Li D, 2003: *Numerical simulation of microfluidic injection processes in crossing microchannels.* Journal of Micromechanics and Microengineering, *vol. 13*(5): 739. 58

Reyes DR, Iossifidis D, Auroux PA and Manz A, 2002: *Micro total analysis systems. 1. Introduction, theory, and technology.* Analytical Chemistry, *vol. 74*(12): 2623–2636. 4

Richter A, Plettner A, Hofmann KA and Sandmaier H, 1991: *A micromachined electrohydrodynamic (EHD) pump.* Sensors and Actuators A: Physical, *vol. 29*(2): 159–168. 6

Rocklin RD, Ramsey RS and Ramsey JM, 2000: *A microfabricated fluidic device for performing two-dimensional liquid-phase separations.* Analytical Chemistry, *vol. 72*(21): 5244–5249. 59

Ruzicka J and Hansen E, 1981: *Flow Injection Analysis* (J. Wiley and Sons, New York). 82

Sano T, Iguchi N, Iida K, Sakamoto T, Baba M and Kawaura H, 2003: *Size-exclusion chromatography using self-organized nanopores in anodic porous alumina.* Applied Physics Letters, *vol. 83*(21): 4438–4440. 107

Sarrion MN, Santos FJ and Galceran MT, 2002: *Determination of chlorophenols by solid-phase microextraction and liquid chromatography with electrochemical detection.* Journal of Chromatography A, *vol. 947*(2): 155–165. 99

Schlautmann S, Wensink H, Schasfoort RB, Elwenspoek M and van den Berg A, 2001: *Powder-blasting technology as an alternative tool for microfabrication of capillary electrophoresis chips with integrated conductivity sensors.* Journal of Micromechanics and Microengineering, (4): 386–389. 48

Schlund M and Gilbert SE, 2004: *Device and process for continuous on-chip flow injection analysis.* International Patent Application PCT/IB2004/001909. 62, 123

Schwarz MA and Hauser PC, 2001: *Recent developments in detection methods for microfabricated analytical devices.* Lab on a Chip, *vol. 1*(1): 1–6. 84

Shang HM, Wang Y, Limmer SJ, Chou TP, Takahashi K and Cao GZ, 2005: *Optically transparent superhydrophobic silica-based films.* Thin Solid Films, *vol. 472*(1-2): 37–43. 51

Shoji S and Esashi M, 1994: *Microflow devices and systems.* Journal of Micromechanics and Microengineering, (4): 157–171. 3

Sinton D, Ren L and Li D, 2003a: *A dynamic loading method for controlling on-chip microfluidic sample injection.* Journal of Colloid and Interface Science, *vol. 266*(2): 448–456. 58

Sinton D, Ren L and Li D, 2003b: *Visualization and numerical modelling of microfluidic on-chip injection processes.* Journal Of Colloid And Interface Science, *vol. 260*(2): 431–439. 58

Slentz BE, Penner NA and Regnier FE, 2002: *Sampling BIAS at Channel Junctions in Gated Flow Injection on Chips.* Analytical Chemistry, *vol. 74*(18): 4835 –4840. 59

Slikkerveer PJ, Bouten PCP and de Haas FCM, 2000: *High quality mechanical etching of brittle materials by powder blasting.* Sensors and Actuators A: Physical, *vol. 85*(1-3): 296–303. 48

Small H, 1974: *Hydrodynamic chromatography a technique for size analysis of colloidal particles.* Journal of Colloid and Interface Science, *vol. 48*(1): 147–161. 106

Small H, Saunders FL and Solc J, 1976: *Hydrodynamic chromatography A new approach to particle size analysis.* Advances in Colloid and Interface Science, *vol. 6*(4): 237–266. 106

Solignac D and Gijs MAM, 2003: *Pressure Pulse Injection: a Powerful Alternative to Electrokinetic Sample Loading in Electrophoresis Microchips.* Analytical Chemistry, *vol. 75*(7): 1652 –1657. 5, 58

Stegeman G, Kraak JC and Poppe H, 1991: *Hydrodynamic and size-exclusion chromatography of polymers on porous particles.* Journal of Chromatography A, *vol. 550*: 721–739. 108

Stegeman G, van Asten A, Kraak j, Poppe H and Tijssen R, 1994: *Comparison of resolving power and sparation time in thermal field-flow fractionation, hydrodynamic chromatography, and size-exclusion chromatography.* Analytical Chemistry, *vol. 66*(7): 1147–1160. 114

Szumski M and Buszewski B, 2002: *State of the Art in Miniaturized Separation Techniques.* Critical Reviews in Analytical Chemistry, *vol. 32*(1): 1–46. 3, 4

Tabeling P, 2003: *Introduction à la microfluidique* (Belin, Paris). 11, 35

Taylor G, 1953: *Dispersion of Soluble Matter in Solvent Flowing Slowly through a Tube.* Proceedings of the Royal Society of London Series A, Mathematical and Physical Sciences, *vol. 219*(1137): 186–203. 15

Terry SC, 1975: *A gas chromatographic air analyzer fabricated on a silicon wafer using integrated circuit technology.* Ph.D. thesis, Stanford University. 1

Terry SC, Jerman JH and Angell JB, 1979: *A gas chromatographic air analyzer fabricated on a silicon wafer.* Electron Devices, IEEE Transactions on, *vol. 26*(12): 1880–1886. 4

Theunissen MJJ, 1972: *Etch Channel Formation during Anodic Dissolution of N-Type Silicon in Aqueous Hydrofluoric Acid.* Journal of the Electrochemical Society, *vol. 119*(3): 351–360. 111

Tijssen R, Bleumer JPA and Van Kreveld ME, 1983: *Separation by flow (hydrodynamic chromatography) of macromolecules performed in open*

microcapillary tubes. Journal of Chromatography A, *vol. 260*: 297–304. 2, 106

Tijssen R, Bos J and Van Kreveld ME, 1986: *Hydrodynamic chromatography of macromolecules in open microcapillary tubes.* Analytical Chemistry, *vol. 58*(14): 3036–3044. 2, 106, 114

Tjerkstra R, De Boer M, Berenschot E, Gardeniers J, van den Berg A and Elwenspoek M, 1997: *Etching technology for microchannels.* In *Micro Electro Mechanical Systems, 1997. MEMS '97, Proceedings, IEEE., Tenth Annual International Workshop on*, pp. 147–152. 25

Tock PPH, Boshoven C, Poppe H, Kraak JC and Unger KK, 1989: *Performance of porous silica layers in open-tubular columns for liquid chromatography.* Journal of Chromatography A, *vol. 477*(1): 95–106. 50

Toth K, Stulik K, Kutner W, Feher Z and Lindner E, 2004: *Electrochemical detection in liquid flow analytical techniques: Characterization and classification - (IUPAC Technical Report).* Pure and Applied Chemistry, *vol. 76*(6): 1119–1138. 84

Tsuda T, Hibi K, Nakanishi T, Takeuchi T and Ishii D, 1968: *Studies of open-tubular micro-capillary liquid chromatography : II. Chemically bonded octadecylsilane stationary phase.* Journal of Chromatography, *vol. 158*: 227–232. 50

Uhlir A, 1956: *Electrolytic Shaping of Germanium and Silicon.* Bell System Technical Journal, *vol. 35*(2): 333–347. 110

Unger M, Chou HP, Thorsen T, Scherer A and Quake SR, 2000: *Multilayer Soft Lithography Monolithic Microfabricated Valves and Pumps by Multilayer Soft Lithography Monolithic Microfabricated Valves and Pumps by Monolithic Microfabricated Valves and Pumps by Multilayer Soft Lithography.* Science, *vol. 288*: 113–116. 56

Vahey PG, Park SH, Marquardt BJ, Xia Y, Burgess LW and Synovec RE, 2000: *Development of a positive pressure driven microfabricated liquid chromatographic analyzer through rapid-prototyping with poly(dimethylsiloxane); Optimizing chromatographic efficiency with sub-nanoliter injections.* Talanta, *vol. 51*(6): 1205–1212. 4, 58

van Deemter JJ, Zuiderweg FJ and Klinkenberg A, 1956: *Longitudinal diffusion and resistance to mass transfer as causes of nonideality in chromatography.* Chemical Engineering Science, *vol. 5*(6): 271–289. 30

Verheggen TPEM, Beckers JL and Everaerts FM, 1988: *Simple sampling device for capillary isotachophoresis and capillary zone electrophoresis.* Journal of Chromatography A, *vol. 452*: 615–622. 5, 58

Verpoorte E, 2002: *Microfluidic chips for clinical and forensic analysis.* Electrophoresis, *vol. 23*(5): 677–712. 7

Verpoorte E and De Rooij NF, 2003: *Microfluidics Meets MEMS.* Proceedings of the IEEE, *vol. 91*(6): 930–953. 5

Viisanen Y, Strey R and Reiss H, 1993: *Homogeneous nucleation rates for water.* Journal of Chemical Physics, *vol. 99*(6): 4680–4692. 63

Vissers JPC, de Ru AH, Ursem M and Chervet JP, 1996: *Optimised injection techniques for micro and capillary liquid chromatography.* Journal of Chromatography A, *vol. 746*(1): 1–7. 57

Wang J, Siangproh W, Thongngamdee S and Chailapakul, 2005: *Continuous monitoring with microfabricated capillary electrophoresis chip devices.* The Analyst, *vol. 130*: 1390–1394. 59

Widder D, 1975: *The heat equation* (Academic Press. New York). 66

Widmer HM, 1983: *Trends in industrial analytical chemistry.* TrAC Trends in Analytical Chemistry, *vol. 2*(1): VIII–X. 1

Zhong J, Yi M and Bau HH, 2002: *Magneto hydrodynamic (MHD) pump fabricated with ceramic tapes.* Sensors and Actuators A: Physical, *vol. 96*(1): 59–66. 6

Curriculum Vitae

Mario Schlund

Date of birth:	June 28, 1976
Nationality:	Swiss
Origin:	Aesch ZH and Zürich
Languages:	German/Swiss german (mother tongue) French (fluent) English (fluent) Spanish (basic knowledge)

Education

2003 – 2007	**Swiss Federal Institute of Technology Lausanne (EPFL)** Ph.D. (Dr. ès sciences).
1996 – 2002	**Swiss Federal Institute of Technology Lausanne (EPFL)** MSc in microengineering (ing. microtechn. dipl. EPF) with special focus on micro- and nanosystems. Master thesis : *Nanopores in microfabricated polyimide/ metal/polyimide membrane chips.*
1999 – 2000	**Virginia Polytechnic Institute and State University, USA** Graduate student at the College of Engineering (student exchange program).
1991 – 1996	**Kantonsschule Zürich-Wiedikon** Matura type B (Highschool).

Professional Experience

2003 – 2007	**Swiss Federal Institute of Technology Lausanne (EPFL)** Ph.D. studies and research assistant in the field of microsystems and microfluidics in particular.
2002 – 2003	**Crystal Vision Microsystems SA, Switzerland** R&D Engineer: Development of an on-chip HPLC chromatography system.
2000 – 2001	**Nestlé Suisse SA – Direction de production** Internship (4 months) and then part-time collaborator. Introduction of a process-oriented management system (ISO 9004), application optimization and user instruction in entire Switzerland.
2001	**University of Neuchâtel, Institute of microtechnology** Semester Project (4 months): *Production and test of optical switch arrays.*
2000	**EPFL, Institut of microelectronics and micro-systems** Semester Project (4 months): *Interface electronics/tissue of bio-electrodes.*

Publications

M. Schlund, A. Bertsch, P. Renaud: *Size-exclusion enhanced, open-tubular hydrodynamic chromatography for microfluidic separations*, to be published.

T. Braschler, J. Theytaz, R. Zvitov-Marabi, H. van Lintel, G. Loche, A. Kunze, N. Demierre, R. Tornay, M. Schlund and Ph. Renaud: *Virtual valve for smooth contamination-free flow switching*, Lab on a chip, 2007.

M. Schlund, S.E. Gilbert, S. Schnydrig and P. Renaud: *Continuous sampling and analysis by on-chip liquid/solid chromatography*, Sensors and Actuators B: Chemical, 123 (2), Pages 1133-1141, 2006.

M. Schlund and S.E. Gilbert: *Device and process for continuous on-chip flow injection analysis.* International Patent Application PCT/IB2004/001909, 2004.